FINAL TECHNICAL REPORT

AF STTR PHASE II

"3-Dimensional Nano-Scale Reinforcement Architecture for Advanced Composite Structures"

Topic #AF04-T020

Contract No. FA9550-05-C-0088

Submitted to Dr. Byung-Lip Lee
Program Manager, AFOSR/NA
875 North Randolph Street
Suite 325, Room 3112
Arlington, VA 22203

Contractor: 3TEX, Inc.
109 MacKenan Drive, Cary, NC 27511

Principal Investigator – Dr. Alexander Bogdanovich
Vice President, Research & Development
Phone: 919-481-2500 ext. 113
E-mail: bogdanovicha@3tex.com

Research Partners: University of Texas at Dallas and North Carolina State University

October 2008

Table of Contents

OBJECTIVES

- Comprehensively study, implement at a laboratory scale and further advance the new method, invented at the University of Texas at Dallas, of processing continuous yarns from Multi Wall Carbon Nanotubes, improve process control and automation, increase production rate and volume of continuous CNT yarns, and verify their applicability in the manufacturing of 3-D braided and 3-D woven textile structures on 3TEX equipment.
- Conduct experimental studies of the spinnability of Multi-Wall Carbon Nanotube (MWCNT) forests and optimize their processing parameters; increase carbon nanotube length in the forests.
- Conduct further experimental studies of drawing with twist continuous carbon nanotube yarns and investigate the effect of different polymer infusion during drawing on mechanical properties of CNT yarns.
- Fabricate on 3TEX's micro-braiding apparatus continuous samples of 3-D braided preform made of carbon nanotube yarns and their hybrid with glass fibers.
- Fully automate new 3TEX's micro-weaving machine and produce in automated regime samples of 3-D woven preform with continuous carbon nanotube yarns incorporated in through-thickness direction.
- Fabricate micro-scale composite samples reinforced with hybrid 3-D braid made of carbon nanotube yarns and glass fibers, and conduct comprehensive study of their electrical conductivity.
- Conduct experimental Dynamic Mechanical Analysis (DMA) of carbon nanotube 3D braid and respective composite samples infused with different viscosity epoxy resins; correlate results with the previously obtained tensile test data.
- Investigate how to further improve processing methods and enhance multi-functional properties of 3-D nanotube textiles and composites.

EXECUTIVE SUMMARY

Multi-walled carbon nanotubes were used in this STTR Phase II project as building blocks for processing twisted continuous "single" yarns, which were further processed into "multi-ply" yarns, 3-D braids, and 3-D weaves. The draw-twist spinning method of processing long continuous single yarns from multi-wall carbon nanotube forest and plying those single yarns was further advanced and automated. The technology of growing multi-wall carbon nanotube forests has been further studied and much better understood. The principal parameters controlling drawability and morphology of the forests were determined, and this moves us closer to the forest optimization solution.

Extensive experimental studies have been conducted in order to understand the effects of different polymer infusion into carbon nanotube yarns on their mechanical properties. Three polymers (PVA, Polystyrene and PBO) have been infused into the processed carbon nanotube yarns and their influence on the yarn mechanical properties was investigated. It was shown that with relatively small concentrations of these polymers the nanotube yarn strength can be raised up to 1 GPa level.

New research equipment for processing 3-D braids incorporating carbon nanotube yarns has been designed and constructed. It was demonstrated, for the first time, that 3-D micro-braids can be made solely of continuous carbon nanotube yarns and used as reinforcement for composites. Multi-walled CNT yarns were fabricated by UTD and further processed by 3TEX into novel 3-D hybrid nanotube yarn/S-glass fiber braids and their composites. The produced carbon nanotube yarn, hybrid 3-D braid and their composites were tested for electrical conductivity. A comparison with electrical conductivities of some other, more traditional materials, was performed.

Comprehensive structural morphology studies and mechanical characterization of the multi-ply nanotube yarns, 3-D braids, and their reinforced micro-composites have been performed. Tensile tests were conducted for micro-composites reinforced with 5-ply and 25-ply nanotube yarns, as well as 3-D nanotube braids. Test results obtained for 3-D braided micro-composites fabricated with several epoxy resin systems differing in their viscosity revealed new, and some unusual features of the mechanical behavior of this new class of nanocomposites.

A novel 3-D micro-weave has been fabricated with replacement of one or more carbon or S-glass Z-yarns by various multi-ply CNT yarns and 3-D CNT braids. The new specialty 3-D micro-weaving machine has been fully automated by 3TEX. Its capability to process very fine, and relatively weak, fibers and yarns, including carbon nanotube yarns, has been demonstrated in automated regime.

Multi-walled 25-ply carbon nanotube continuous yarns were fabricated by UTD and further processed by 3TEX into a novel type hybrid 3-D woven fabric. In the produced 3-D weave, several rows of regular S-glass roving were replaced by the plied carbon nanotube yarn. This

fabric can be used for further studies of mechanical and electrical properties, and can also be processed into composite material samples.

The results of tensile tests of epoxy matrix composites reinforced with plied nanotube yarns and 3-D braids, obtained earlier in this project, have been revisited and analyzed with more polymer physics insight. The proposed physical hypotheses were verified through experimental Dynamic Mechanical Analysis studies of five epoxy matrices differing in the epoxy modifier content, of carbon nanotube braids, and of composites made with these constituents. New effects have been revealed by the DMA studies; they showed clear correlation with the earlier obtained mechanical test data. These results enabled us to develop a nano-scale hypotheses about interactive behavior of macromolecules in epoxy resins surrounded by carbon nanotubes, which explained the earlier observed unusual mechanical behavior of epoxy matrices reinforced with carbon nanotube yarns and 3-D braids.

Various potential applications of CNT yarns, 3-D braids and 3-D weaves have been revealed and studied in the course of this project. This is supported by numerous interactions/transitions (listed in the next section). Among most exotic potential applications is the space station tether made of 3-D braided CNT yarns. Other realistic applications include various type sensors (joint project on this topic involving NASA Langley Research Center and 3TEX will start soon) and actuators, artificial fuel-powered muscles, devices for energy storage and conversion.

CUMULATIVE INTERACTIONS/TRANSITIONS

1. Bogdanovich, Paper presentation at the 37th SAMPE Fall Technical Conference, October 31-November 3, 2005, Seattle, WA

2. Bogdanovich, Paper presentation at the 27th International SAMPE Europe Conference 2006, Paris, France, March 27-29, 2006.

3. Bogdanovich, Keynote plenary paper presentation at the XIY International Conference on Mechanics of Composite Materials, Riga, Latvia, May 29-June 2, 2006.

4. Bogdanovich, Presentation at the AFOSR Annual Review Meeting, "Mechanics of Multifunctional Materials and Microsystems, " Seattle, WA, August 28-September 1, 2006.

5. Meeting at 3TEX facility with NASA Langley Research Center scientists in June 2007 and follow-on interactions have resulted in a new proposal submitted to internal NASA Innovative Partnership Program. Proposal title: "Carbon Nanotube Yarn Multifunctional Sensors in Composite Structures", Dr. Kahng K. Seun (NASA Langley) Principal Investigator and External Co-Principal Investigator Dr. Alexander Bogdanovich (3TEX) The proposal has been awarded and contract between NASA Langley and 3TEX is currently in preparation.

6. A.E. Bogdanovich, Presentation at the AFOSR Annual Contractor's Review Meeting, "Mechanics of Multifunctional Materials and Microsystems", Monterey, CA, June 25-28, 2007.

7. A.E. Bogdanovich, paper presentation at SAMPE Fall Technical Conference 2006, Dallas, Texas, November 6-9, 2006. 1st Place Outstanding Paper Award.

8. R.H. Baughman, Keynote paper presentation at SAMPE Fall Technical Conference 2006, Dallas, Texas, November 6-9, 2006.

9. A.E. Bogdanovich, Keynote paper presentation at the 16th International Conference on Composite Materials, ICCM-16, Kyoto, Japan, July 8-13, 2007.

10. P.D. Bradford, Paper presentation at the 16th International Conference on Composite Materials, ICCM-16, Kyoto, Japan, July 8-13, 2007. Finalist of the Steve Tsai Award competition for Best Student's Paper.

11. A.E. Bogdanovich, Poster paper presentation at the Nanomaterials for Defense Applications Symposium, San Diego, CA, 23-26 April, 2007.

12. "3 Dimensional Nano-Scale Reinforcement Architecture for Advanced Composite Structures", *Presentation at the AFOSR Annual Contractor's Review Meeting*, "Mechanics of Multifunctional Materials and Microsystems" (Arlington, VA, August 18-20, 2008).

13. "Solid-State Fabrication, Structure, and Multifunctional Applications of Carbon Nanotube Yarns and Transparent Sheets", *Presentation at Department of Aerospace Engineering, University of Illinois* (Sept. 24, 2007, Urbana-Champaign, Illinois).

14. "NanoTech Institute Inventions: Transparent Metallic Sheets, Fuel-Powered Muscles and More", *MetroCon (IEEE) Conference* (Oct. 10, 2007, Arlington, TX).

15. "From Multifunctional Carbon Nanotube Yarns and Transparent Sheets to Fuel-Powered Muscles and Devices for Energy Harvesting, Storage, and Conversion", *Presentation at General Electric* (Oct. 23, 2007, Niskayuna, NY).

16. "Nanotechnology for Fun and Profit", *Carnegie Mellon University Lecture Series* - Lecture preceding receipt of 2007 Distinguished Alumni Award (Oct. 26, 2007, Pittsburgh, PA).

17. "From Electrical to Fuel-Powered Artificial Muscles", *Plenary Lecture at 2007 National Nano Engineering Conference*, prior to receiving Nano 50 Award for Fuel-Powered Artificial Muscles (Nov. 14, 2007, Boston, Massachusetts).

18. "Nanotechnology for Fun and Profit", *Presentation at Petersen Institute of NanoScience and Engineering, University of Pittsburgh* (Feb 4, 2008, Pittsburgh, PA).

19. "Diverse Carbon Nanotube Artificial Muscles Meet an Exciting New Family Member", *Presentation at Monash University* (Feb. 21-22, 2008, Melbourne, Australia).

20. "Diverse Carbon Nanotube Artificial Muscles Meet an Exciting New Family Member", *Presentation at the US AFRL-Israeli Bio/Nano Workshop for Materials* (March 24-25, 2008, San Francisco, CA).

21. "Diverse Carbon Nanotube Artificial Muscles Meet an Exciting New Family Member", *Presentation at ChemOnTubes 08*, (April 6-9, 2008, Zaragoza, Spain).

22. "Diverse Carbon Nanotube Artificial Muscles Meet an Exciting New Family Member", *Presentation at Nano for Defense Applications* (April 21-23, 2008, Arlington, Virginia).

23. "Nanotechnology for Fun and Profit", *Presentation at Hoby Youth Leadership Conference* (May 16, 2008, Dallas, TX).

24. "Fabrication and Multifunctional Applications of Carbon Nanotube Yarns and Self-Woven Sheets", *Paper presentation at Third International Conference on Smart Materials Structures and Systems* (June 8-13, 2008, Acireale, Sicily).

25. "Solid-State Fabrication, Structure, and Multifunctional Applications of Carbon Nanotube Yarns and Transparent Sheets", *Keynote Lecture, 2nd New Diamond and Nano Carbon* (May 26-29, 2008, Taipei, Taiwan).

26. "Solid-State Fabrication, Structure, and Multifunctional Applications of Carbon Nanotube Yarns and Transparent Sheets", *Paper presentation at POLYMER FIBRES 2008* (July 9-11, 2008, University of Manchester, UK).

27. "Nanotechnology for Fun and Profit", *Presentation at Technology Club of Dallas* (August 12, 2008, Dallas, TX).

CUMULATIVE PUBLICATIONS

A. Journal Articles

1. A. Bogdanovich, P. Bradford, D. Mungalov, S. Fang, M. Zhang, R.H. Baughman, and S. Hudson, "Fabrication and Mechanical Characterization of Carbon Nanotube Yarns, 3-D Braids, and Their Composites", SAMPE Journal, 2007, Vol. 43, No. 1, pp. 6-19.
2. R.H. Baughman, "Towering Forests of Nanotube Trees", Nature Nanotechnology, Vol. 1, pp. 94-96, 2006.
3. T. Mirfakhrai , J. Oh, M. Kozlov, E.C.W. Fok, M. Zhang, S. Fang, R.H. Baughman, and D. Madden, "Electrochemical Actuation of Carbon Nanotube Yarns", Invited Paper in Journal of Smart Materials and Structures, Vol. 16, pp. S243-S249, 2007.
4. K.R. Atkinson, S.C. Hawkins, C. Huynh, C. Skourtis, J. Dai, M. Zhang, S. Fang, A.A. Zakhidov, S.B. Lee, A.E. Aliev, C.D. Williams, and R.H. Baughman, "Multifunctional Carbon Nanotube Yarns and Transparent Sheets: Fabrication, Properties, and Applications", Physica B: Condensed Matter, Vol. 15, pp. 339-343, 2007.
5. A.A. Zakhidov, R. Nanjundaswamy, A.N. Obraztsov, M. Zhang, S. Fang, V.I. Klesch, and R.H. Baughman, "Field Emission of Electrons by Carbon Nanotube Twist-Yarns", Applied Physics, 2007, A 00, pp. 1–8.
6. P.D. Bradford and A.E. Bogdanovich, "Electrical Conductivity Study of Carbon Nanotube Yarns, 3-D Hybrid Braids and their Composites," Journal of Composite Materials, 2008, Vol. 42, No. 15, pp. 1533-1545.
7. P. Galvan-Garcia, E.W. Keefer, F. Yang, M. Zhang, S. Fang, A.A. Zakhidov, R.H. Baughman, and M.I. Romero, "Robust Cell Migration and Neuronal Growth on Pristine Carbon Nanotube Sheets and Yarns," Journal of Biomaterials Science: Polymer Edition, Vol. 18, pp. 1245-1261.
8. A.E. Aliev, C. Guthy, P.A. Heiney, M. Zhang, S. Fang, A.A. Zakhidov, J.E. Fischer, and R.H. Baughman, "Thermal Transport in MWNT Sheets and Yarns," Carbon, 2007, Vol. 45, pp. 2880-2888.
9. L. Qu, Q. Peng, L. Dai, G.M. Spinks, G.G. Wallace, and R.H. Baughman, "Carbon Nanotube Electroactive Polymer Materials: Opportunities and Challenges," Materials Research Society Bulletin, 2008, Vol. 33, pp. 215-224.
10. T. Mirfakhrai, M. Kozlov, S, Fang, M. Zhang, R.H. Baughman, and J.D. Madden "Carbon Nanotube Yarns: Sensors, Actuators, and Current Carriers", Proc. SPIE, 2008, Vol. 6927, 692708.

B. Conference Publications

1. A. Bogdanovich, "Long Carbon Nanotube Fibers – Processing, Properties, and Some Application Concepts", CD Proceedings of the 37th SAMPE Fall Technical Conference, October 31-November 3, 2005, Seattle, WA.
2. A. Bogdanovich, D. Mungalov, R.H. Baughman, S. Fang, and M. Zhang, "3-D Braided Material Made of Carbon Nanotubes," CD Proceedings of the 27th International SAMPE Europe Conference 2006, Paris, France, March 27-29, 2006, pp. 455-460.

3. A. Bogdanovich, "Long Continuous Nanotube Yarns as a Reinforcement for Composites: Processing, Properties, and Potential Applications," Book of Abstracts, XIY International Conference on Mechanics of Composite Materials, Riga, Latvia, May 29-June 2, 2006, p. 36.
4. A. Bogdanovich, P. Bradford, D. Mungalov, S. Fang, M. Zhang, R.H. Baughman, and S. Hudson, "Fabrication and Mechanical Characterization of Carbon Nanotube Yarns, 3-D Braids, and Their Composites", CD Proceedings of SAMPE Fall Technical Conference 2006, Dallas, Texas, November 6-9, 2006. **1st Place Outstanding Paper Award, SAMPE Fall 2006 Technical Conference, Dallas**.
5. P.D. Bradford and A.E. Bogdanovich, "Fabrication and Properties of Multifunctional, Carbon Nanotube Yarn Reinforced 3-D Textile Composites", Proceedings of the 16th International Conference on Composite Materials, ICCM-16, Kyoto, Japan, July 8-13, 2007.
6. A.E. Bogdanovich, "Advancements in Manufacturing and Applications of 3-D Woven Preforms and Composites", Proceedings of the 16th International Conference on Composite Materials, ICCM-16, Kyoto, Japan, July 8-13, 2007.
7. R.H. Baughman , M. Zhang, S. Fang, A.A. Zakhidov, M. Kozlov, S.B. Lee, A.E. Aliev, S. Lee, C.D. Williams, and K.R. Atkinson, "Multifunctional Carbon Nanotube Yarns and Textiles for Fun and Profit: Artificial Muscles, Electronic Textile, Energy Storage and Harvesting, Display, Electron Emission, and Other Applications", 49th Annual Conference Proceedings- Society of Vacuum Coaters, pp. 466-469, 2006.
8. A.E. Aliev, C. Guthy, M. Zhang, A.A. Zakhidov, J.E. Fischer, R.H. Baughman, "Thermal Transport in MWNT Sheet: Extremely High Radiation from the Carbon Nanotube Surface," Proceedings of Materials Research Society Symposium 2007, Vol. 963E, (Nanowires and Carbon Nanotubes - Science and Applications).

C. Defended Thesis

Philip David Bradford, "Mechanical Characterization and Morphology Study of a Novel Class of Carbon Nanotube Textiles and Composites," Master of Science Thesis, North Carolina State University, Raleigh, NC, April 2007. Available at NCSU library.

CUMULATIVE HONORS/AWARDS

1. First Place Best Paper Award at the SAMPE Fall Technical Conference 2006, Dallas, Texas, November 6-9, 2006. To: A. Bogdanovich, P. Bradford, D. Mungalov, S. Fang, M. Zhang, R.H. Baughman, and S. Hudson.
2. Nano 50 Award for Carbon Nanotube Sheets and Yarns. To: Zhang M., Fang S., Zakhidov A. A., Lee S. B., Aliev A. E., Williams C. D., Atkinson K. R., and Baughman R. H., Nanotech Briefs Magazine, 2006
3. The NanoVic Prize from Australia. To: Zhang M., Fang S., Zakhidov A. A., Lee S. B., Aliev A. E., Williams C. D., Atkinson K. R., and Baughman R. H., Nanotechnology Victoria Ltd., a venture involving the Australian state of Victoria, 2006.
4. Scientific American Magazine 50 List Recognition for outstanding technological leadership. To: Zhang M., Fang S., and Baughman R. H., Scientific American Magazine. This recognition is for discoveries on carbon nanotube sheets and yarns, 2006.
5. Chancellor's Entrepreneurship and Invention Award. To: Baughman R. H., University of Texas at Dallas. This recognition is for discoveries on carbon nanotube sheets and yarns, 2007.
6. Publication on nanotube-based solar cells was selected, out of 3,100 oral and poster presentations, as one of the "Top Five Hot or Cool Papers" at the Spring 07 Materials Research Society Meeting. To: R. Ulbricht, S.B. Lee, X. Jiang, K. Inoue, M. Zhang, S. Fang, R.H. Baughman, and A.A. Zakhidov, *Materials Research Society*.

CUMULATIVE RESEARCH PERSONNEL SUPPORTED

3TEX, Inc.:

Dr. Alexander Bogdanovich, Vice President, R&D – Principal Investigator
Dr. Dmitri Mungalov, Senior Product Development Engineer
Patrick Duke, Product Development Engineer
Lee Odom, Product Development Engineer
Philip Bradford, Hourly Employee (Research Assistant)

University of Texas at Dallas:

Dr. Ray H. Baughman, Professor and Director of the NanoTech Institute
Dr. Shaoli Fang, Research Associate
Dr. Mei Zhang, Research Associate
Dr. Anvar Zakhidov, Research Associate
Raghuveer Yarlagadda, Graduate Student Worker
Anjanadri K. Venkatasubbareddy, Graduate Student Worker
Xavier Lepro, Graduate Student Worker
Deepthi Durgempudi, Graduate Student Worker
Sravan Vegunta, Graduate Student Worker
Pragna Paranji, Graduate Student Worker
Amelia Lin, Casual Undergraduate Student Worker

North Carolina State University:

Dr. Samuel Hudson, Professor, Department of Textile Engineering, Chemistry and Science
Philip Bradford, MS Graduate Student

ACCOMPLISHMENTS/NEW FINDINGS

Introduction

There are at least five possible ways of using carbon nanotubes for improving existing and developing novel composite systems: (I) modifying matrix material by mixing it with carbon nanotubes, (II) modifying interfaces in composite laminates by adding carbon nanotubes, (III) modifying interfaces between conventional fibers/yarns and matrix by adding carbon nanotubes, (IV) modifying certain types of existing continuous fibers by adding carbon nanotubes during their processing, and (V) replacing conventional continuous fibers/yarns with the ones made solely of carbon nanotubes. A large volume of research work has been performed in directions (I) – (IV), while the group of researchers working on this project has pioneered direction (V) and showed most substantial up-to-date progress in this direction. This statement was supported by several prestigious awards, including First Place Best Paper Award at SAMPE 2006 Fall Technical Conference (Dallas, TX, November 2006).

There are several essential tasks which had to be attacked for the sake of success of this project. The first one is achieving controlled growth of carbon nanotube forests which can be then effectively spun with twist into continuous yarns using UTD's proprietary draw-spin process. The second is the draw-spin process itself, which has been comprehensively studied, continuously improved and enhanced in its capabilities by developing new automated CNT yarn draw-spin equipment. The third is advancing with 3-D braiding and 3-D weaving processes at the micro-level and developing special machines and devices that would allow using very fine (tens of microns in diameter) CNT yarns, having relatively low breaking force values (measures in tens of grams), in the textile formation processes. The fourth is developing special methods of composite materials fabrication by infusing various polymeric resins into nanotube yarns, weaves and braids and consolidating them into composites. The fifth is related to a broad area of mechanical, electrical and thermal property characterization of polymer matrix composites reinforced with CNT yarns, 3-D braids and 3-D weaves. It is believed that this novel type of nanocomposites will show many unique and highly useful multi-functional properties.

Principal technical accomplishments of this research team in all five aforementioned directions are described in the following sections of this Final Technical Report.

SECTION 1

Growing Carbon Nanotube Forests and Yarn Spinning

1.1. Introduction

A very important step in the progress of nanotechnology was the production of nanotubes in macroscopic quantities achieved in 1996 and 1997, using laser ablation [1,2] and electric-arc discharge [3] methods. Later, the new method of high-pressure decomposition of CO (HiPco method) became available [4]. Another very promising method of carbon nanotube synthesis, intensively explored most recently, is based on well-established chemical vapor deposition (CVD) from hydrocarbons [5,6]. Authors of [7] have recently reported the synthesis of 4 cm long individual Single Wall Nanotubes (SWNTs), at a high growth rate of 11 μm/sec by catalytic CVD. Their results show the possibility of growing SWNTs continuously, and without any apparent length limitation. Recent advancements in this area of research have been presented in papers [8-10] among others. In CVD technique, iron nanoparticles on an oxide-coated silicon substrate catalyze the decomposition of hydrocarbon vapours to produce nanotubes on the surface. The technique depends critically – and in largely unpredictable ways – on catalyst composition and structure, gas pressure and flow rates, and the compositions of precursor reactants and carrier gases not to mention the temperature for any catalyst pre-treatment and the CVD growth itself. A comprehensive study of the aforementioned factors' effect on the nanotube forest growth and drawability, conducted during Year 2 of this project at the University of Texas at Dallas (UTD), is presented in the following sections of this report chapter.

As reported in [10], a major breakthrough in nanotube synthesis has been achieved, see [11-13] at the National Institute of Advanced Industrial Science and Technology (AIST) in Tsukuba, Japan, where by growing and characterizing over 1400 samples, researchers have been able to identify the optimum reaction conditions and catalyst structure for the production of ultrahigh forests of double-walled carbon nanotubes. Kenji Hata, Sumio Ijima and their co-workers described a new process for the size-selective growth of ultrahigh forests of double-walled carbon nanotubes containing negligible amounts of catalyst. The nanotubes were synthesized by CVD method. In 2004 this Japanese team has discovered that just the right trace amount of water dramatically increases catalyst lifetime, because the water wapour oxidizes the harmful carbon coating that forms on the catalyst during the growth process. A longer catalyst lifetime means that there is more time for nanotube to grow, which permits the synthesis of 2.5mm high forests of SWNTs that contain less than 0.02% by weight of catalyst. The new aspects in that technological advancement is a thorough investigation of how the thickness of the iron films, used as a catalyst precursor, determines the type (SWNT, DWNT, MWNT) and diameter of the nanotubes. When heated, the iron film (which is typically 1-2 nm thick) breaks up into an array of iron particles, each forming a possible catalytic base for growing one of the nanotubes in the forest. Thicker films tend to break up into larger particles, which catalyze nanotubes with larger diameters.

It is anticipated that nanotubes of such length will significantly impact a wide spectrum of applications. Note that individual carbon nanotubes possess remarkable mechanical properties, and strong belief exists that it will be possible to effectively convert their superior stiffness and strength into respective high properties of various type carbon nanotube reinforced composites. Which type of nanotubes is most useful, will depend on whether the application benefits from high surface area (like in sensors and super capacitors) or on high density of nanotube packing (like in mechanical structures, good thermal and electrical conductors). MWNTs provide the highest density of nanotube walls that can carry currents, transport heat, and support stress (as long as the inner walls are similar in diameter to the SWNTs). However, for electrochemical devices, where high gravimetric surface area is needed (such as super capacitors, fuel cells and artificial muscles), SWNTs or DWNTs might be best.

The nanotube yarn drawing process requires certain amount of bonding between the nanotubes in the forest, which can be achieved by intermittingly bundling the nanotubes together. If either this bundling or the density of nanotubes in the forest is too low (or too high), the fabrication process fail. Conventional wisdom says that that unbundled SWNTs provide the best properties. However, this conclusion largely rests on the data for nanotubes that are just microns in length. Such short nanotubes cannot provide efficient mechanical stress transfer and electron and phonon transport – either between the walls in MWNTs or DWNTs, or between bundled nanotubes. With ever-longer nanotubes becoming available, the highest bulk mechanical stiffness and strength, and electrical and thermal conductivities will likely come from MWNTs that are closely packed, well aligned, and minimally curved.

1.2. Spinning Continuous Carbon Nanotube Yarns from Nanotube Forests

A number of sophisticated and, at the same time, very distinct methods aimed at processing long continuous fibers and yarns from carbon nanotubes have been developed in the past 6 years. There are several papers containing reviews on this topic and extensive lists of references, see [14-19]. Particularly, paper [19] provides and extensive review and discussion of several most promising methods, state-of-the-art summary, and essential literature on this topic. The primary challenges of making nanotube fibers/yarns with desirable properties are: (i) achieving the maximum possible alignment of the building blocks (nanotubes or their bundles) within continuous fiber/yarn and (ii) increasing internal force, heat, electrical current, etc. transfer between the building blocks.

An interesting discovery was occasionally made by authors of [20] who found that carbon nanotubes can be self-assembled into yarns up to 30 cm long, simply by being drawn out of aligned arrays of carbon nanotubes. That approach has been substantially modified and advanced by the authors of [21]. They purposefully added twist during nanotube drawing. Figure 1.1 shows an SEM image of yarn assembly during the spinning process, in which ~10 nm diameter Multi-Walled Nanotubes (MWNTs) were simultaneously drawn from their forest and twisted. The yarn diameter was set by controlling the width of the forest sidewall that was used to generate an initial wedge-shaped ribbon, which is shown converging from about the thickness of the forest to that of the yarn at the apex. About a hundred thousand MWNTs pass through every micron square area of the produced yarn.

Figures 1.2a and 1.2b show SEM images of MWNT single yarn and 5-ply yarn, respectively. The 5-ply yarn was produced by over-twisting five individual single yarns and, subsequently, allowing them to twist relax around itself until a torque balanced state is reached.

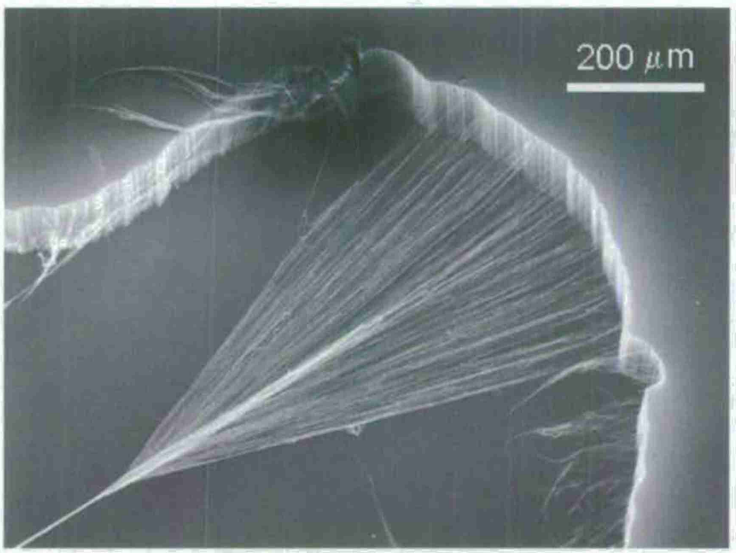

Figure 1.1. SEM image of a nanotube yarn captured in the process of being simultaneously drawn and twisted from a nanotube forest [21].

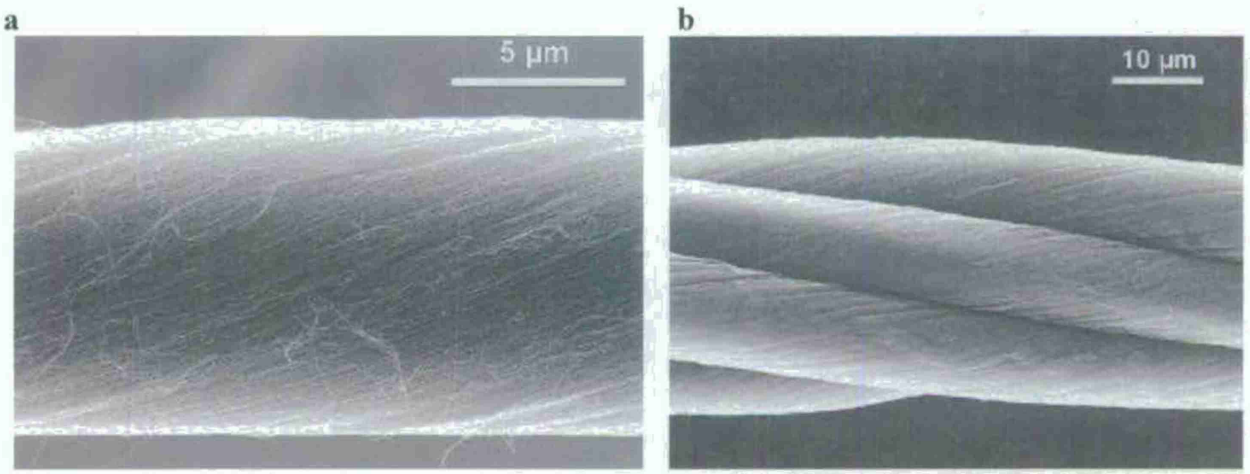

Figure 1.2. SEM images of a single (a) and 5-ply (b) MWNT yarns [21].

The Mark 3 first-generation spinner developed at UTD has been the sole fabrication tool for 3TEX MWNT yarn delivery during Year 1 of this project. Although Mark 3 spinner has high production efficiency and its operation is very user-friendly, it does not provide precise control of twist insertion. By leveraging the knowledge learned from the development of Mark 3 and using direct spinning approach, UTD and their Australian collaborators have developed a more sophisticated, continuous spinning apparatus (Mark 4), which introduces twist as it winds the twist-spun yarn onto a bobbin and builds a yarn package. Figure 1.3 a picture of Mark 4.

The advantage of this new system is the precise control of twist level and sophisticated electronic interfaces which offers real-time adjustment during spinning. Also, Mark 4 provides more precise control in plying single-ply or multi-ply yarns together to continuously make more complex multi-ply yarns. In such a case, the nanotube forest is replaced by reels of unplied single yarns, and the single yarns are passed through an initial yarn guide. The twist level of the multi-ply yarns is again determined by winding speed, which can be continuously adjusted, and by diameter of the bobbin. This process provides precise control of twist insertion and sophisticated electronic interfaces which offers real-time adjustment during plying to continuously make multi-ply yarns.

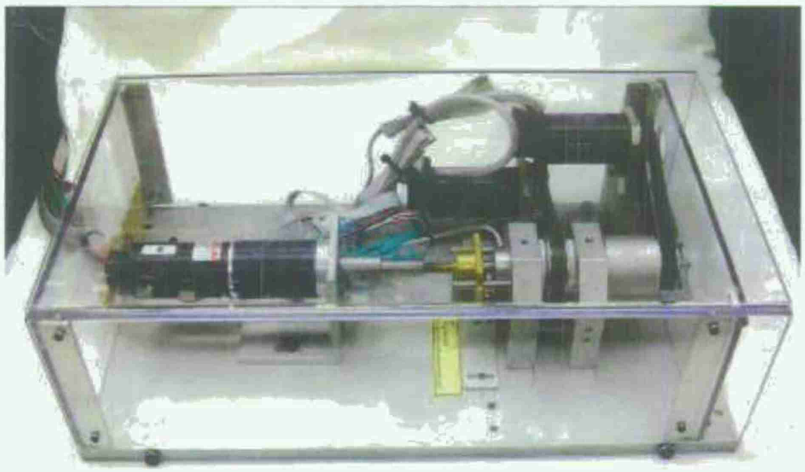

Figure 1.3. Mark 4 apparatus developed at UTD for spinning continuous single yarn from nanotube forest and for plying yarns.

UTD produced on Mark 4 device eighteen pieces (each about 25 inch long) of 6-ply yarns which were used in 3TEX's 3-D braiding process. The hybrid 3-D nanotube yarn/glass fiber braid, to be described further in this report, has been produced utilizing that yarn. Recently UTD produced 20 ft of 25-ply CNT yarn which was used by 3TEX's in the first 3-D weaving trials on the new, fully automated 3-D weaving machine.

1.3. Further Studies of Nanotube Forest Growth

Catalyst film quality (uniformity and thickness) plays a vital role for growing spinnable carbon nanotube (CNT) forests. The key problem with the current solid state spinning process developed at the University of Texas at Dallas (UTD) is that synthesis of CNT forests enabling fast "continuous" draw often fails. The nanotube drawing process depends totally on the intimate connections between nanotube bundles in the forest. The failures during draw are due to the non-uniform structure (connectivity) of CNT forests, which largely stems from the non-uniformity of the catalyst layer.

The catalyst deposition is accomplished using e-beam evaporation onto the Si substrates. UTD's current catalyst deposition system is a home-made e-beam evaporator, which is not robust

enough for reliable uniform catalyst deposition. Although some high-quality spinnable forests have been produced using this e-beam evaporator, the yield of the entire process has been relatively low. Recently, UTD personnel has encountered problems with the catalyst layer deposition, and the resulting CNT forests are largely unspinnable. It was found that the reasons for not being able to obtain reliable uniformity and precise thickness control for the catalyst deposition are the following (it is illustrated in Fig. 1.4):

1) The inability to rotate the deposition substrate in the e-beam evaporator.
2) Irreproducible location of the thickness monitor, which correspondingly causes thickness calibration to be unreliable.
3) Irreproducibility in the shutter position.
4) Overheating in the auto E-beam mode, causing wild fluctuations in evaporation rate.

Figure1.4. Current E-beam evaporation system (left) and inside view of the deposition chamber (right).

UTD's current e-beam evaporator, with these inherent problems, is highly unsuitable for development of upscaled processes. In order to solve these problems, it is planned to develop the catalyst film deposition recipe using the newly accessible CHA Industries e-beam evaporator (shown in Fig. 1.5). The new evaporator provides the following advantages compared with the current e-beam evaporator:

1) Built for industrial process application.
2) Rotating substrate insures uniform deposition.
3) Fixed position of the thickness monitor.
4) Reliable and repeatable shutter position.
5) Deposits simultaneously on six substrates (6" diameter).
6) Increases throughput 4.5 x 5 = 23 times for currently employed 3" CVD furnace.

Figure 1.5. Newly accessible CHA Industries E- Beam Evaporator.

1.4. CNT Yarn Properties and Their Relationship to CNT Properties

Inter-bundle, intra-bundle, and intra-wall mechanical stress transfer all increase with nanotube length. All of these effects are expected to result in an increase of yarn strength and yarn modulus with increasing nanotube length. The goal of the present study is to identify the most important critical link (inter-bundle, intra-bundle, or intra-wall) in stress transfer for our nanotube yarns that are typically 10 nm in diameter, hundreds of microns long, and contain about eight co-axial walls in each nanotube.

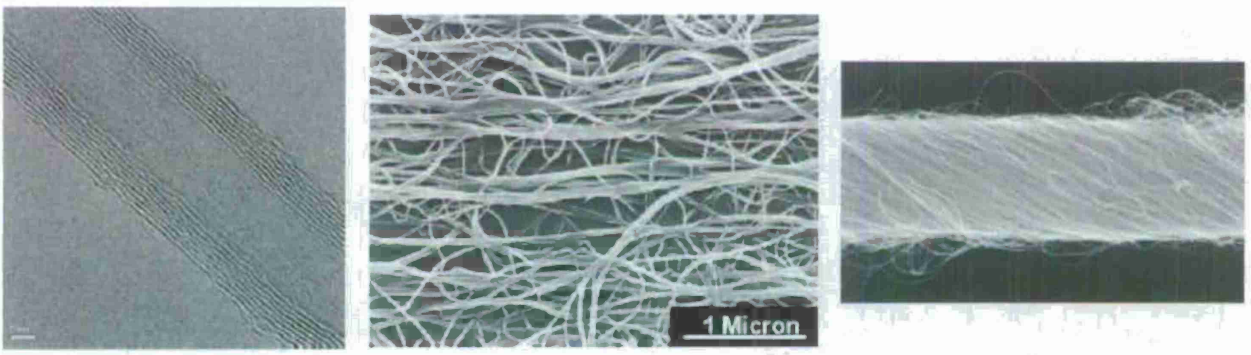

Figure 1.6. Micrographs illustrating different levels of hierarchal assembly and associated stress transfer for MWNTs: inter-wall coupling in MWNT (left), inter-tube bundling (with about a hundred nanotubes per large bundle) and bundle forking before twist (middle), and inter-bundle coupling by twist for a 2.2 micron diameter yarn (right). The lateral extent of the middle micrograph is less than a percent of the length of the individual MWNTs.

Yarn properties vs. MWNT length is potentially a function of structure on vastly different scales: from inter-wall coupling in MWNTs, to inter-tube bundling and bundle forking, and to inter-bundle coupling by twist (as illustrated in Fig. 1.6). The results show that the most critical link in mechanical stress transfer for our MWNT yarn is the stress transfer between walls in a MWNT. This result contrasts with that for poorly oriented nanotube arrays, like filtration-produced nanotube sheets, where stress transfer at the intersection between poorly oriented nanotubes has paramount importance.

The ratio of yarn tensile strength σ_y to the tensile strength of the component bundles σ_f is approximately $\sigma_y/\sigma_f \approx \cos^2\alpha(1-k\cos ec\alpha)$, where $k=(DQ/\mu)^{1/2}/3L$, α is the helix angle that the bundles make with the yarn axis, D is the bundle diameter, μ is the friction coefficient between bundles, L is the bundle length, and Q (the bundle migration length) is the distance along the yarn over which a bundle shifts from the yarn surface to the deep interior and back again. When k is very small, permanent twist degrades mechanical properties, except to the extent that twist increases yarn density. The main effect of permanent twist is densification of the initial aerogel yarn.

As expected, we find that nanotube yarn strength increases with increasing MWNT length (as seen in Fig. 1.7). All tensile strengths are for yarns with the same twist angle and diameter. How long must our 10 nm diameter, eight-wall MWNTs be, before stress is supported by all nanotube walls? Our collaborator Rod Ruoff and co-workers showed (Experimental Mechanics (2006)) sword-in-sheath rupture for 1-8 μm long MWNTs and the measured sheath strength (considering only the outer wall) was 12 GPa - 41 GPa. Results of others (Hong *et al.*, Proc. Natl. Acad. Sci. USA (2005)) for 1.5-20 nm diameter MWNTs show stress transfer from the outer wall to one adjacent inner wall when MWNT length is one centimeter (Fig. 1.8). Complete stress transfer to all walls by going to longer nanotube lengths could increase yarn strength up to 6 times.

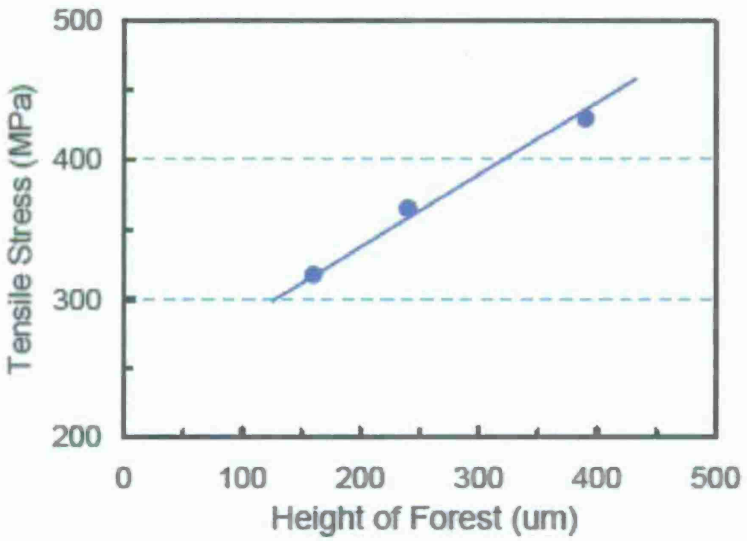

Figure 1.7. Dependence of MWNT yarn strength on MWNT length.

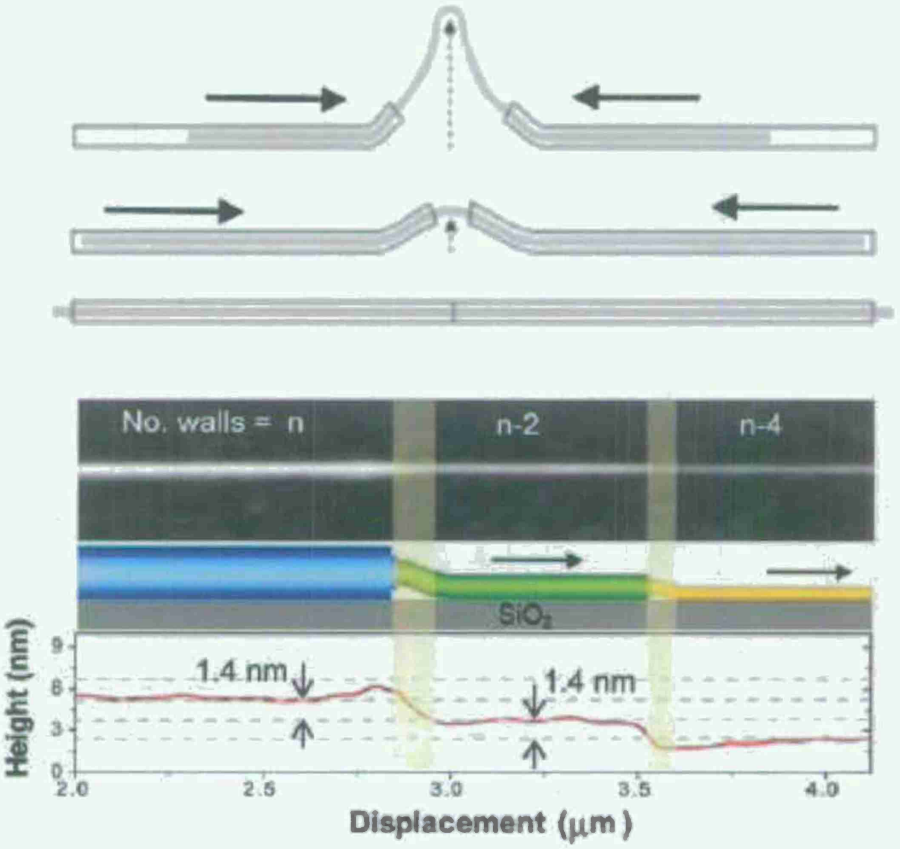

Figure 1.8. Sword-in-sheath rupture for MWNTs.

Slippage between bundles is another weak link for achieving yarns with the mechanical properties of individual MWNTs. Micrograph in Fig. 1.9 shows slippage in the rupture region of broken CNT yarn. We can either decrease the CNT yarn migration length Q by processing prior to twist (using false twist and or liquid-based densification) or use yarns having ultra-long nanotubes for which permanent twist is not needed. The surface-to-volume ratio of nanofiber bundle determines force needed for slippage (pull-out) and this ratio is ~ 12 times larger for a single MWNT than for a 100 MWNT bundle.

This increased surface-to-volume ratio for individual MWNTs or small MWNT bundles, versus that for large MWNT bundles, explains some fascinating new results. Small MWNT bundles or unbundled MWNTs could not be pulled from the yarn (Fig.10) without their breaking into a few micron long segments (versus the starting 300 micron CNT length). Hence, slippage between individual nanotubes in the yarn does not limit strength. This conclusion, that individual nanotubes (or small bundles) do not slip, is also confirmed by inspection of the broken nanotube ends, while slippage of large bundles is evident. The high concentration of broken individual nanotube ends and small bundle ends indicates that they are not slipping (Fig. 1.11). Measurements of the failure strengths of individual nanotube segments and small bundle segments provide a tensile strength of from 2.9 to 13.8 GPa.

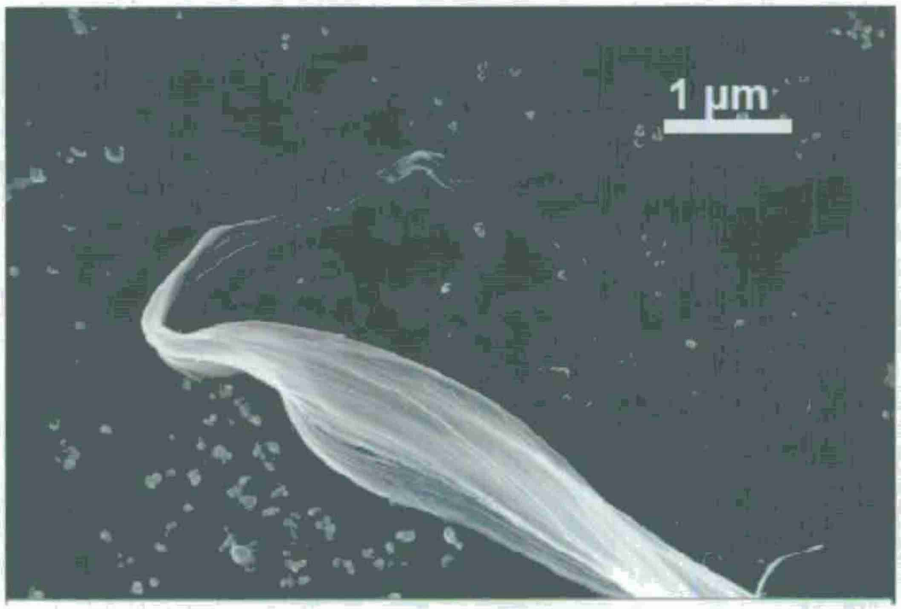

Figure 1.9. SEM image showing slippage in the rupture region of a broken MWNT yarn.

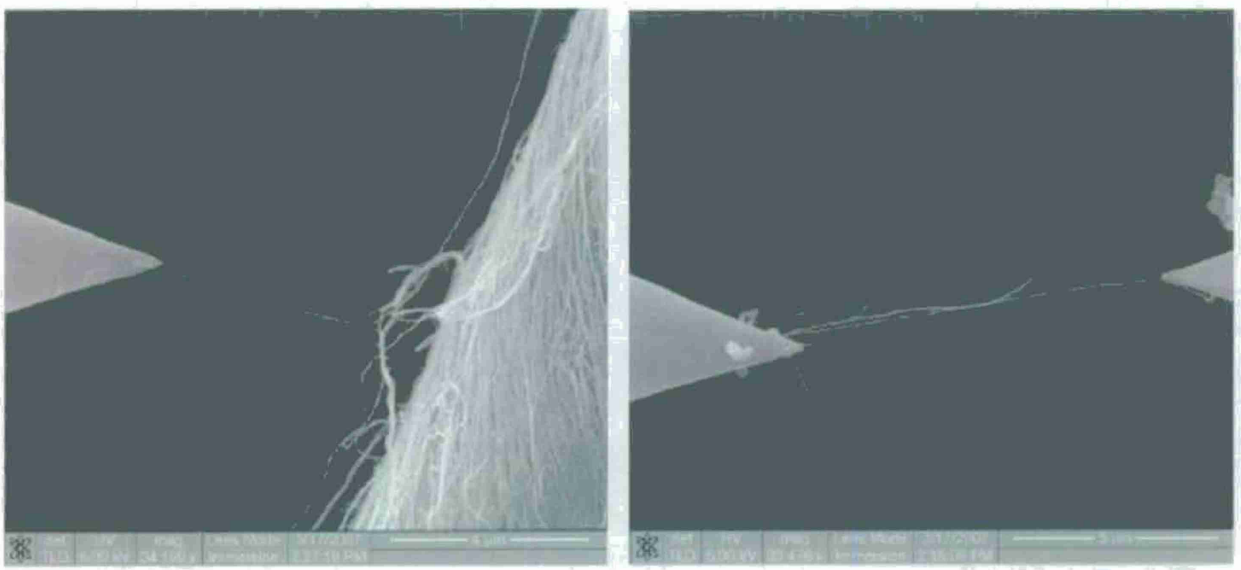

Figure 1.10. Show extraction of a small nanotube bundle from a 10 micron diameter twist-spun yarn using a AFM tip (left). Tensile strength measurement by stretching a small diameter MWNT bundle between two AFM cantilever tips (right).

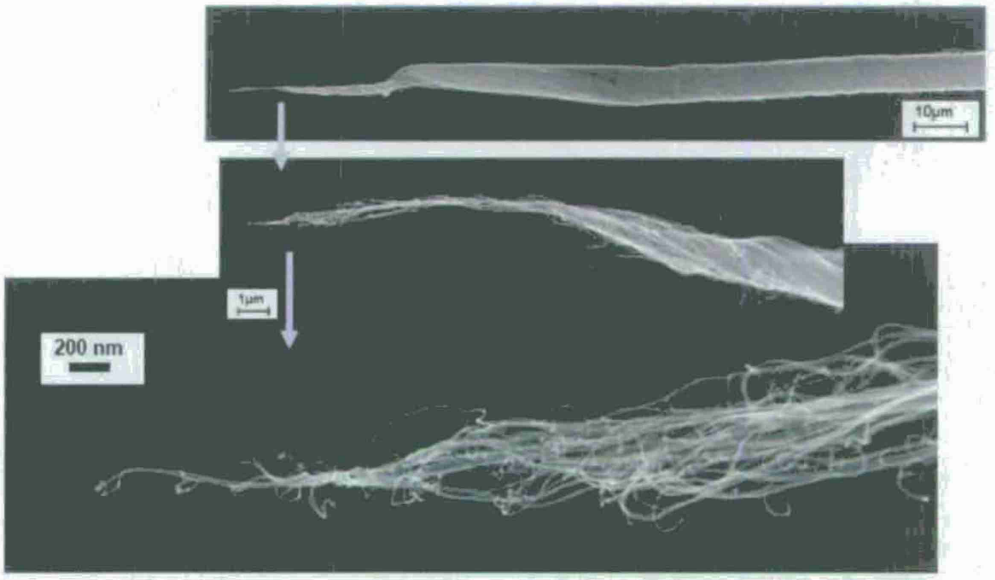

Figure 1.11. SEM micrographs at progressively higher magnification showing the broken end of a MWNT yarn. Slippage occurs for large bundles (~ 130 nm in diameter, containing about a hundred MWNTs). Very small bundles or individual CNTs break rather than slip (as evidenced by the high density of CNT ends seen in the highest magnification above micrograph).

1.5. CNT Yarn Fabrication and Evaluation

A final shipment of 25-ply carbon nanotube yarns was provided to 3TEX from UTD. The total length of the shipment was measured to be five meters. Each 25-ply yarn was produced from singles which were then plied with four others to make 5-ply yarns. Five of these yarns were then plied together to create the final product. To monitor the progress of yarn development at UTD the yarns were compared to 25-ply yarns that were received in the previous year. Tensile testing of the 25-ply yarn was conducted by 3TEX on an Instron tensile tester with a 5N load cell. These tests showed almost identical breaking load and elongation at failure as compared to a sample saved from the previous year. The yarns were also viewed in a SEM to compare the physical morphology of the yarns.

Figs. 1.12-1.14 show images of the newest 25-ply CNT yarns. These images reveal that the level of twist in the yarns and plies was comparable to the previous plied CNT yarn samples. Interestingly, the uniformity of the single yarns within the plies is still low.

Fig. 1.12 shows the large range of yarn diameters present.

Fig. 1.14 shows a side by side view of the new yarn on the left and the previously studied yarn on the right. Their evident almost identical morphology explains the closeness in the measured mechanical characteristics of the " new" and "old" CNT yarn samples.

Figure 1.12. SEM image of the "new" 25-ply CNT showing non-uniformity of single CNT yarns.

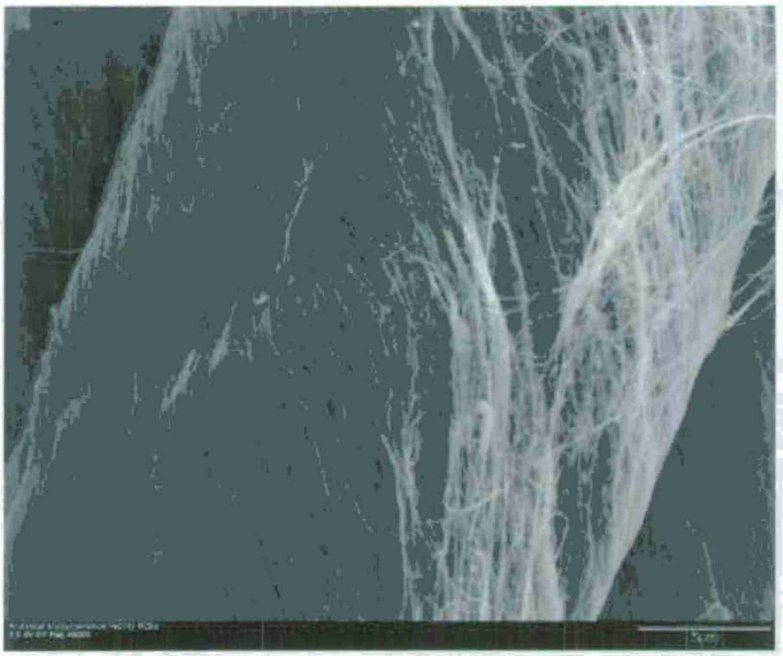

Figure 1.13. Close up SEM image of a single CNT yarn showing the twist orientation of the CNT bundles.

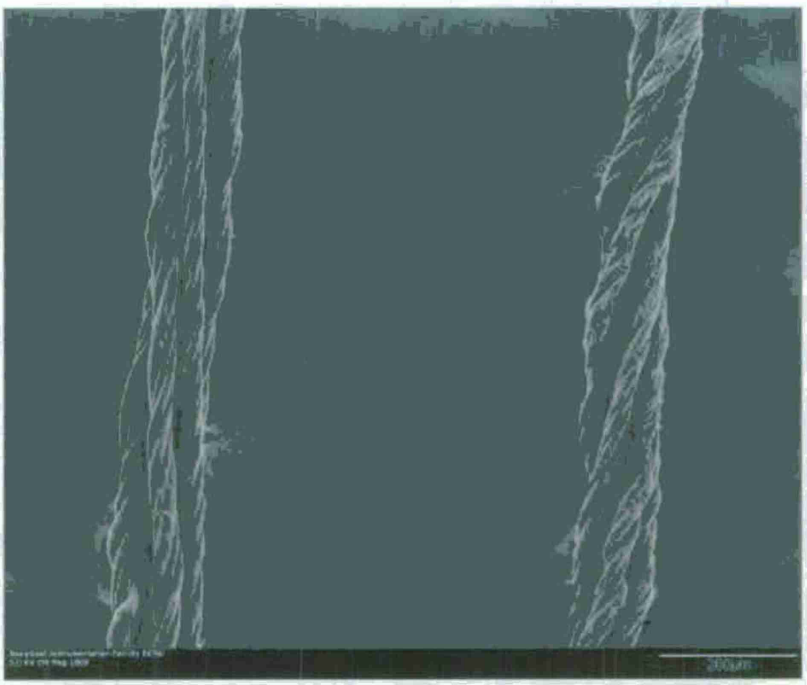

Figure 1.14. Side by side SEM images of the "new" 25-ply yarn (left) and "old" 25-ply yarn (right).

SECTION 2

2.1. Synthesis and Characterization of Multi-Wall Carbon Nanotube Forests

2.1. Introduction

The synthesis of carbon nanotube forests is the key for solid-state fabrication of carbon nanotube yarns. Processability and the properties of resulting yarns strongly depend on nanotube length and morphologies of nanotubes in the forests. One of the important project goals is to synthesize drawable carbon nanotube (CNT) forests having longer nanotube length, smaller diameter, and fewer number of walls in MWNTs.

UTD personnel has successfully fabricated drawable forest using single layer Fe film as catalyst and acetylene gas as carbon source. However, the maximum height of the forests using this approach is only about 500 micron. Recently, several groups reported growth of millimeter high vertically-aligned CNTs using Fe/Al_2O_3 film in C_2H_4, see [24-27]. Table 2.1 summarizes their synthesis conditions and the best results. Currently, the UTD group efforts are focused on synthesis of CNT forests over a millimeter high by leveraging the information listed in Table 2.1, and the simultaneous maintenance of small nanotube diameters.

Table 2.1. Summary of conditions determined for synthesizing millimeter high CNT forests from the recent literature.

Reference	Substrate Si SiO_2/Al_2O_3 (nm)	Catalyst Fe (nm)	Tube furnace Dia. (inch)	Gas (sccm) He or Ar	H_2	C_2H_4	Water ppm	Temp. °C	Best height (mm)	Height (mm) in 15 min	Tubes	Dia. (nm)
1 and 2	600/10	1	1	600	400	100	100	750	2.5 in 10 min	0.9	SWNT or DWNT	2 ~ 3
3	?/10	1	1	115	80	15	250	750	7 in 12 hr.	0.6	DWNT	10
4	500/15	2	1.5	350	200	150	775	750	0.4 in 5 min		DWNT or TWNT	10
5	0/20	1.2	1	200	500	100	0	750	1.8 in 1 hr.	0.9	MWNT	9
6	1000/10	1	1	94	6	100	0	750	3 in 1.5 hr.	0.8	MWNT	10
7	500/?	2	2	0	200	200	200sccm Ar	750	2		MWNT	15

UTD conducted a systematic study of CNT forest growth using a Fe/Al_2O_3 catalyst deposited by e-beam evaporation, and demonstrated uniform, and conformal, growth of over millimeter high CNT forests by atmospheric-pressure thermal chemical vapor deposition (CVD). The height of CNT forest grown was increased from 0.5 mm to ~1.7 mm using the newly developed CVD process.

2.2. Materials

The substrates are plain (100) silicon wafers (p-type, 725 μm thickness, Silicon Quest International). The buffer layer Al or Al_2O_3 and catalyst Fe are deposited on Si wafer by e-beam evaporation using a Temescal BJD-1800, with a Inficon XTM film deposition controller. A catalyst film of 11 nm Al_2O_3 and 1.2 nm Fe is deposited by e-beam evaporation in a single pump-down cycle. The Al_2O_3 is deposited by direct evaporation from a crucible of high-purity

crystals, rather than by evaporation of Al with a slight background pressure of O_2, or by other methods such as spin-coating of a sol–gel precursor. In the case of Al/Fe, the film of Al is deposited first, and then oxidized naturally in air before depositing Fe film. After catalyst deposition, no further cleaning or dedicated oxidation is necessary prior to nanotube growth. The catalysts used in this report are listed in Table 2.2. The change in thicknesses both for buffer layer and catalyst was aimed for the investigation of their effects to CNT forest growth. During CVD process, substrates with all 6 types of catalysts were placed side by side inside the furnace.

Table 2.2. List of Catalysts Used.

Table 2. Catalysts

	Buffer layer / Catalyst	Thickness (nm)
Cat 1	Al / Fe	10 / 3.5
Cat 2	Al / Fe	10 / 2.2
Cat 3	Al / Fe	>10 / 2.2
Cat 4	Al / Fe	>10 / 1.5
Cat 5	Al / Fe	5.5 / 1.5
Cat 6	Al2O3 /Fe	11 / 1.2

2.3. CVD Procedure

CNT forest growth is performed in a conventional three-zone atmospheric pressure quartz tube furnace, with a 6.8-cm inner diameter and a 50-cm long heating zone. Flows of helium (He, 99.999%), ethylene (C_2H_4, 99.95%), and hydrogen (H_2, 99.999%) are controlled using mass flow controller. After loading the substrates in the tube, the chamber is pumped and filled with He to atmospheric pressure. Next, the furnace temperature is ramped linearly to the set point temperature with a flow of 700 sccm He. Then the reactant gases are introduced during the growth period, which is typically 15 min. A constant 700 sccm He flow is maintained for displacing the growth gases from the quartz tube and for furnace cool-down.

2.4. CNT Forest Characterization

The height of the forest was measured using a 100x optical microscope. Scanning electron microscopy (SEM) of as-grown samples was also performed using a LEO 1530 VP in high-vacuum mode at 15 keV. The samples were also characterized by high-resolution transmission electron microscopy (TEM) using a JEM-2100F at 200 keV with samples pulled directly from the forest and fixed on a holey carbon grid.

2.5. CNT Forest Growth

From Table 2.1 we can see that most of the researchers use 1 inch diameter quartz tube and 750°C process temperature; and water is not very critical for growing millimeter high forest. The big differences in growth conditions among the research groups are the total gas flow rate and gas composition. Therefore, first of all in our experiments, we investigated the effects of gas composition and then the relationship between the forest height and reaction times. Because

substrates with all 6 types of catalysts are used in all CVD processes, the effects of catalysts on CNT growth are also investigated.

To evaluate the effect of gas composition on CNT growth, experiments were conducted using ~1x1 cm samples at 750°C for 15 min. The total gas flow of 1000 sccm and the C_2H_4 flow rate of 100 sccm are fixed. The ratio of H_2 in the gas phase is changed by varying the flow rates of H_2 and He. Failure of CNT growth occurs from the process without H_2. Fig. 2.1 shows the dependence of CNT height on the partial flow rate of H_2 using different catalysts. Generally, H_2 can increase the activity of the metal catalyst for cracking hydrocarbons. It can also clean the catalytic surface by etching polycyclic hydrocarbon species, which tend to encapsulate metal surfaces. Reduction of the catalyst to metallic Fe by H_2 might improve CNT nucleation, but prolonged treatment with H_2 might suppress growth, thereby engendering sintering of metal particles or altering metal–support interactions. The optimized H_2 flow rate is related to carbon source gas and catalysts.

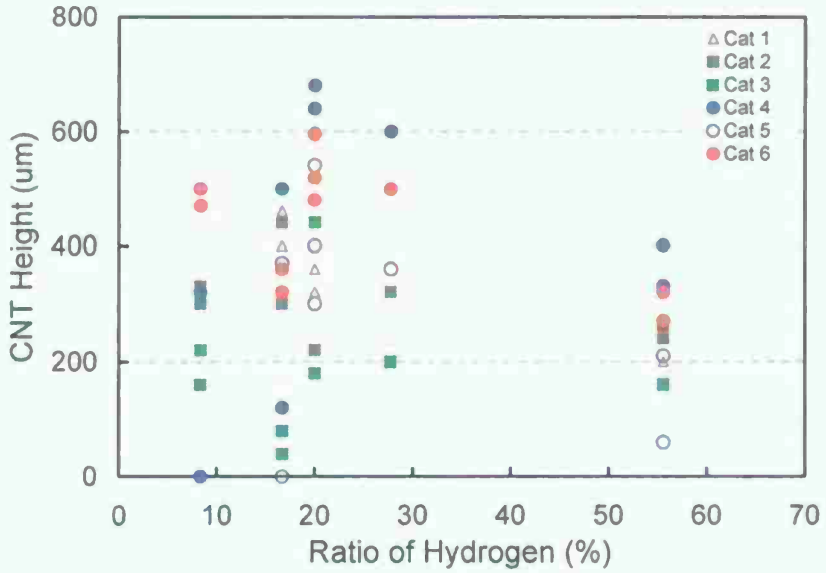

Figure 2.1. Dependence of CNT height on the ratio of the flow rate of H_2 to the total flow rate using different catalysts.

Fig. 2.2 shows the dependence of CNT height on growth time using different catalysts. The highest CNT forest achieved is about 1.7 mm high, using Cat 4 (see Table 2.2) substrate. In the experiments, the H_2 flow rate is maintained at 20% of the total flow rate. Increase of CNT height was achieved for the samples with longer growth time (close to 1 hr) using Cat 4, Cat 5, and Cat 6. Without water and at low H_2 flow rate, the catalyst nanoparticles are still active after one hour CVD growth, which is an important milestone and provides a high possibility for growing longer CNTs.

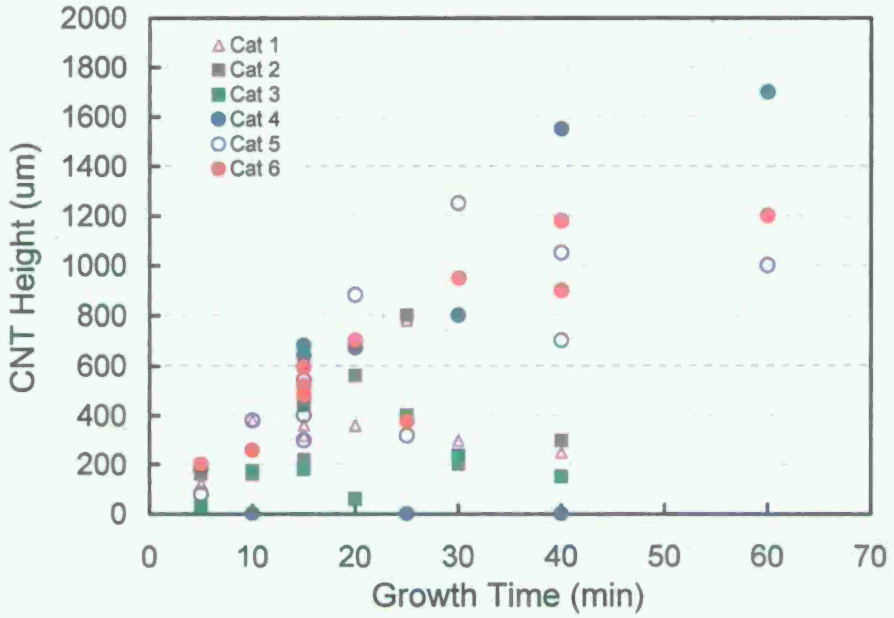

Figure 2.2. Dependence of CNT height on growth time with different catalysts from Table 2.2.

Images of the over millimeter long aligned CNTs are shown in Fig. 2.3. The largest substrate used is less than 3cm x 3cm, however, there are no major obstacles to growing uniform and high CNT forest over lager substrates.

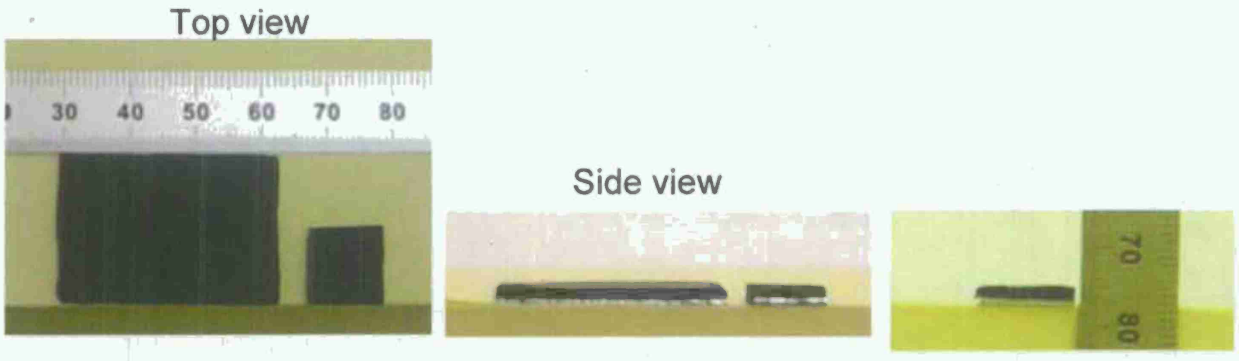

Figure 2.3. Images of the over millimeter long aligned CNT forests.

TEM image of the 700 μm long CNTs grown on Cat 1 are shown in Fig. 2.4. Nanotubes with 2 to 5 walls have been observed. It is clear that tubes made by our new ethylene process have fewer walls than the tubes made by the acetylene process. SEM images in Fig. 2.5 show that the tubes in the high forest are aligned well and form small bundles. Up to now, centimeter long CNT yarn was drawn from some of the high forests, however, continuous drawing have not been achieved yet.

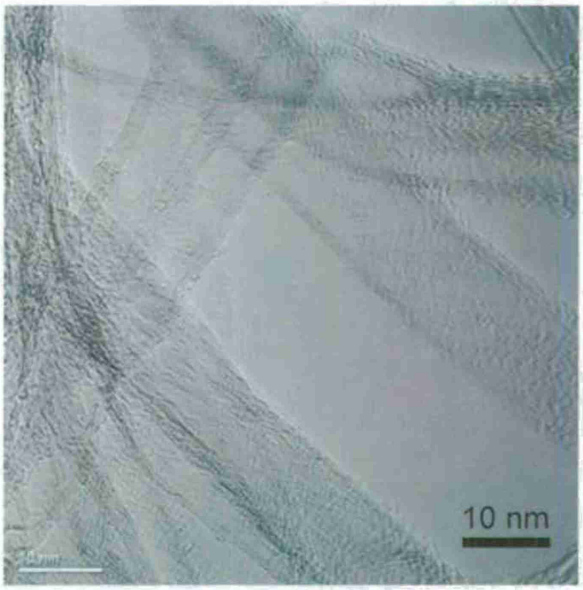

Figure 2.4. TEM image of CNTs grown on Cat 1.

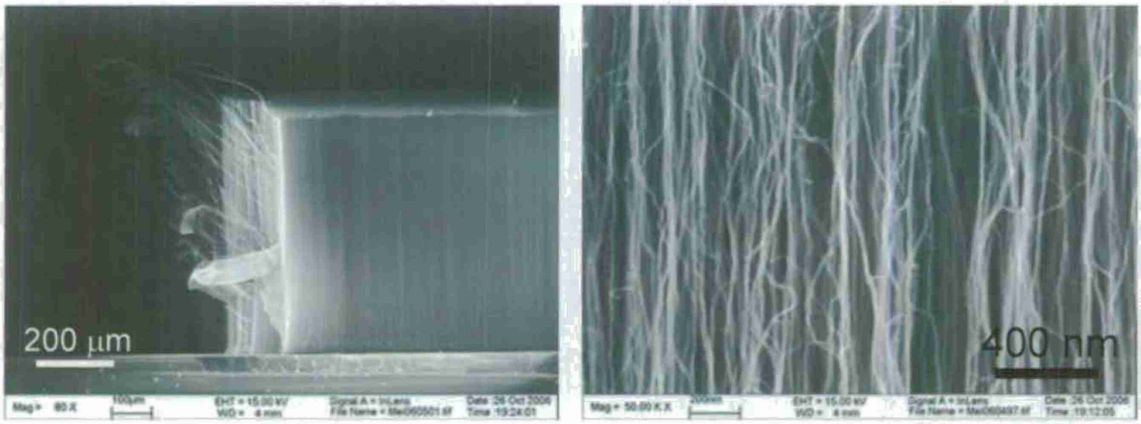

Figure 2.5. A low-magnification SEM image of the 700 μm high CNT forest grown on Cat 6 for 15 min. Small CNT bundles are being teased out from the sidewall of the forest (Left). A high-magnification SEM image of nanotubes in forest (Right).

2.6. Preliminary Conclusions: Effects of Catalyst and Other Growth Conditions

The process using Fe-coated bare Si substrates produces only sparse tangled, non-aligned CNTs. Aligned CNTs were only obtained using Fe/Al and Fe/Al_2O_3 substrates. However, as shown in Figs. 2.1 and 2.2, different thicknesses of Fe/Al and Fe/Al_2O_3 catalysts give very different growth rates and lifetime of catalyst under the same CVD conditions. It is clear that synergy between the metal catalyst and the supporting material is critical for efficient and high-yield CVD growth process.

Although we have successfully grown CNT forests that are nearly millimeters high using our new process, the growth conditions are yet to be optimized. Balancing the relative levels of

ethylene, H_2, temperature, combination of substrate as well as catalysts, is crucial for achieving super-long aligned CNTs. The work performed in this direction and obtained results are described next.

2.7. Further Studies of Nanotube Forest Growth

Further efforts have been made to investigate the growth conditions for synthesis of CNT forests. The conditions investigated included total gas flow, ratio of He or C_2H_4 in gas phase, reaction temperature, temperature ramp-up time, and catalysts. Another focus is on growing uniform forest on larger substrates, which is very important for increasing production capacity of CNT yarns. The gases used were He as carrier gas, C_2H_4 as carbon source gas, and H_2 as "helper". The substrate is silicon and the reactor is a 3" quartz tube. The forest synthesis time was 15 min. The catalysts used in this report are listed in Table 2.3 for reference.

Table 2.3. Catalysts used in this stage of nanotube forest growth study.

	Buffer Layer / Catalyst	Thickness (nm)
Cat 1	Al / Fe	10 / 3.5
Cat 2	Al / Fe	10 / 2.2
Cat 3	Al / Fe	>10 / 2.2
Cat 4	Al / Fe	>10 / 1.5
Cat 5	Al / Fe	5.5 / 1.5
Cat 6	Al_2O_3 / Fe	11 /1.2

2.8. The Effect of Gas Ratio

The total gas flow rate is a crucial factor in CNT forest synthesis because it affects the gas residue time inside the reactor, the ratio of reactant gases, and the temperature distribution in the reactor. To investigate the effects of gas flow rate, the temperature was maintained at 760°C, the total flow rate was varied between 900 and 1200 sccm, while the flow rate of carrier gas He was varied from 300 to 1020 sccm. Fig. 2.6 (left) shows the height of the forest versus the ratio of He flow rate. The optimal carrier gas percentage in the gas phase for forest growth is about 70 %.

Besides the total flow rate, the percentage of carbon source gas also has significant impact on CNT growth. In the conducted experiments, the total flow rate was maintained at 1000 or 1020 sccm and the flow rate of C_2H_4 was varied from 68 sccm to 110 sccm. The dependence of forest height on the ratio of C_2H_4 is shown in Fig. 2.6 (right). A carbon source gas in the gas phase of 10 % or less (depending upon the catalyst) seems to be best for forest height optimization.

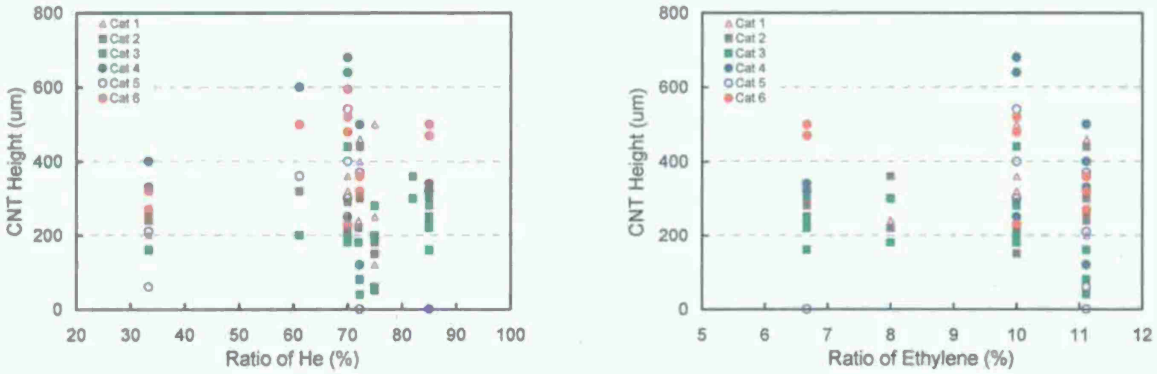

Figure 2.6. The relationship between the forest height and the ratio of carrier gas and carbon source gas in gas phase.

2.9. The Effect of Temperature

Reaction temperature influences the growth of CNT forest because the reactivity of the catalysts and the gas decomposition rate are strongly related to the temperature. In this report period, we only explored a narrow range from 740 to 780°C. As shown in Fig. 2.7, forest height increases as reaction temperature increases for every kind of catalyst investigated.

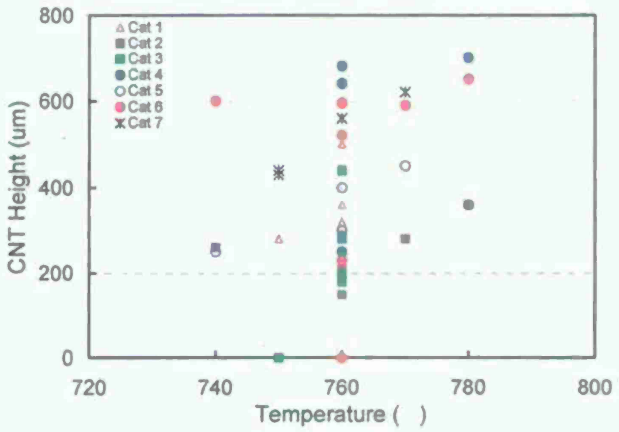

Figure 2.7. The forest height dependence on temperature.

2.10. The Effect of Temperature Ramp-up Time

Due to there are no post treatments to the substrate after catalyst films are prepared, the catalyst particles are formed during temperature ramp-up and before CNT growth. The purpose of this particular experiment is to investigate whether the formation of catalyst particles and its reactivity depends on ramp-up time. The ramp-up time was varied from 17 to 33 min. 17 min is the maximum ramp-up capability of the furnace plus temperature overshot time. As shown in Figure 2.8, the ramp-up time does not have significant impact on the growth of CNT forest. This

is important conclusion, which allows us to use the shortest ramp-up time; it saves both time and energy.

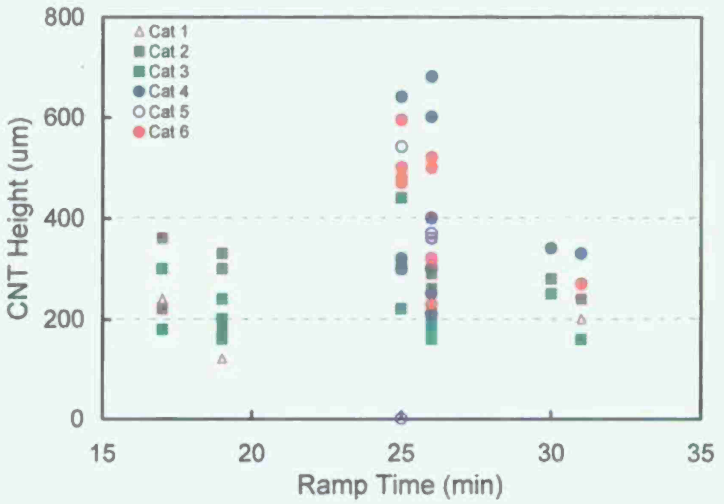

Figure 2.8. The height of forest vs. temperature ramp-up time.

2.11. The Effect of Catalyst

Catalyst is another important parameter for CNT forest growth. The effects of the catalysts revealed earlier can be seen in Figures 2.1 and 2.2. In some cases, catalyst could be a critical factor. Fig. 2.9 shows a photo image of the Si substrates with different catalysts after a CVD growth process, in which two of the substrates had almost no CNT growth in this CVD run. However, the same two substrates achieved very good CNT growth in other CVD growth conditions. For different catalysts, it is clear that other synthesis conditions (gases, temperature, etc.) must be collectively adjusted for achieving best results.

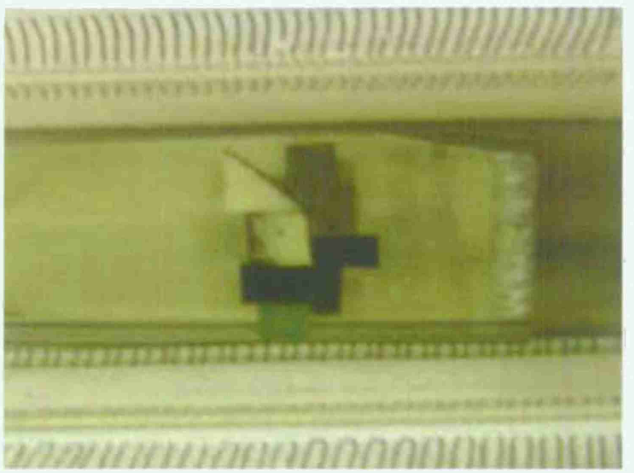

Figure 2.9. A photo image of the substrates with different catalysts in the reactor after a CVD run. There are eight substrates with eight different combinations of catalysts. Only three of them (black) had very good nanotube forest growth in this run.

2.12. The Effect of Substrate Size

Several experiments were carried out on substrates with size of 6 cm x 8 cm. The CVD process was kept under identical conditions. We got uniform growth on the whole substrate. We also got partial growth sometimes. The reliability and repeatability of the process is still a challenge, which contributes to the relatively large data distributions in Figs. 2.1, 2.2 and 2.6-2.8 presented above.

Further research devoted to the exploration of CNT forest synthesis and investigation of the morphologies of the forests and nanotubes is described next. In most of the published papers on CNT synthesis using C_2H_4 as carbon source gas, the substrates used are silicon wafers covered with a few hundred nanometers or a few micrometer thick silicon dioxide. The function of the silicon dioxide layer has not been well understood. In this report period, we tried to better understand the impacts of the buffer layers, SiO_2 as well as Al_2O_3. The structure and morphology of nanotubes was characterized by TEM, and the relationship of the CNT area density and the drawability was explored.

2.13. Effects of Buffer Layers

Table 2.4 shows list of substrates with various configurations of SiO_2, Al_2O_3 and Fe layers experimented in this report period. The 500 nm thick SiO_2 layer was thermally formed on the silicon wafer, while Al_2O_3 and Fe films were coated onto the substrate by e-beam evaporation in a single pump-down cycle.

Table 2.4. Catalysts used in this stage of research.

	Thickness (nm)		
	SiO2	Al2O3	Fe
Cat 6	0	11	1.2
Cat 9	0	25	1.4
Cat 10	0	10.8	1.6
Cat 11	500	10.8	1.6
Cat 12	0	20	6.3
Cat 13	500	20	6.3

As our earlier results showed, the buffer layer (Al or Al_2O_3) and the iron film are crucial for growing CNT forests. Here, Cat 10 and Cat 11, Cat 12 and Cat 13 were used for comparison with and without SiO_2 layer. Cat 6 serves as a reference for monitoring the reliability of the process. Cat 6, 9 10 and 12 were used to investigate the effect of the alumina layer. In most of the experiments, all of the substrates listed in Table 2.4 were placed side by side inside the reaction tube furnace for CNT growth. Unless mentioned otherwise, the flow rates for He, H_2, and C_2H_4 are taken 700 sccm, 200 sccm, and 100 sccm, respectively. The forest synthesis temperature was set at 760°C and the growth time was set at 15 min.

Fig. 2.10 shows the relationships of CNT forest height with the flow rate ratio of the hydrogen in gas phase and the growth time. The CNT grown on Cat 6 (also on Cat 5) are comparable with

that of the previous results, indicating that our CVD process is well repeatable. Cat 10 has similar outcome as Cat 6. Comparing the CNT height of Cat 10 and Cat 11, and of Cat 12 and 13, it is seen that adding SiO_2 layer does not have positive effect on CNT growth. It is also more economical to use substrates without SiO_2.

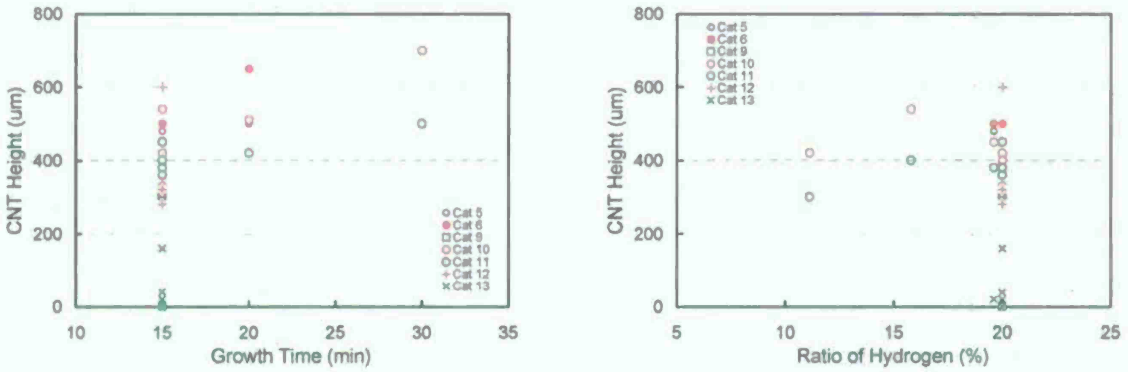

Figure 2.10. The relationship of the forest height to the flow rate ratio of hydrogen gas in gas phase (left) and growth time (right).

It is known that CNT forest cannot form without an Al_2O_3 layer, which is critical for CNT growth. Typically, the thickness of Al_2O_3 used for CNT forest synthesis is reported to be from 10 nm to 30 nm. We varied the thickness of alumina from 11 nm to 25 nm in our experiments. As shown in Fig. 2.11, it seems that increasing the thickness of Al_2O_3 layer does not benefit CNT growth rate. However, the impact of alumina layer on the morphology of CNT forest is presently unclear.

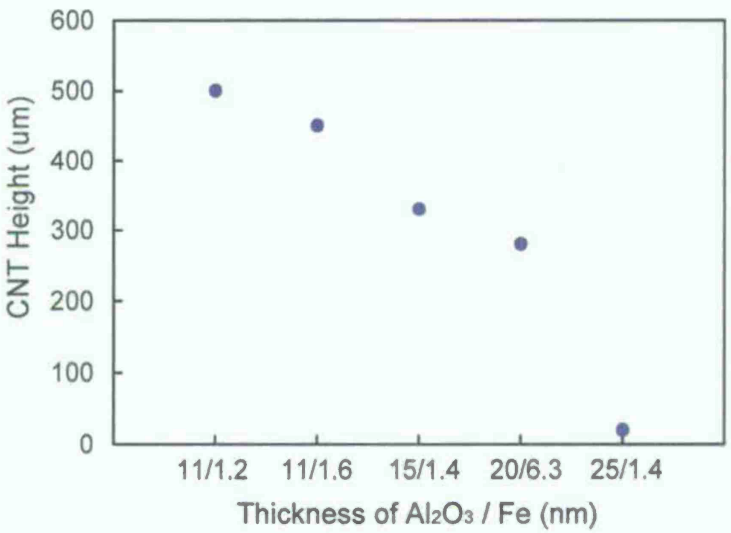

Figure 2.11. Dependence of CNT forest height on the total thickness of alumina and iron layers.

2.14. Structure and Morphology of the Nanotubes

Several typical CNT samples were characterized by high-resolution transmission electron microscopy (TEM) using a JEM-2100F at 200 keV. Samples were collected directly from the forest and loaded onto a holey carbon grid. Fig. 2.12 shows the TEM images of the tubes grown on substrate Cat 6 for 15 min. We observed that most of the tubes are double-walled carbon nanotubes with the diameter close to 10 nm and that many tubes have open ends. The tubes tend to collapse and flex due to a larger inner wall diameter and fewer walls.

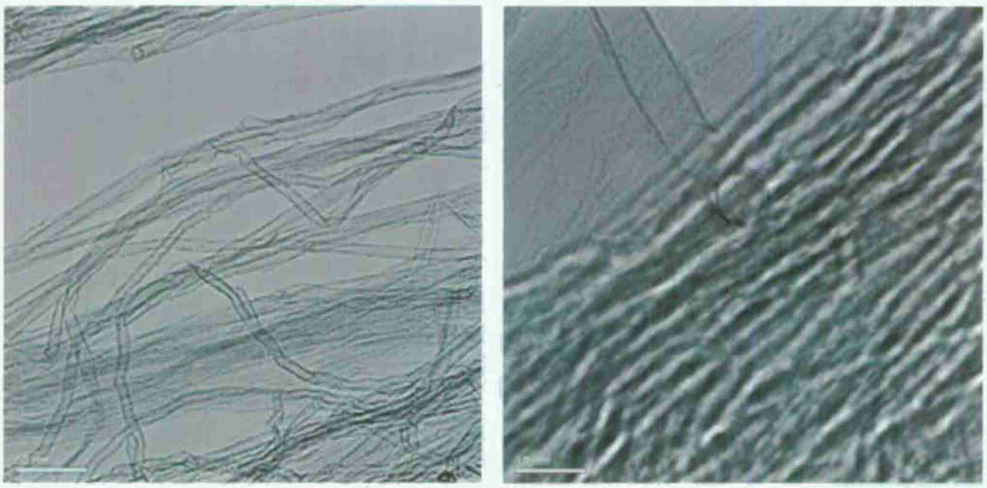

Figure 2.12. TEM images of the nanotubes grown on substrate Cat 6 for 15 min.

Fig. 2.13 further shows the structure of the nanotubes grown on substrate Cat 6 for 30 min. Although the catalyst layer has the same configuration, the tubes shown in Fig. 2.13 have more walls and thicker amorphous carbon deposit on the outside wall of the tubes. Amorphous carbon formed on nanotubes is likely due to extended growth time. Thick a-C deposited on tubes could lock the structure of the tube network, which makes the forest undrawable. More TEM observations are needed to study the relations of nanotube morphology with different catalyst configurations and synthesis conditions.

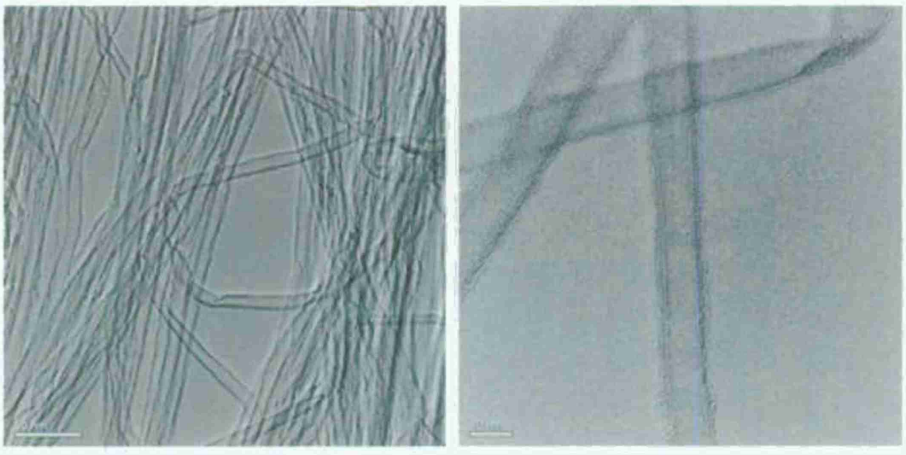

Figure 2.13. TEM images of the nanotubes grown on substrate Cat 6 for 30 min.

2.15. Concluding Remarks: Drawability of the CNT Forest

We believe that the key factors that affect the drawability of CNT forests are the purity of the nanotubes, the height of the forest, the morphology of the forest (especially the 3D network formed by self-assembly during CVD growth), and the area density of the nanotubes. Among these factors, area density (number of nanotubes grown per square centimeter of substrate) plays a very important role. As illustrated in Fig. 2.14, carbon nanotubes start to form forest when the tube area density surpasses a critical value. Drawable forest must have a sufficiently high areal density of CNTs to form intimate interactions in the forest. The value of the area density of the drawable forests is related to the tube diameter.

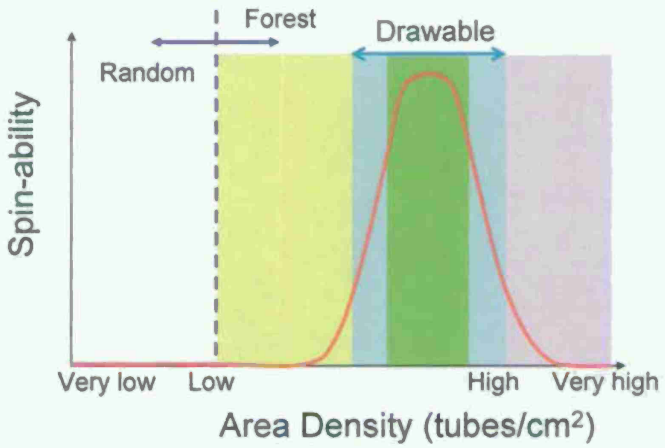

Figure 2.14. Illustration of the relationship between the forest drawability and CNT area density.

Experimentally the area density of CNT forest is determined from counting the roots of the tubes on the substrate after removing the forest. Fig. 2.15 shows the surface of the substrates after removing undrawable (left) and drawable (right) forests, where both forests were prepared by C_2H_2 process. It was found that the area density of undrawable forest is around $10^{10}/cm^2$, while the area density of well drawable forest is $\sim 10^{11}/cm^2$.

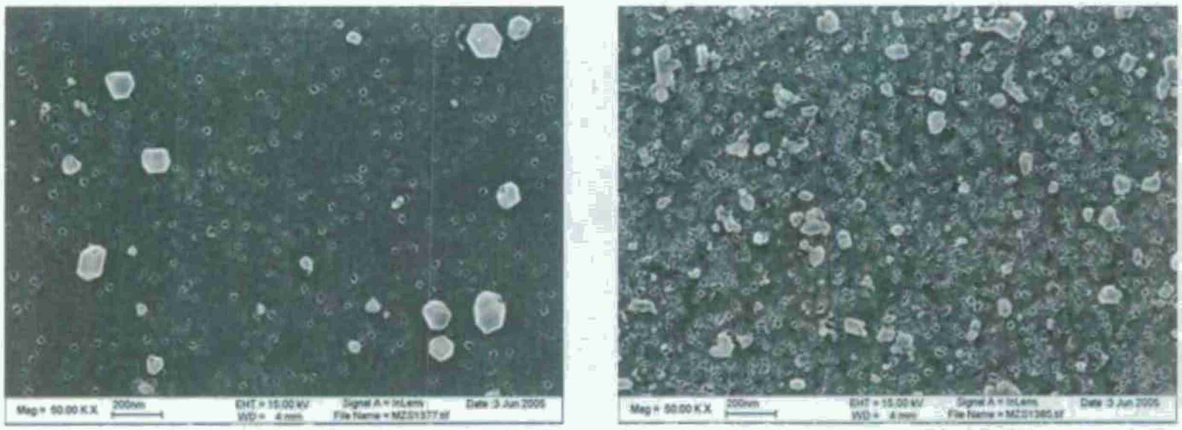

Figure 2.15. The surfaces of the substrates after removing the forests synthesized using C_2H_2, undrawable forest (left) and well drawable forest (right).

Fig. 2.16 shows the typical surfaces of the substrates after removing forests made by C_2H_4 process. The image on the right in Fig. 2.16 corresponds to a drawable forest. The drawability is not as good in the case of the left image in Fig. 2.16. Comparing Figs. 2.16 and 2.15, we can see that the size of the tubes in Fig. 2.16 is smaller, and the area density is still not dense enough for continuous drawing.

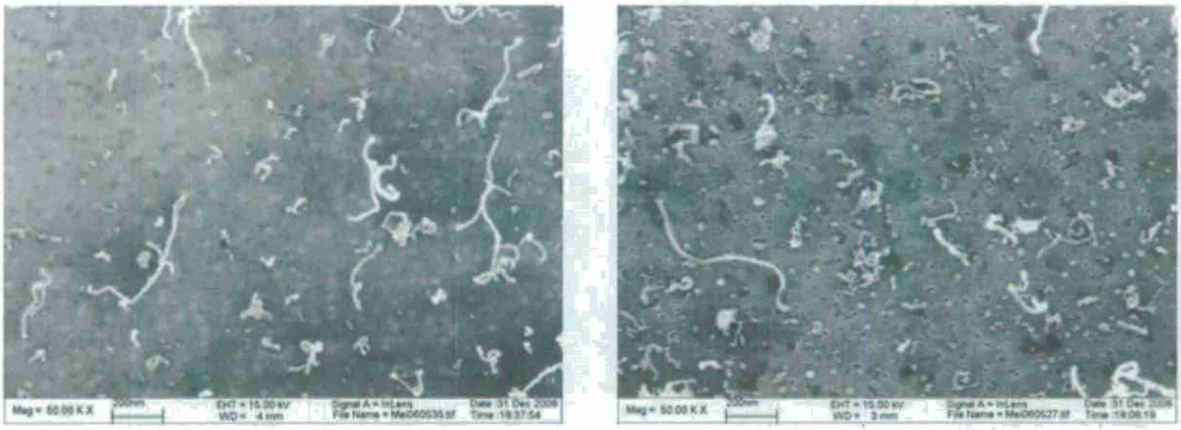

Figure 2.16. The surfaces of the forests synthesized using C_2H_4, undrawable forest (left) and drawable forest (right).

SECTION 3

Infiltration of Binding Polymers in Carbon Nanotube Yarns and Its Effect on Mechanical Properties

3.1. Introduction

Though major advances have been made on the fabrication of nanotube yarns, no one is yet able to assemble carbon nanotubes into yarns and composite structures that retain the spectacular properties of the individual nanotubes: (i) over a ten-fold higher strength than existing yarns, (ii) a higher thermal conductivity than diamond, (iii) a thousand-fold higher current carrying capability than copper, and other fascinating and useful properties for active devices.

There are generic problems with using any technology involving nanotube dispersion in a liquid for making nanotube yarns or composites that are most useful for active, high performance devices. *First*, the ability to disperse nanotubes into a liquid and to fabricate oriented nanotube yarns from liquid dispersions decreases with increasing nanotube length. This is a problem since the properties of the individual nanotubes cannot be retained in indefinitely long nanotube yarns unless the component nanotubes are quite long. *Second,* simultaneously assembling a polymer binder and nanotubes during yarn formation degrades electrical and thermal transport by interrupting electronic and phononic pathways between carbon nanotubes. While this polymer binder can be added as a post-fabrication treatment for solution-fabricated yarns to avoid this problem, the polymer binders needed to provide high strength for short solution-processable nanotubes are often not those that provide the desired multi-functionality.

Enhancing the inter-tube binding (interaction) is a promising route to utilize the spectacular mechanical properties of individual carbon nanotubes. The previous work of UTD showed that the mechanical properties of twisted yarns can be increased by infiltration of polyvinyl alcohol (PVA). MWNT/PVA impregnated yarns were made either by soaking a single yarn for 15 hours in 5 wt% aqueous PVA solution or by passing a single yarn through a drop of this solution during spinning, and then drying in air. The molecular weight of the PVA was in the range 77000 – 79000, and it was 99.0-99.8% hydrolyzed.

The studies performed earlier in this project led to several conclusions. The PVA infiltration results indicate that infiltration conditions play very important role in the resulting mechanical properties of the investigated yarns. The ideal case is to use PVA to serve as an inter-tube binding media and limit excessive PVA filling of the void space in the twisted-spun yarns. The current infiltration conditions are still far from being optimized. The SEM images included in that report show excessive PVA infiltration (PVA beads) along the yarn and PVA shell structure formation owed to a very high concentration of PVA solution. The PVA beads and shell

structures do not provide mechanical improvement to the infiltrated yarns, while decreasing yarn's gravimetric strength.

In the follow-on experiment reported here, we tried to eliminate excessive PVA infiltration using lower concentration PVA solutions and also tried to optimize tension conditions to further improve the mechanical properties of PVA infiltrated nanotube yarns. Also, infiltration experiments with an organic solvent-based solution: polystyrene (PS)/chloroform, has been conducted. Finally, the third polymer, namely poly(p-phenylene benzobisoxazole) (PBO), which is a member of the polybenzoxazole class of polymers, one of the various types of highly heat resistant polyheteroarylenes, has been infiltrated into carbon nanotube yarns, and the results of that were investigated.

3.2. New Studies of PVA Infiltration

In the earlier study PVA infiltration of CNT yarns was arranged so that the yarns were under tension during the infiltration. This was achieved by attaching a small weight to one end of a ~8 cm length of yarn (with silver paint), attaching the other end (with sticky tape) to a wire support, and then lowering the whole yarn into a conical flask of PVA solution (as illustrated in Fig. 3.1). The weights were made from half a standard paper staple, having masses on the order of 15 mg (in air, these would produce tensile stresses of about 1.5 MPa in the yarns, which is well below 1% of the yarns' typical breaking stresses).

In the later work, we have experimented with another low tension approach. Here, a ~10 cm length of yarn was suspended – from both ends – off a wire support frame (the yarn affixed with silver paint). The frame's support spacing was only ~8 cm, and thus the yarns were allowed to droop, loosely, meaning that they would experience the tension from only their own weight. This yarn (and wire frame) was then suspended within a dish of PVA solution for infiltration, as shown in Fig. 3.2. A piece of yarn is attached to the ends of a wire support (the vertical sections of wire), and lowered into a dish of PVA solution. The length of yarn is longer than the spacing of the wire support, so that it hangs loosely within the solution, receiving tension only from its own weight. The ends of the vertical wire sections extend about 5 mm into the PVA solution. Contact with the solution (infiltration time) was 2.5 hrs.

Figure 3.1. Photograph showing weight attached to the end of a MWNT yarn sample with silver paint (left). Photograph showing a conical flask full of PVA solution, on top of which there is a wire support for attaching the upper end of a yarn sample (right).

Figure 3.2. Schematic and photograph showing the mounting frame for "low-tension" infiltration of a MWNT yarn sample.

Similar to the profile of PVA infiltration at high tension, the addition of PVA at low tension can produce a large increase in tensile strength. Untreated yarns have tensile strengths of around 330 MPa, while yarns infiltrated with 5 wt% PVA solution have strengths of 800 MPa, see Fig. 3.3. From the first plot, there does not appear any significant difference in resultant yarn strength between the two infiltration methods. Neither is there any significant difference between the methods in terms of failure strain, as Fig.3.4 indicates. It may be expected that there will be some difference, since excess tension during the infiltration stage might be able to induce extra alignment of the nanotubes. However, it may happen that the actual tension experienced by these staple weights is simply too small to effect any change.

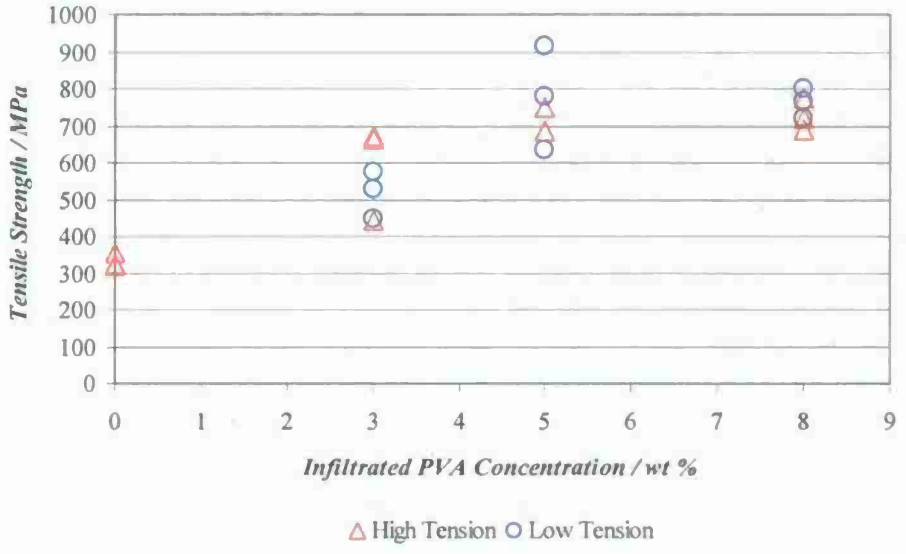

Figure 3.3. Graph showing the difference in tensile strength of thick, PVA infiltrated yarns, when infiltrated under 'high' and 'low' tension conditions. The point at 0 wt% concentration corresponds to untreated yarns.

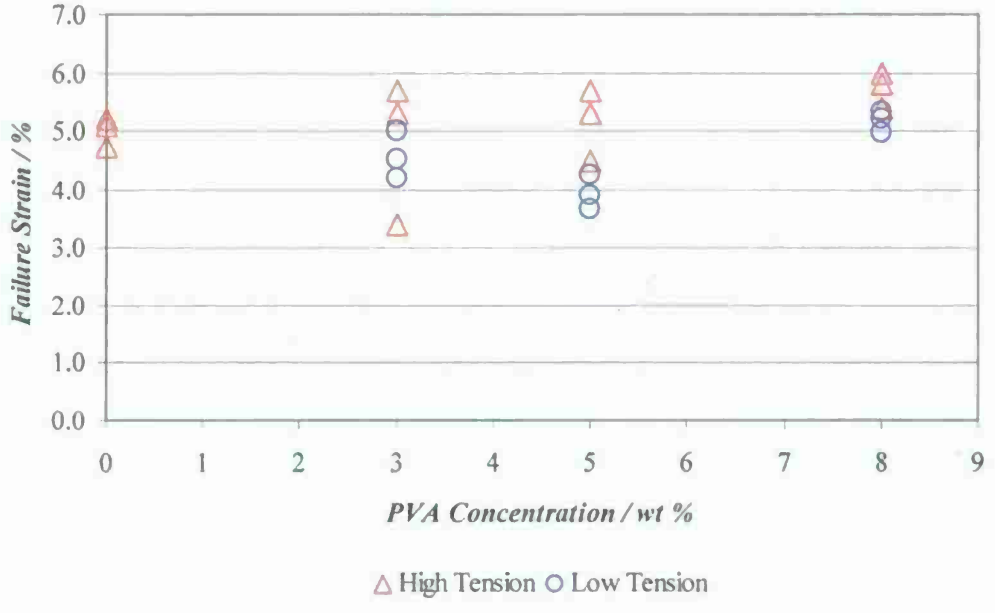

Figure 3.4. Graph showing the difference in the failure strain of thick, PVA infiltrated yarns, when infiltrated under 'high' and 'low' tension conditions. The point at 0 wt% concentration corresponds to yarn placed in water only.

3.3. Infiltration of PS/chloroform

Continuing the efforts of searching for better inter-nanotube binders, we conducted infiltration experiments with an organic solvent-based solution: polystyrene (PS)/chloroform, following PVA infiltration of nanotube yarns presented in the previous reports. It was found that PS/chloroform solutions have much lower viscosities compared to PVA/water solutions at the same polymer concentrations. This allowed us to evaluate PS infiltration up to the higher PS concentrations without encountering serious over-coating problem.

As shown in Fig. 3.5, the ultimate tensile stress of our twist-spun yarn decreases with increasing yarn diameter. One reason for that is that increasing the ratio of nanotube length to yarn circumference increases inter-nanotube binding and, consequently, leads to higher yarn strength. Another reason is that the larger the diameter, the larger the stress variation across the yarn, which results in uneven stress distribution among nanotubes and, as the result, the yarn strength decreases with increasing yarn diameter.

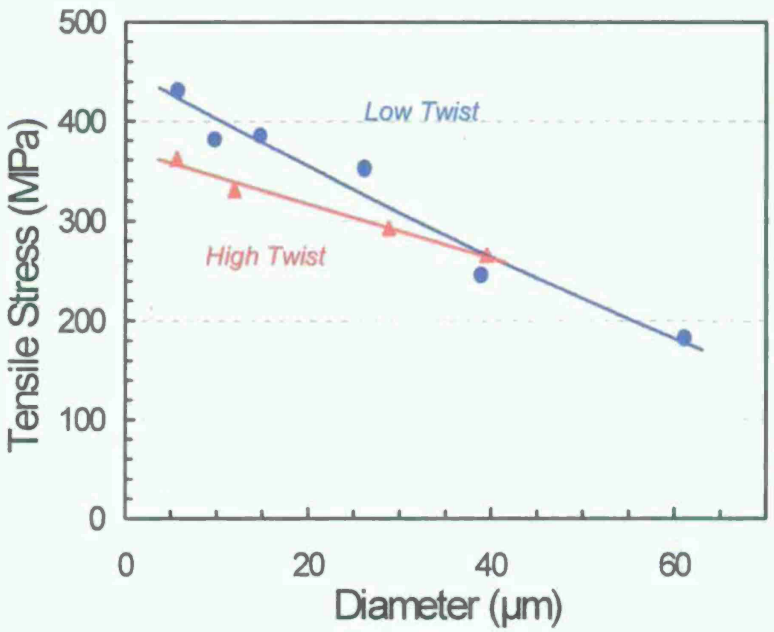

Figure 3.5. Dependence of the ultimate tensile strength as function of yarn diameter for 'low' and 'high' yarn twists.

In the new set of experiments we conducted PS infiltration using nanotube yarns with two different diameters: 12 micron (thick yarn) and 4.5 micron (thin yarn). Polystyrene granules (Arcos Organics manufactured, with a rated polystyrene molecular weight of 250 000) were dissolved into chloroform, in concentrations of 3–20 wt%. The PS/chloroform solution was stirred at room temperature until granules were no longer visible (this process usually took several hours). Smaller volumes of solution were then prepared for the PVA experiments and so

a different infiltration technique was used. Here, small lengths of yarn were mounted onto wire frames, as shown in Fig. 3.6. The left hand image shows a single frame, which is approximately 5 cm in width. The right hand image shows the bottom of this frame, magnified, displaying a single yarn threaded through two eyelets (loops). The yarn is attached to the wire frame using pieces of sticky tape, which are visible in the upper half of the right hand image.

The frames contained two spokes, joined by a handle, with eyelets formed at the ends of the spokes. Yarn was threaded through the eyelets, so as to cross the spacing between the ends of the spokes. The ends of the yarn were attached to the upper part of the frames with small pieces of sticky-tape. In initial investigations, it was found that chloroform fumes are capable of dissolving silver paint, although sticky tape remains mostly intact. The wire frames were then inserted into a small beaker, containing a shallow amount of PS solution, and left for two hours to allow for infiltration to take place.

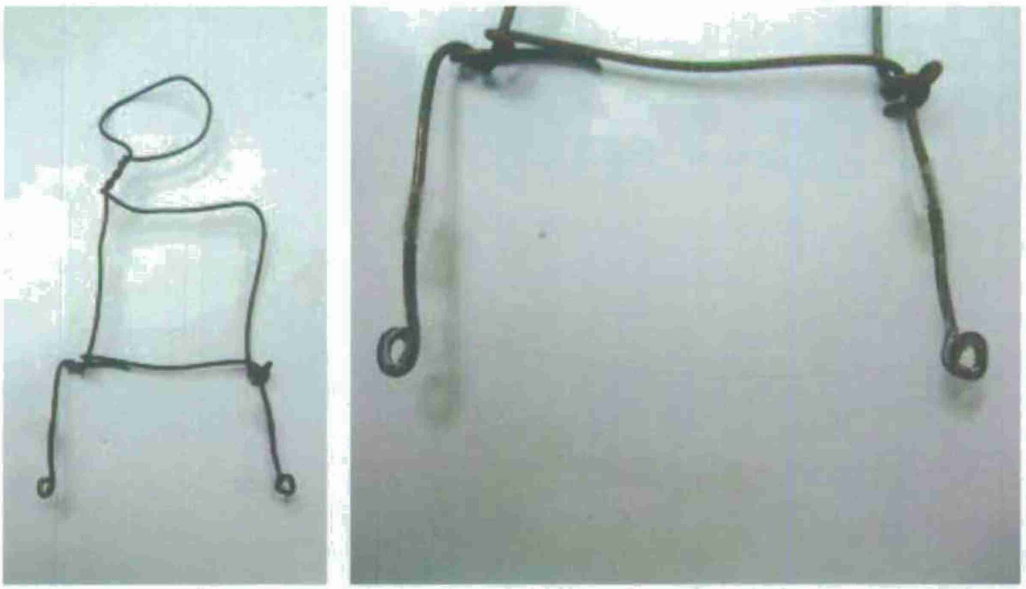

Figure 3.6. Photographs showing wire frames used to insert sections of yarn into polystyrene solution.

The process of removing the yarn introduced a problem of 'beading' - as the frame and yarn is lifted out of the polymer, the solution would tend to cling to the rising frame. After certain small height, this plume of polymer would fall back, level (under its own weight). As the surface of the polymer splits across the raised yarn, it was particularly prone to leaving small droplets along the yarn. Because the chloroform evaporates so readily, these droplets dry quickly, and it was not generally possible to remove them. However, their effect could be minimized by initially drawing only part of the yarn from the solution (i.e, by lifting the frame at an angle). The section of yarn displaying the resultant droplet features could be usually avoided when mounting the yarns for mechanical testing. Alternatively, sections showing this beading were reserved for SEM imaging only.

Each frame was large enough to support sufficient length of yarn for two mechanical testing samples. Hence, two yarn segments were infiltrated at each concentration. Yarn segments were labeled 'A' and 'B', thus producing four yarn samples: 'A1', 'A2', 'B1', 'B2'. SEM imaging was generally performed only on one sample (for example, B1). This may have led to inaccuracies in the stress calculations (if the yarn diameter varied significantly between the A and B segments). However, the relative consistency of the tensile test data suggests that any such inaccuracies were small.

If the SEM images were collected from a sample showing beading (and over-coating), then diameters had been measured from the regions of yarn between the beads. If such over-coated region of the yarn was excessively large (compared to the non over-coated region), then the measurements would produce systematic under-estimates of the yarn strength. Additionally, SEM imaging was performed on the sample with 'worst' over-coating; therefore the tested segments will likely having less over-coating, and smaller cross sections.

3.4. Thick Yarns: Tensile Test Results

Fig. 3.7 shows how the tensile strength of 'thick' polystyrene-infiltrated yarns varies with the concentration of the polymer solution. It is seen that tensile strength generally increases with concentration, reaching a maximum of around 820 ± 30 MPa, which is ~2.3 times higher than the strength of untreated yarn. At 10 wt%, the tensile strength appears 'abnormally' low; this is likely due to an over-coating problem that creates an abnormally large yarn diameter, which is clear from Fig. 3.8. At a concentration of 20 wt%, the yarn strength falls dramatically below the level for untreated yarns. This, again, is due to an over-coating issue, with the resultant yarns having diameters almost twice as large as the untreated yarns. The polystyrene solution becomes particularly viscous at this concentration, and it would seem difficult to prevent this effect.

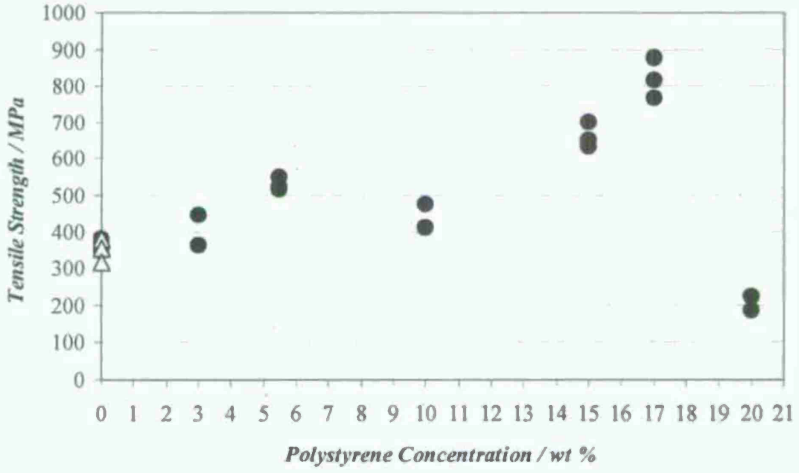

Figure 3.7. Graph showing the tensile strength of 'thick' polystyrene infiltrated MWNT yarns, as a function of the concentration of the polystyrene solution. Closed circles show yarns infiltrated with polystyrene/chloroform solution. Triangles correspond to untreated yarns.

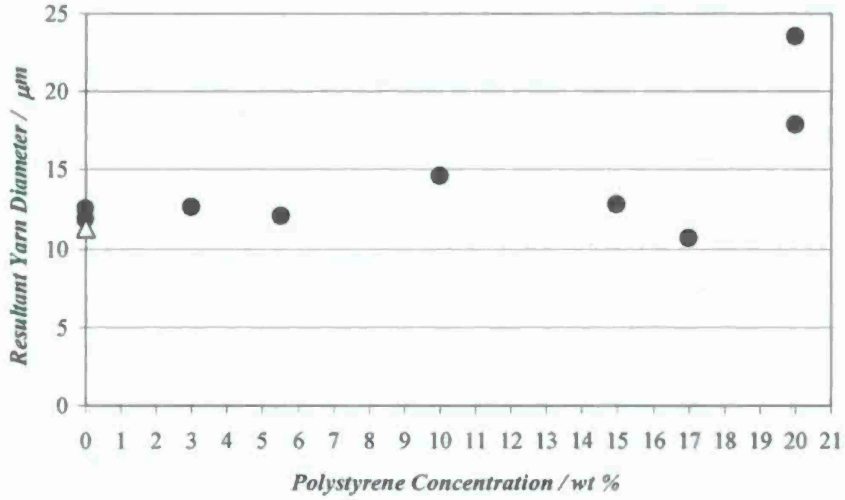

Figure 3.8. Graph showing the diameter of 'thick' dried yarns, after infiltration with polystyrene solutions of various concentrations. Closed circles represent yarns infiltrated with polystyrene/chloroform solution. Triangles indicate the diameter of untreated yarns.

In the case of PVA infiltrated yarns over-coating can be removed by physically wiping excess polymer from the treated yarn before drying. Contrary to that, the chloroform solvent used in the polystyrene preparation evaporates too quickly and it is difficult to remove any lumps from the coating. Particularly large over-coating lumps are visible in Fig. 3.9, which is an SEM micrograph of a 15 wt% polystyrene-infiltrated yarn.

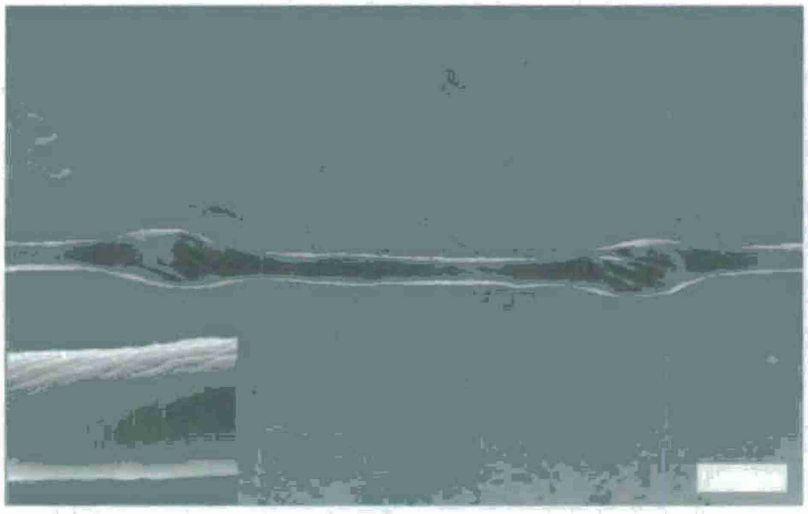

Figure 3.9. SEM micrograph of a 'thick' MWNT yarn infiltrated with 15 wt% polystyrene solution. The scale bar is 40 μm long. The insert image shows an enlarged portion of the yarn. Twist and individual nanotube bundles are still visible, suggesting that there is minimal over-coating outside of the 'lump' areas.

Fig. 3.10 shows a similar yarn, but after infiltration of 5 wt% polystyrene. The periodic, 'lumpy' over-coating is still present, but the lumps are much thinner than in the previous case.

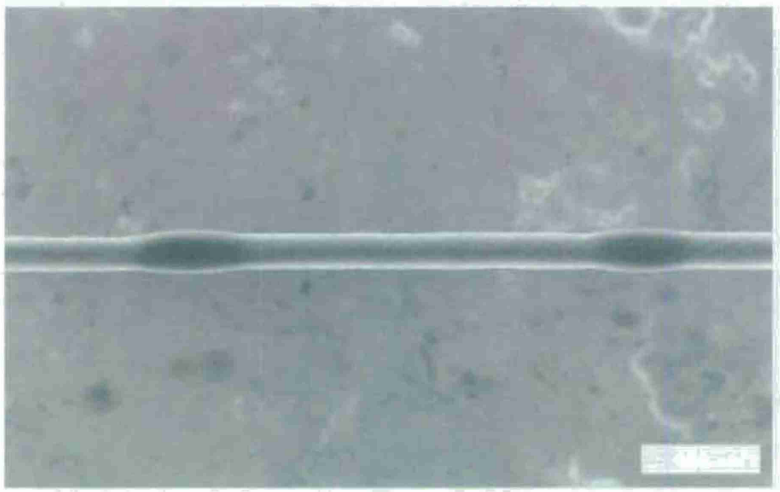

Figure 3.10. SEM micrograph showing a portion of thick yarn, after infiltration with 5 wt% polystyrene solution. The scale bar is 40 μm long.

Fig. 3.11 shows strain to failure variations for thick yarns after infiltration with increasing concentrations of polystyrene solution. The strain to failure value is approximately (5.2 ± 0.2) % for 0 wt% (i.e., for yarns dipped in chloroform only). The strain to failure then decreases slightly, as the polystyrene concentration is increased. Above 10 wt% its value is only about 3-4 %. In general, infiltration appears to make the yarn "less ductile". Interestingly, exactly the same effect has been observed when infusing nanotube yarns and braids with epoxy resins, as will be discussed further in report.

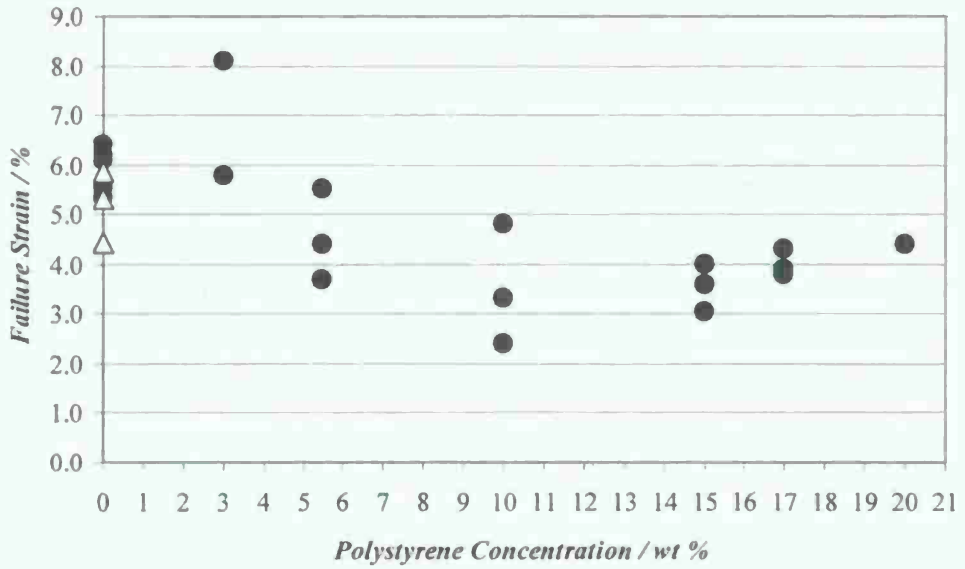

Figure 3.11. Graph showing the failure strain of 'thick' MWNT yarns as a function of the concentration of infiltrated polystyrene solution (closed circles). Triangles correspond to untreated yarns.

3.5. Thin Yarn: Tensile Test Results

Fig. 3.12 shows variation of tensile strength of 'thin' polystyrene-infiltrated yarns. Similarly to the thick yarns, the addition of polystyrene leads to an increase in yarn tensile strength. After infiltration with 10 wt% polystyrene, the strength of the thin yarns reached 1.04 GPa. This corresponds to an increase of around 1.3 times, compared to the untreated thin yarns. However, this relative increase is much less than that for the 'thick' yarns reported above. This reduced effectiveness of strength increase is, possibly, due to a higher density of the thin yarn, which makes their complete polymer infiltration more difficult.

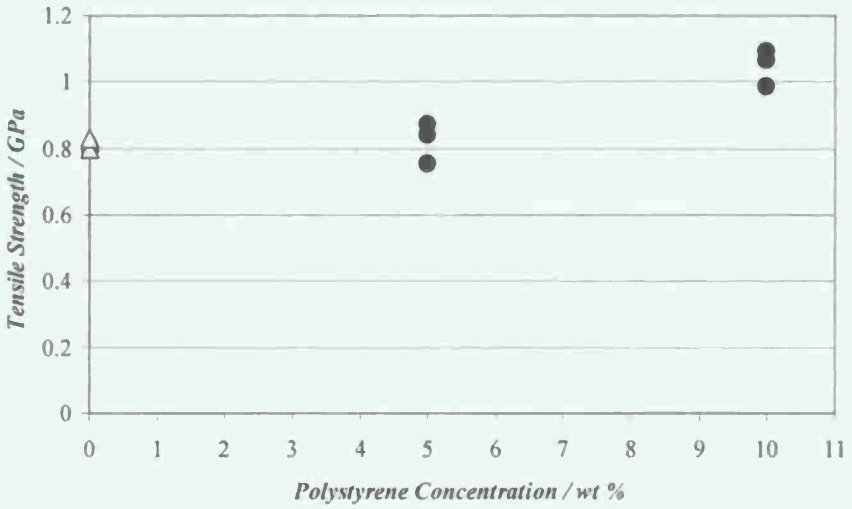

Figure 3.12. Variation of tensile strength for 'thin' polystyrene infiltrated MWNT yarns as a function of concentration of the polystyrene solution (closed circles). Triangles correspond to untreated yarns.

Fig. 3.13 shows the corresponding strain to failure variation for each concentration of infiltrated polymer. This value is seen to decrease – relative to that of untreated yarns – after infiltration, similarly to the trend observed for thick yarns, above, see Fig. 3.11.

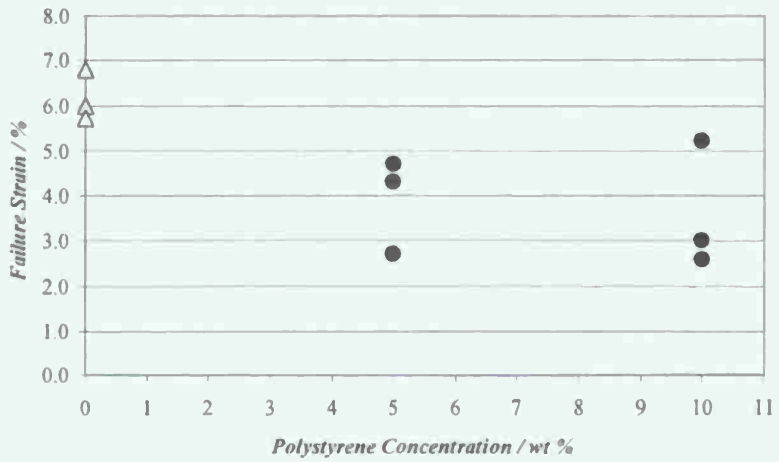

Figure 3.13. Variation of strain to failure of 'thin' MWNT yarns as a function of concentration of infiltrated polystyrene solution (closed circles). Triangles correspond to untreated yarns.

Note from Fig. 3.14 that the diameters of these yarns remain quite constant for different polymer concentrations.

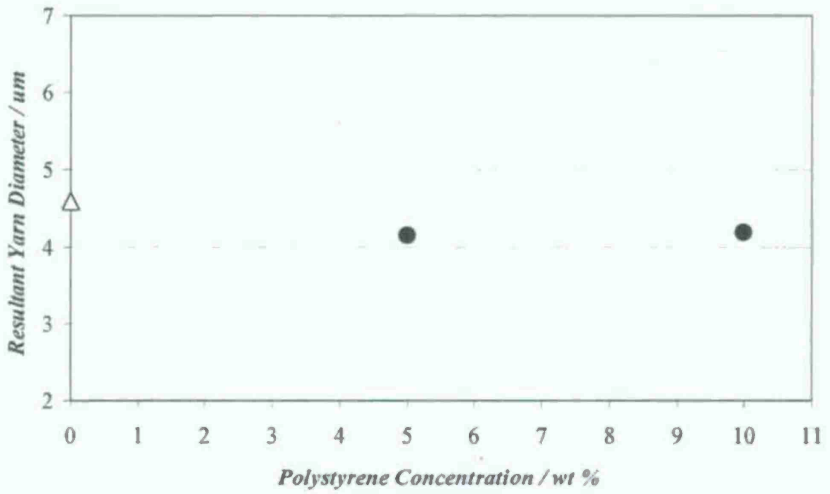

Figure 3.14. Variation of the diameter of 'thin' MWNT yarns after infiltration with polystyrene solution, and drying for 2 hrs (closed circles). Triangle corresponds to untreated yarns.

Fig. 3.15 shows SEM image of the 10 wt% infiltrated nanotube yarn; it is similar in appearance to the one for thick yarns: it contains a semi-regular series of polymer over-coating 'lumps', while the yarn between the lumps displays very little excess polymer.

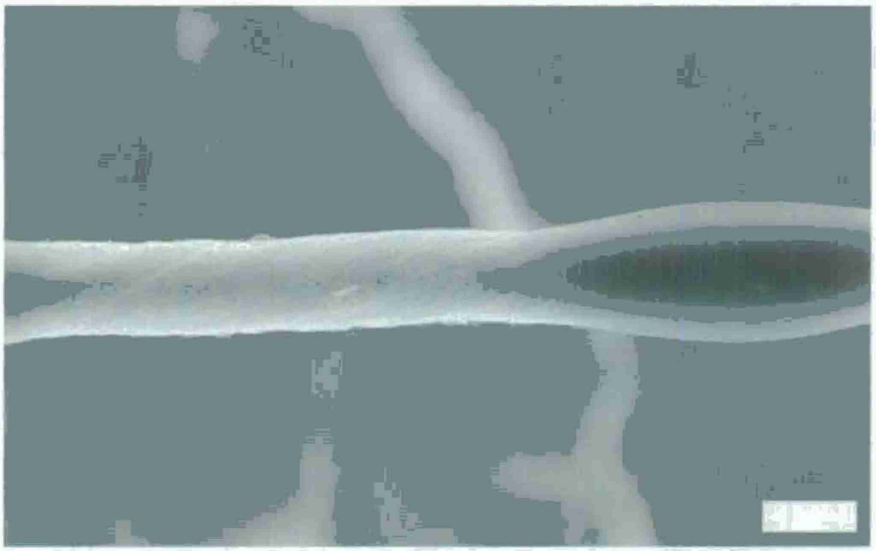

Figure 2.31. SEM micrograph of a thin MWNT yarn after infiltration with a 10 wt% polystyrene/chloroform solution. The scale bar is 4 μm long.

3.6. Infiltration of PBO and Effect on Strength

Poly(p-phenylene benzobisoxazole) (PBO), is a member of the polybenzoxazole class of polymers, one of the various types of highly heat resistant polyheteroarylenes. PBO has properties which make it unique among the known organic fibers. It has higher tensile strength

and modulus than Kevlar, and it is flame resistant. Its oxygen index varies between 56 percent and 72 percent, depending on sample treatment and structure. PBO is unique because it has both the thermo-oxidative and the tensile properties so desired in many aerospace applications. PBO, like the other synthetic organic thermostable fibers, has an aromatic structure which contributes to its thermal properties. In aromatic systems, the phenomenon of resonance stabilization increases the primary bond strength and, consequently, influences the heat resistance. This is the principal mechanism which makes polybenzoxazoles, polyimides, polybenzimidazoles, as well as aramids (to a lesser extent) heat resistant fibers.

In order to explore the possibility of carbon nanotube yarn strength improvement, infiltration by the polymer PBO was performed and its effect on the mechanical properties of the twist-spun yarns was investigated.

Because the tensile strength of our twist-spun yarn varies with yarn diameters, we conducted PBO infiltration using nanotube yarn with diameter of 11.3 μm in this experiment. For PBO infiltration, 3-inch long pieces of CNT twist-spun yarns were submersed in a solution of PBO monomer diluted with NMP for lower viscosity. The CNT yarns were soaked in PBO solution for 24 hour period, before performing the curing process. A standard temperature profile was used for PBO polymerization. First, the samples were heated up to 210°C and held at this temperature for 30 min to remove solvent. Second, the samples were cooled down to 100°C and held at this temperature for 30 min. Then, the samples were heated up to 350°C and held for 90 min in argon environment to polymerize the PBO monomer.

After PBO polymerization, scanning electron microscopy analysis was performed on the pristine and PBO infiltrated CNT yarns. Fig. 3.16 shows representative SEM images of the yarns. The PBO infiltrated yarn exhibits a distorted surface morphology, as compared to CNT yarns infiltrated with other polymers. Twist and individual nanotube bundles are still visible, suggesting that over-coating is minimal, although over-coating is common for infiltration with high-viscosity polymers. The distortion of surface morphology might be due to the polymerization process of PBO. The average diameter of PBO infiltrated yarns is 10.3 μm, which is slightly lower than that of the pristine nanotube yarn (11.3 μm).

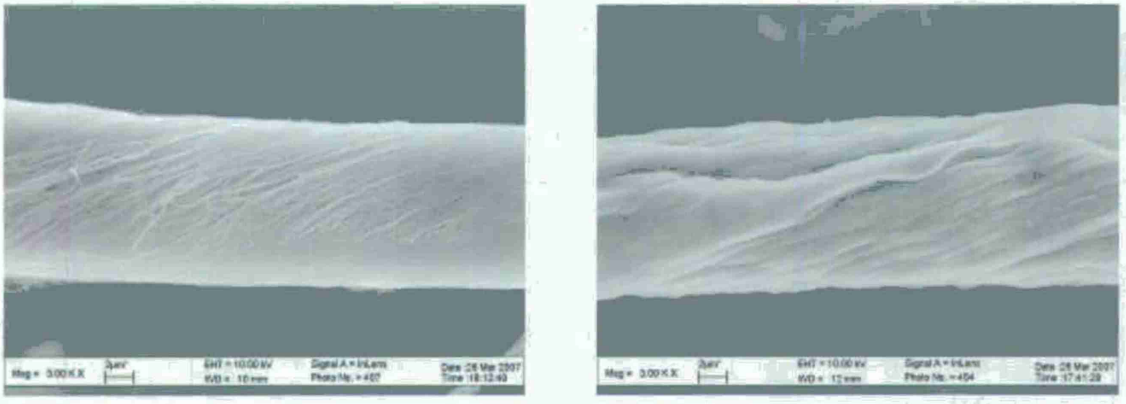

Figure 3.16. SEM images of pristine (Left) and PBO infiltrated (Right) MWNT yarns.

Figs. 3.17 and 3.18 show typical stress/strain dependencies of pristine and PBO infiltrated CNT yarns. It is seen that the tensile strengths of the pristine and PBO infiltrated yarns are 419 MPa and 877 MPa, respectively. This means that there is about 2.1 times strength increase of the PBO infiltrated yarn as compared to the pristine yarn.

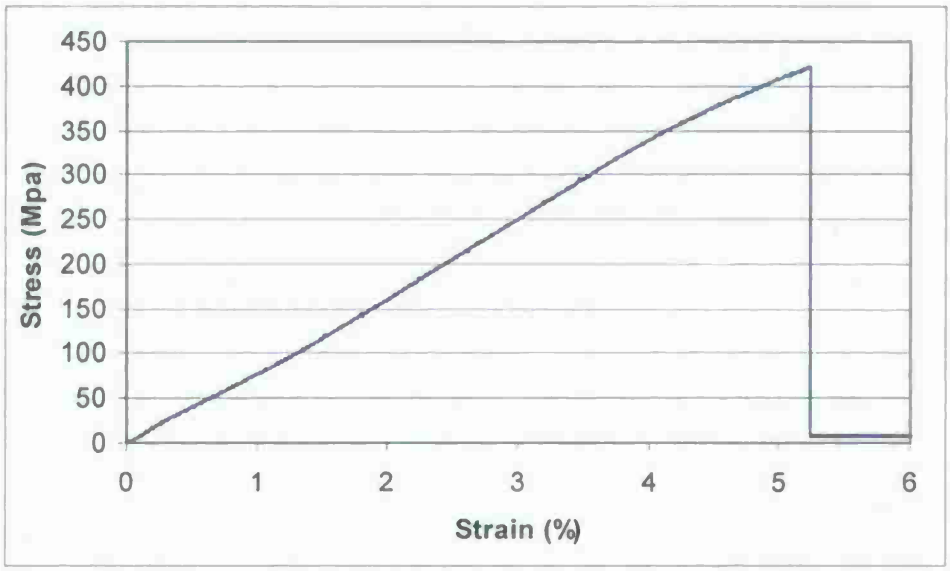

Figure 3.17. Typical stress vs. strain variation for pristine MWNT yarn.

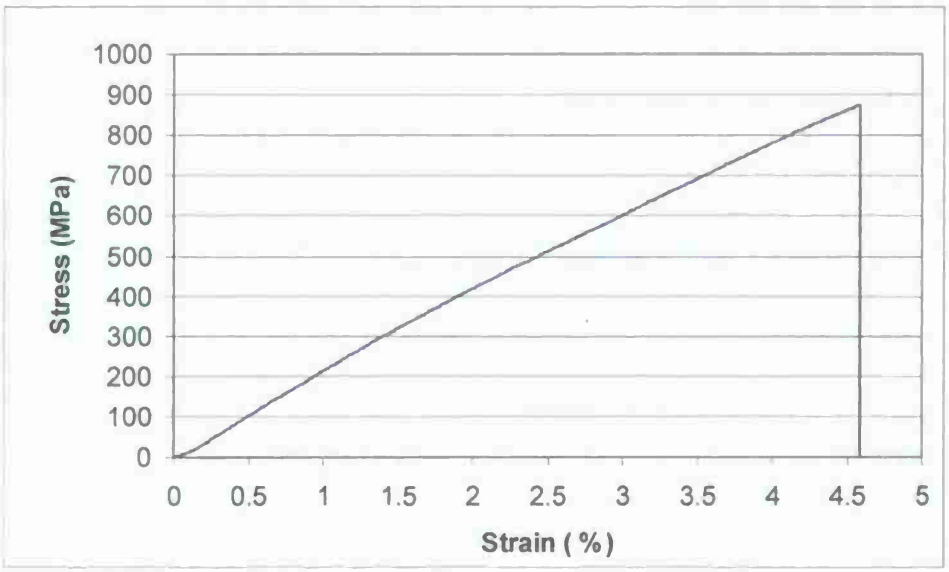

Figure 3.18. Typical stress vs. strain variation for PBO-infiltrated MWNT yarn.

SECTION 4

3-D Braiding with CNT Yarns

4.1. Introduction

The motivation for using continuous nanotube reinforcements for various type composites was discussed in detail in the Phase I Final Technical Report and in paper [19]. Several generic design concepts were proposed there for 3-D woven and 3-D braided preforms. The anticipated effects of substantially reducing size of Z-directional (through thickness) yarns in 3-D woven composites were explained using specific examples. Though 3-D woven and 3-D braided fiber architectures are very different in nature, the main goals of those innovative design concepts are very similar: (i) to increase as much as possible total fiber volume fraction (V_f) in the composite, (ii) to improve their "primary" mechanical properties in the principal loading direction(s), (iii) to ensure sufficient strength and fracture toughness in the "secondary" direction(s), and (iv) to provide unique multi-functional physical properties to the composite. Hypothetical 3-D woven preforms dominated by straight, tightly packed warp and fill yarns with very small diameter nanotube Z-yarns, form one specific class of such innovative materials. The other is 3-D braided preforms dominated by straight, tightly packed axial yarns and very small diameter braided nanotube yarns. Various kinds of hybridization using yarns of different nature will further enhance these design concepts.

4.2. New Equipment for 3-D Braiding with CNT yarns and First Product Samples

First fabrication trials of novel engineered textiles, namely 3-D CNT braids, were performed on 3TEX's designed and built equipment. Fig. 4.1a shows a picture of 3-D braiding device. In the braiding process illustrated in Fig. 4.1b, 3TEX used 36 ends of 5-ply CNT yarns fabricated by UTD. The produced first sample of all-nanotube 3-D braid, approximately 2.5" (6 cm) long, is illustrated in Fig. 4.2. Due to a small length it was used only for demonstration and SEM investigation.

One can see in the SEM image of Fig.4.3 the three upper levels of structural hierarchy: the braid level, the 5-ply yarn level, and the single yarn level. This new textile material has uniquely smooth surface (no typical ends of broken fibers are seen), high consistency of its shape and cross-sectional dimensions (the cross section is nearly a square with 211 micron side length), it is also characterized with high flexibility. The latter property is especially useful for yarn processing into different textile forms. Hence, this 3-D CNT braid can be further used at the next structural level weaving or braiding instead of some regular yarns or rovings.

The further needs of mechanical characterization of the braid and composite sample preparation requested to fabricate more of such 3-D braided material. The single MWNT yarns used in this 3-D braid fabrication were made on UTD's Mark 3 apparatus, with the typical twist level for the

single yarns ~25 turns/mm in counter-clockwise direction. The diameter of the single yarn is ~ 10 μm. It was estimated that at least 15g breaking-force is required for the yarn that can be braided on 3TEX apparatus. The produced single yarns did not satisfy this requirement; besides, they tend to "coil" due to their inherent twist. This made them unusable for braiding or any other textile processing.

a

b

Figure 4.1. A novel 3TEX's device equipped with optical microscope for 3-D braiding nanotube yarns (a); 36 ends of carbon nanotube plied yarn in the apparatus set up (b).

a

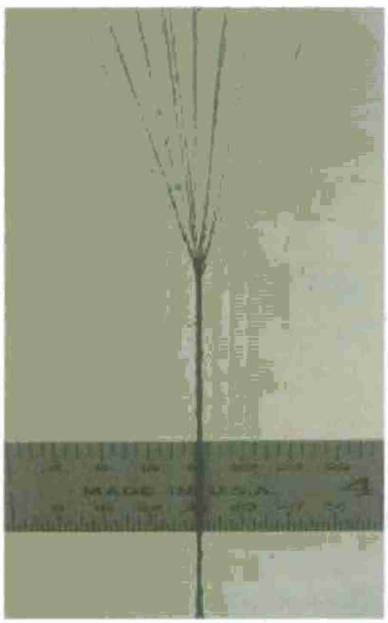

b

Figure 4.2. Fabrication of the first nanotube 3-D braid in progress (a) and produced 2.5" (6 cm) long piece of 3-D carbon nanotube braid (b);

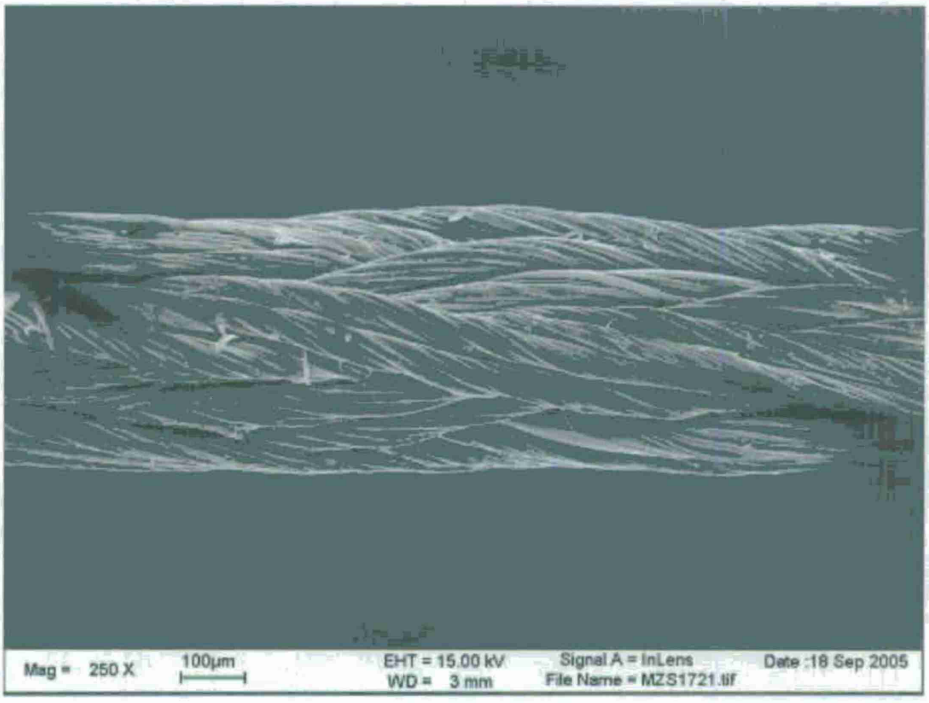

Figure 4.3. SEM image of the first 3-D nanotube braid.

To overcome this obstacle, five single yarns were placed side-by-side between two parallel glass bars 11 inch apart. With one end of the yarn assembly fixed, a twist rate ~4 turns/mm was applied in clockwise direction to achieve a balanced multi-ply yarn. The resulting yarns were sufficiently strong to hold at least 15-20g of weight, and it was possible to keep them straight under slight tension. Therefore, the principal requirements for using them in 3-D braiding were satisfied. UTD produced 40 pieces of such 5-ply yarn, each piece 1 meter long.

This delivery enabled 3TEX to fabricate two more samples, each 20" (50 cm) long, using the same 3-D braiding apparatus, braiding method, and 5-ply nanotube yarns as the "raw material". One of the braids in fabrication is shown Fig. 4.4. Having previous experience, a better uniformity of the braid with less surface loops and other irregularities was achieved, compare Figs. 4.2a and 4.4.

Also, it is evident from SEM image of the braid shown in Fig. 4.5 that the braid structure is very tight and the braid angle looks uniform along the length. The average side length of this nearly square cross section 3-D braid was evaluated at 211 µm using Scion Image technique with 17 measurements taken along the braid length. One of the produced samples was used as one Z-yarn incorporated in 3-D woven fabric, as described later in this report. The produced 3-D braid was also used for its mechanical characterization, as reported further, and for 3-D braided composite fabrication and mechanical characterization.

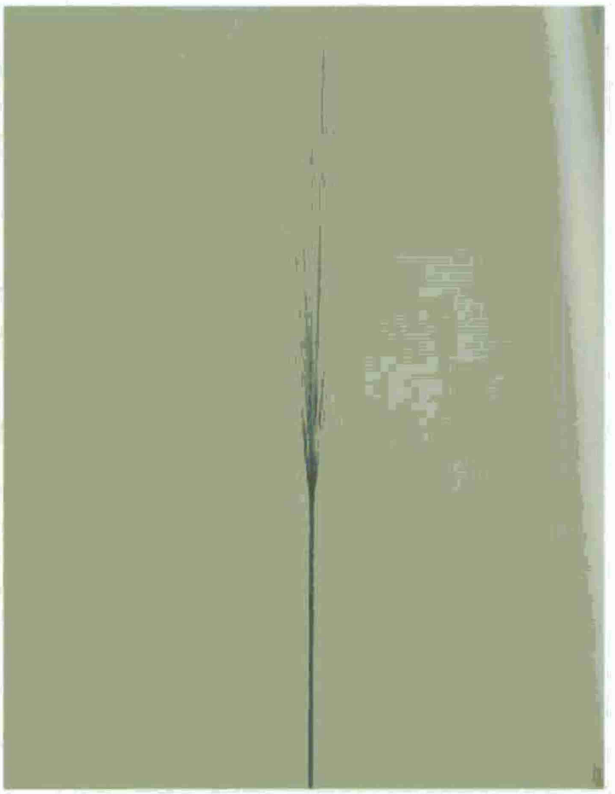

Figure 4.4. Fabrication of 50 cm long nanotube 3-D braid sample in progress.

Figure 4.5. SEM image of the 3-D braid fragment.

4.3. The need of Hybrid CNT 3-D Braids

Long continuous yarns, 3-D braids, 3-D weaves and other textile reinforcements consisting solely of carbon nanotubes, or hybridized with other fiber materials, may be the future of specialty composites requiring unique multi-functional properties. Fig. 4.6 illustrates a conceptual 3-D braided material, first presented in [19], that contains a large amount of aligned axial tows (green), with very fine off-axis carbon nanotube yarns (red), which are being 3-D braided around the axials. The principal design objectives in this case are: (i) to increase as much as possible the total fiber volume fraction (V_f), (ii) to improve 'secondary' mechanical properties of a composite (e.g., properties in the directions perpendicular to the braiding axis) with as little sacrifice of its axial properties as possible, and (iii) to improve as much as possible fracture toughness, damage tolerance, impact resistance, fatigue life and other characteristics of special interest. So, it is desirable to use as little braided fiber amount as possible and also keep the braid angle sufficiently small in order to minimize the reduction of the longitudinal elastic and strength properties vs. the respective properties of the 'baseline' unidirectional composite. Using continuous carbon nanotube yarns in such hybrid 3-D braided structure is one possible path to practical realization of this concept.

Figure 4.6. A conceptual hybrid 3-D braid with braided carbon nanotube yarns.

To succeed with the proposed approach at real life industrial scale, several conditions should be met. First, a reliable source of substantial (meaning, far beyond the laboratory research needs) volume of continuous, sufficiently strong and tough carbon nanotube yarns has to establish its place in the market. Second, those commercially available yarns should be affordable. Third, special 'micro-weaving' and 'micro-braiding' devices and automated machines capable of gently manipulating very fine and relatively weak nanotube yarns shall be designed and built. Fourth, special composite fabrication methods and tooling have to be developed.

Although several different methods of processing continuous yarns from single-wall and multi-wall carbon nanotubes have been proposed and demonstrated, those materials are still produced

in very small quantities and are extremely expensive. As one can reasonably project, even when long continuous carbon nanotube yarns will become commercially available, they will still be a very expensive material even for the specialty low-volume applications. Accordingly, composites solely reinforced with such yarns or their textile structures might be also cost prohibitive. Therefore, hybrid 3-D textile preforms for composites could prove to be a much more economical first application of carbon nanotube yarns, due to they could capitalize on the best possible combinations of mechanical, thermal, electrical, etc. properties, while the nanotube yarn volume content would only account for a small percentage of the total fiber volume in the preform.

4.4. Fabrication of the First Hybrid 3-D Braid with the Use of Carbon Nanotube Yarns

About 100 m long 'single' yarn was fabricated for this study at UTD by drawing it with twist from multi-wall carbon nanotube forest. The yarn was further plied with counter-twist and used on 3TEX's proprietary device. Along with thirty six 6-ply carbon nanotube yarns, the 3-D braiding process incorporated 9 small axial bundles of S-2 glass fibers. Further, composite materials reinforced with the plied nanotube yarns and hybrid (nanotube yarn/glass fiber) braid, were fabricated by infusing epoxy resin. The main objective of this work was to experimentally study some mechanical properties and electrical conductivity of the produced nanotube yarns, 3-D braids and composites made thereof.

As with much larger commercial 3TEX's 3-D braiding machines, the manual device used for this study has the ability to add axial fiber bundles between the braiding yarns. The axial fibers remain nearly straight in the final preform. S-2 glass fibers were chosen for such axial bundles owed to two reasons. One is that they provide a bright color contrast with carbon nanotube yarns and thus allow one to visually study the texture of the hybrid 3-D braided structure. The other is that, like any kind of glass material, S-2 glass provides a non-conductive fiber component for the hybrid 3-D braid. Hybridizing the carbon nanotube yarns with another conductive material, such as carbon fiber, would have resulted in a 'smearing' of electrical conductivity between the two components. The fiberglass is an insulator, so any electrical conductivity gain in the hybrid braid has to be attributed to the carbon nanotube yarns. In order to meet the objective of high axial fiber volume fraction (i.e. staying close to unidirectional composite, the preform incorporated 9 relatively thick axial fiber bundles. Those were extracted from an AGY 463-1250 S-2 glass roving. That particular roving type consists of 12 fiber bundles which are sized individually, so they can be easily separated. Nine of such 12 fiber bundles were removed from the roving and used as axial fibers in the braiding.

On this particular 3-D braider setup, 36 yarns (each of them being a 6-ply carbon nanotube yarn) were tied to the movable braiding positions. The total cross sectional area of S-2 glass fibers, 0.131 mm^2, was taken from the manufacturer's data sheets. The total cross-sectional area of the carbon nanotube yarns was evaluated as 0.047 mm^2 (the cross-sectional area measurement technique described in [23] was used for this purpose). The side length of the produced hybrid 3-D braid was measured as ~0.45 mm. The volume fraction of axial fiber in the preform was estimated as ~74%. An optical micrograph of the produced hybrid 3-D braid is shown in Fig. 4.7. The braid architecture is clearly seen on one side of the square-shaped braid. Three of the nine S-2 glass axial bundles can be seen along the length of the preform. The produced braid is uniform

along its length, and it appears from the optical microscope pictures, that the braided structure is very tight.

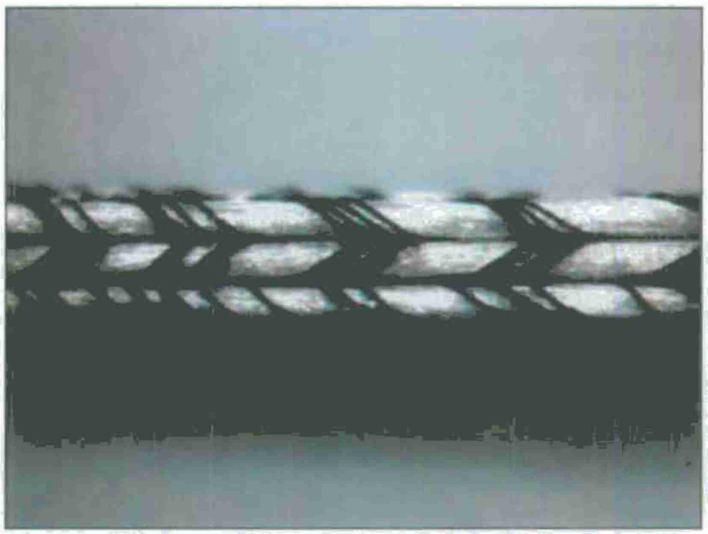

Figure 4.7. Hybrid glass fiber/carbon nanotube yarn 3-D braid, 40x magnification.

One primarily important feature of 3-D braided preforms in general is, that the braiding yarns 'consolidate' entire structure and provide support for the axial yarns. This effect was observed even for the small samples produced in this study. Fig. 4.8 compares two structures being suspended horizontally. Both samples are 15 cm long. The one, which stays nearly horizontal, is the hybrid 3-D braid of Figure 3.5. The other one, which is bent by its own weight, is a loose fiber assembly containing same nine S-2 glass fiber bundles. Therefore, the number of glass fibers is the same in both samples, but in the latter one they are not intertwined by nanotube yarns. The effect of such intertwining is obvious from the picture – 9 bundles of S-2 glass fibers become self-supporting under gravitational force.

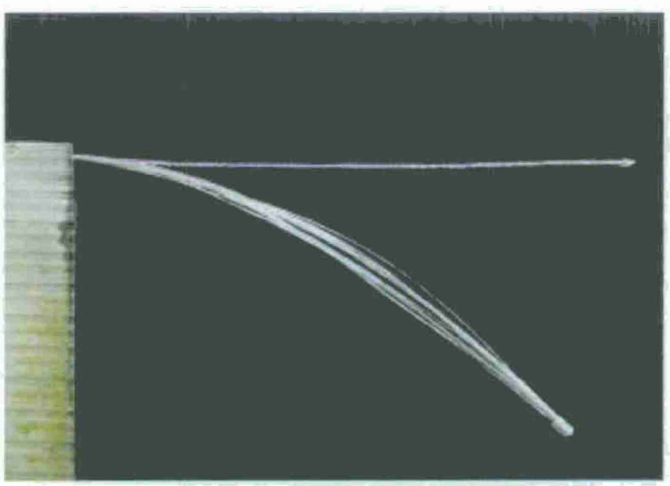

Figure 4.8. Illustration of comparative bending stiffness of the hybrid 3-D braid and the bundle of individual S-2 glass fibers.

SECTION 5

3-D Weaving with CNT Yarns

5.1. New Specialty 3-D Weaving Machine

In order to perform 3-D weaving with carbon nanotube yarns and their larger hierarchical assemblies, a specialty 3-D weaving machine shown in Fig. 5.1 was designed and built by 3TEX in the framework of this STTR project. The machine is capable of weaving very small diameter yarns. The machine's sensitivity to small yarns arises from its reduced size, careful design, and ability to be either hand operated or driven by small electrical motors. Fig. 5.1 illustrates that the weaving machine is capable of sitting on a large tabletop.

Figure 5.1. A novel 3TEX's specialty 3-D weaving machine aimed at processing carbon nanotube yarns.

The frame was designed using extruded aluminum that supports both the weaving mechanism and the creel. Letters (A-E) on the picture point out the major components of the weaving machine. In the right side of the picture the creel can be seen under (A). Aluminum rods support the packages of yarn, which are bobbins commonly used on braiding machines. Three sets of two rows are visible. The top and bottom set each hold twenty eight (28) AS4 3K bobbins and comprise the two warp layers. The middle layer has thirty two (32) T300 1K bobbins, which were the original Z-yarns used in the production of the 3-D woven fabric. The heddles, used to raise and lower the Z-yarn are located under (B). They have a large radius, which minimized the amount of abrasion on the yarns during weaving. The reed used has 40 dents per inch (dpi) and is seen under (C). This is 2-4 times more than the warp yarn draw density found in common 3-D woven fabrics commercially produced by 3TEX. Three weft layers of AS4 3K were inserted by the mechanism under (D). Three 2 mm diameter rapiers were capable of inserting the weft yarns into very small shed openings. A stepping motor was used to take up the fabric. The fabric clamping platform, as seen under (E) in the picture, moves on the acme rod guided by a track. The fabric could be taken up a set distance by the push of a button.

5.2. First 3-D weaving Trials

Initial weaving trials showed abrasion and breakage of some Z-yarns. The 1K T300 yarns used in the Z-direction were not capable of sustaining much abrasion before failing. A method commonly used for adding tension to yarns was found to be causing much of the abrasion. Abrasion of the 1K yarns was almost eliminated by reducing the tension on the yarns. This was accomplished by using much smaller hanging weights. In Fig. 5.2, the original weight is seen on the left yarn while the much smaller weight is seen on the right. .

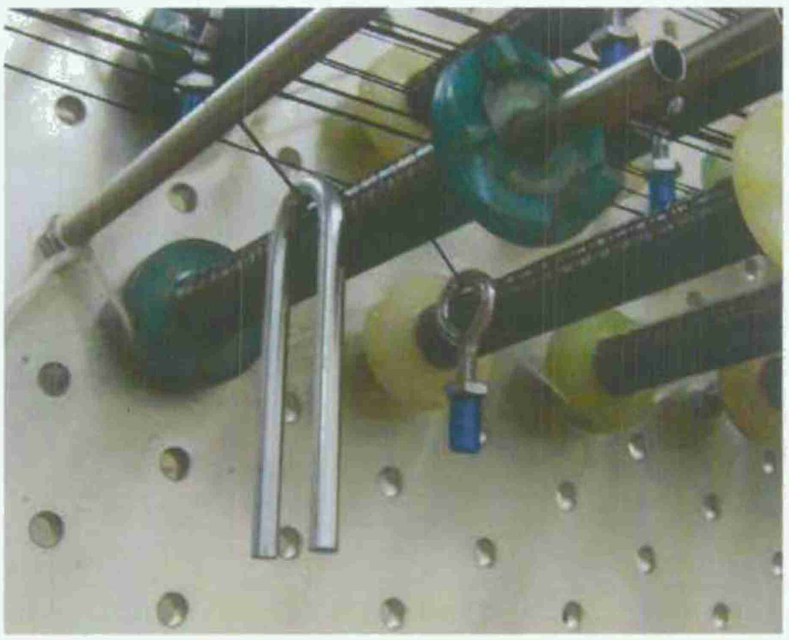

Figure 5.2. Different size tension weights used in weaving for warp yarns and Z yarns.

The first fabric made on this machine was very uniform, as is observed in Fig. 5.3. The filling yarn insertion density is thirty eight (38) picks per inch (ppi) along the length of the fabric.

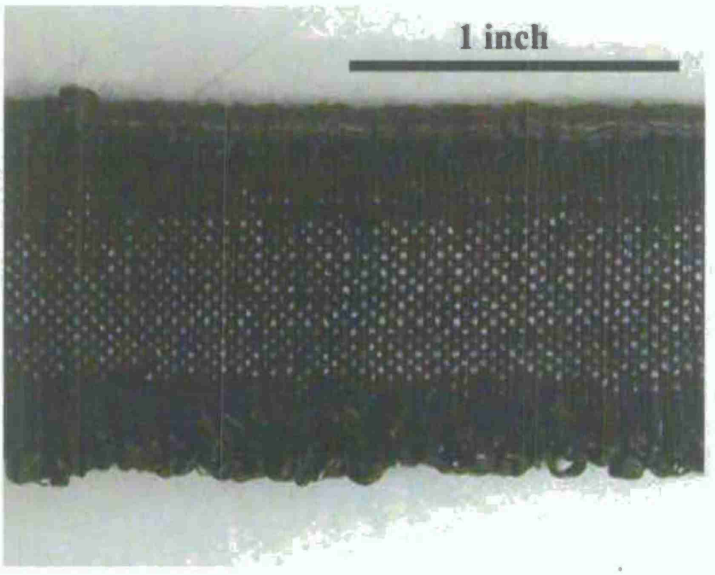

Figure 5.3. The first 3-D woven carbon fiber fabric fabricated on the new 3-D weaving machine.

5.3. First 3-D Weaving Trials with 3-D Carbon Nanotube Braid Replacing One 1K Z-Yarn

The first trial of weaving with carbon nanotube material used part of one of the 20" long 3-D braids, described in Section 4.2, as the replacement for one of regular 1K T300 carbon yarn. Of the braid produced, a portion went to characterize the mechanical properties, while a 6" (15 cm) long piece was used in 3-D weaving. Because this material had never been woven before, special care was taken of handling and a gentle touch was used when weaving. The force needed to break the fresh braid was measured to be greater than 700 grams, which is absolutely sufficient for using this material as Z-yarn in 3-D weaving. However if significant damage from careless handling and/or abrasion during weaving was imparted to the braid, this number would be drastically reduced.

Constant tension had to be applied to the braided nanotube Z-yarn during weaving, and it had to take the same path through the reed and heddles as the regular 1K yarn. The best solution was to cut the 1K Z-yarn at the fabric production point, hold one end of the braid in place at the fabric production point and glue the other end of the braid to the end of the 1K carbon yarn still on the bobbin. Once the glue cured, the 1K yarn glued to the braid was back wound through the reed to take out any slack. Weaving produced the fabric shown in Figs. 5.4 and 5.5. Individual plied yarns in the braid can be seen through careful inspection of the picture at 65x magnification. Near the end of its length, the superglued connection was snagged on the reed during beat-up and the connection broke, terminating the weaving process. Minimizing the amount of superglue at this point would be the key in future trials.

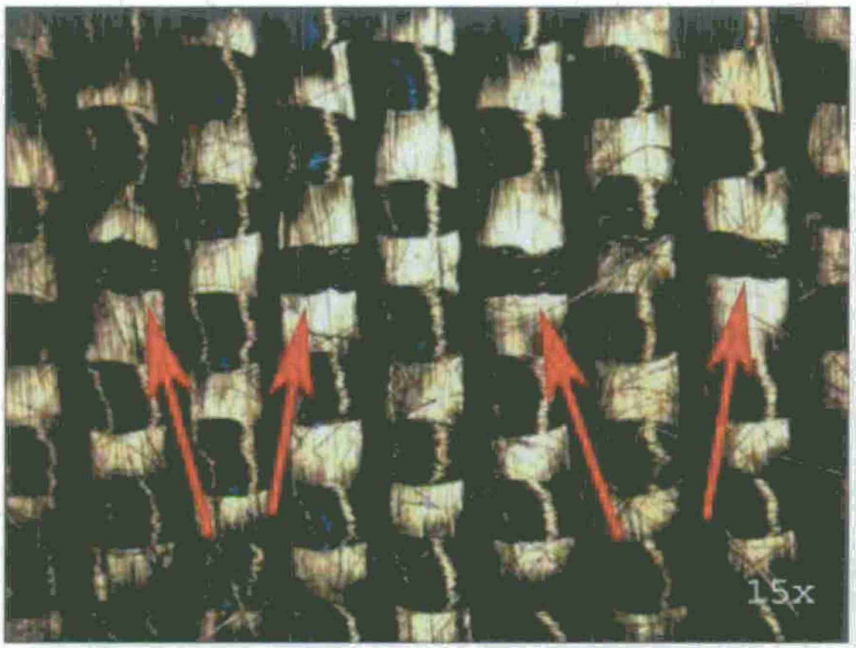

Figure 5.4. 3-D nanotube braid used as Z-yarn in 3-D woven fabric (15x magnification).

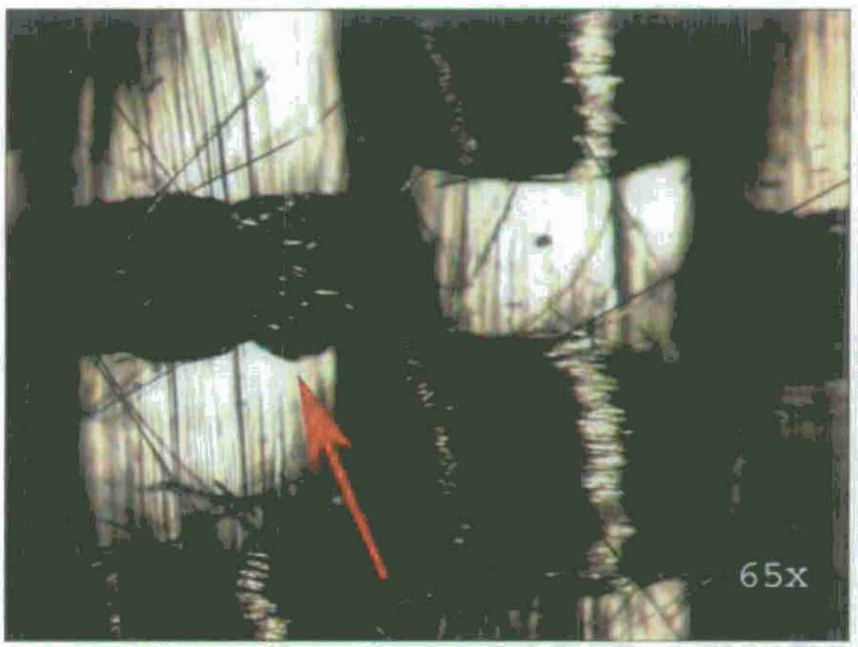

Figure 5.5. 3-D nanotube braid used as Z-yarn in 3-D woven fabric (65x magnification).

The 3-D nanotube braid Z-crowns seen in Figs. 5.4 and 5.5 are smaller in width and are obviously of a totally different construction than their neighboring Z-crowns of 1K T300 carbon yarns. It looks like the latter ones do not conform to the filling yarns below them as well as the nanotube braid does. Damage to the 1K yarns is apparent, while there is absolutely no fraying of the nanotube braid, which is much more flexible and allow for a much higher failure strain.

From the calculations based on SEM images, the cross-sectional area of the braid was determined to be about 70-80% of the area of a 1K T300 carbon yarn. This is not a dramatic area difference that is desirable for fulfilling the objective of reducing the out-of-plane fiber volume fraction as much as possible. A much smaller carbon nanotube yarn would serve the purpose. Next section describes the process of 3-D weaving with much smaller nanotube yarns.

5.4. 3-D Weaving with 25-Ply Carbon Nanotube Yarns Replacing 1K Z-Yarns

An individual 5-ply yarn used in 3-D braiding described above were found to have a breaking force of around 15-20 grams. This very small allowable force, coupled with the fact that these yarns are very hard to see, required that a nanotube yarn with substantially larger cross section and, accordingly, much higher breaking force, should be used in the 3-D weaving process. To meet this requirement, UTD produced 25-ply yarns by twisting five 5-ply yarns together. The spool of five meters of this yarn is shown in Fig. 5.6. This picture gives some idea of the scale of 3-D weaving with carbon nanotube yarns that was performed.

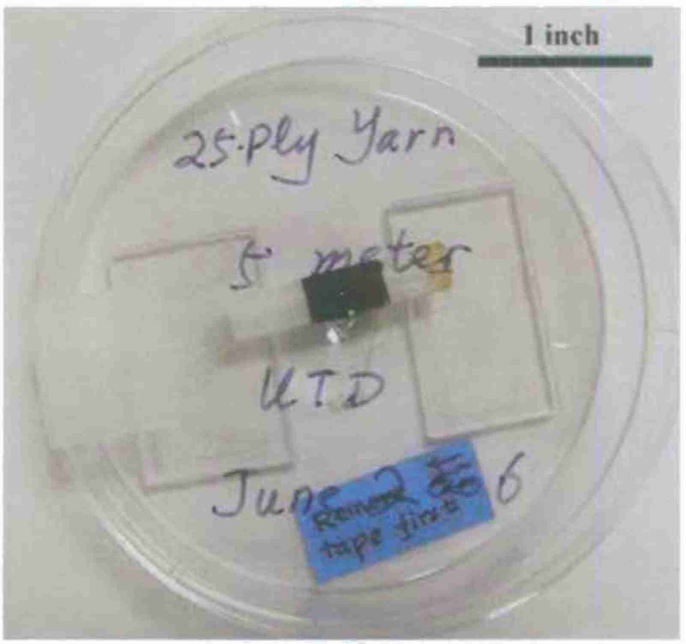

Figure 5.6. Five meters of 25-ply carbon nanotube yarn.

Five 1K Z-yarns were replaced on the weaving machine with the new 25-ply nanotube yarns in the same manner as was described before for the case of 3-D nanotube braid. However, there is a great difference between the two weaving trials: in the 3-D braid case there are 180 single yarns within the Z-yarn used, compared to only 25 single yarns in the Z-yarn we have to deal with now. This means that weaving with 25-ply yarns requires to manipulating much smaller Z-yarns than regular 1K.

Care was taken to only use a very small amount of superglue by dabbing it onto both the 1K yarn and the 25-ply nanotube yarn with a needle. Fig. 5.7 shows the connection made between the two types of yarn. To ensure that the breaking force was not exceeded, even smaller hanging weights

were used during weaving to lower the tension. Extreme care was taken during the first cycles of weaving with the 25-ply yarns. Damage that can be caused by the headels was not apparent when viewed by a handheld magnifying glass after multiple cycles.

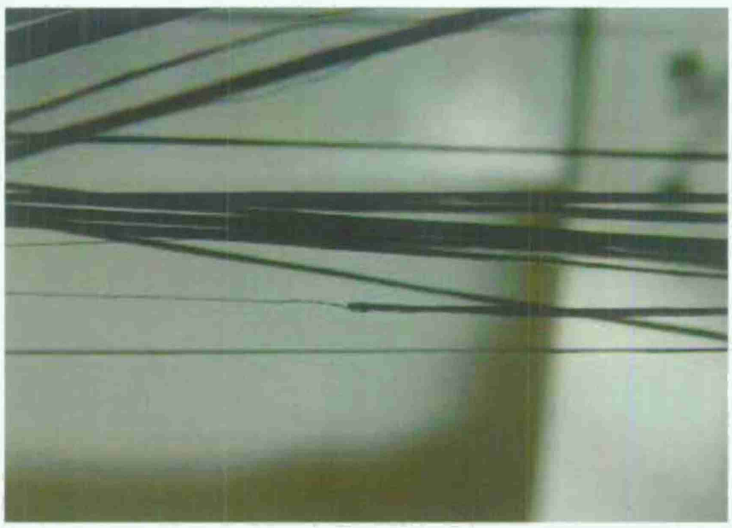

Figure 5.7. Connection made between regular 1K T300 carbon yarn and 25-ply carbon nanotube yarn.

Fig. 5.8 shows the nanotube yarns going through the heddles during weaving with no apparent damage.

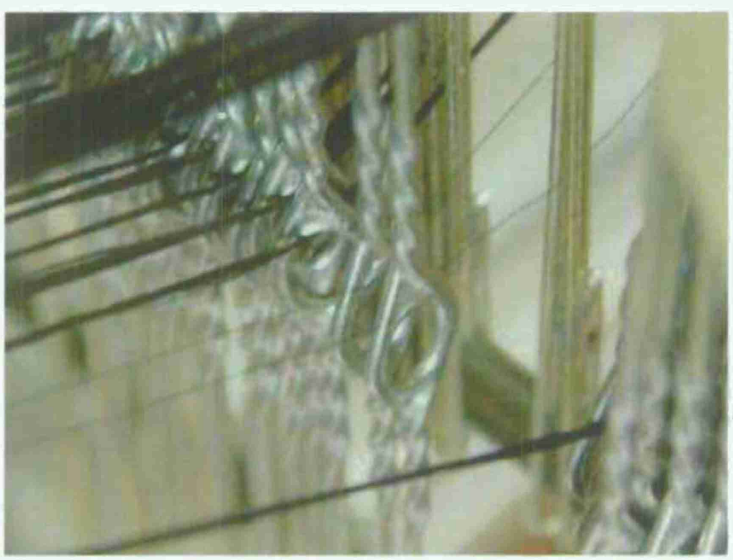

Figure 5.8. 25-ply nanotube yarns passing through 3-D weaving heddles.

Weaving at a normal pace of about 4 picks per minute resumed for the rest of the 35 cm length of nanotube yarns. Pictures of the fabric produced are shown in Figs. 5.9-5.12. Figs. 5.9 and 5.10 were taken with a high quality digital camera at close range. Both of these pictures show the 25-ply nanotube yarns integrated as Z-yarns (first five from the bottom of the fabric in both

pictures). They appear as crowns over the filling yarns and are approximately one tenth of the size of the regular 1K Z-yarns. A separation was drawn on Fig. 5.10 to show where the nanotube yarns stop and the 1K carbon yarns begin. Figs. 5.11 and 5.12 were taken on an optical microscope with picture capture capabilities in order to show the crowns of the nanotube Z-yarns more clearly.

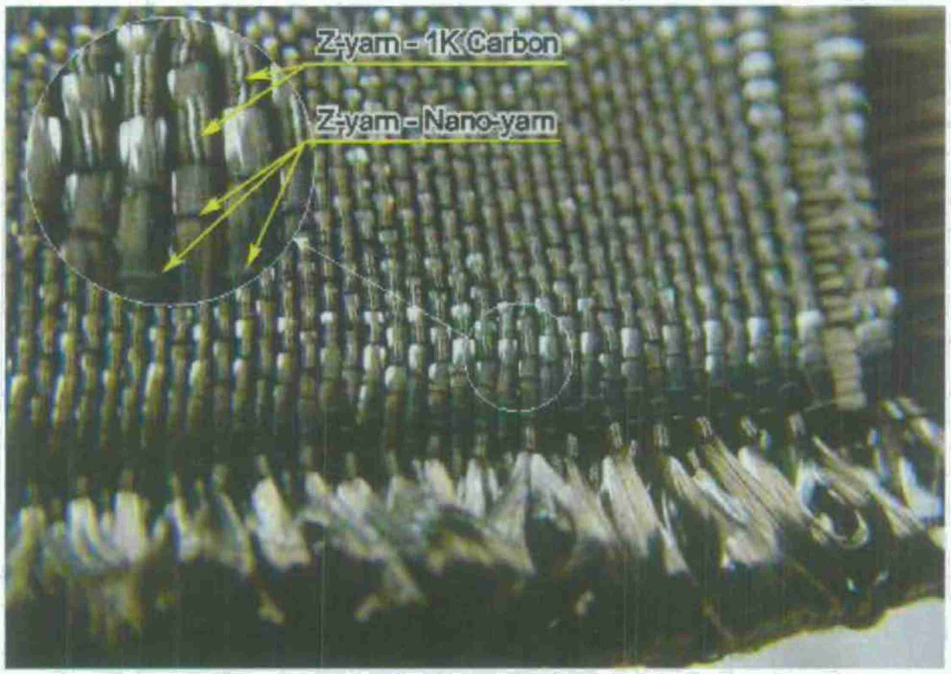

Figure 5.9. Fabricated 3-D woven fabric with 25-ply nanotube yarns incorporated as the first five Z-yarns from the bottom.

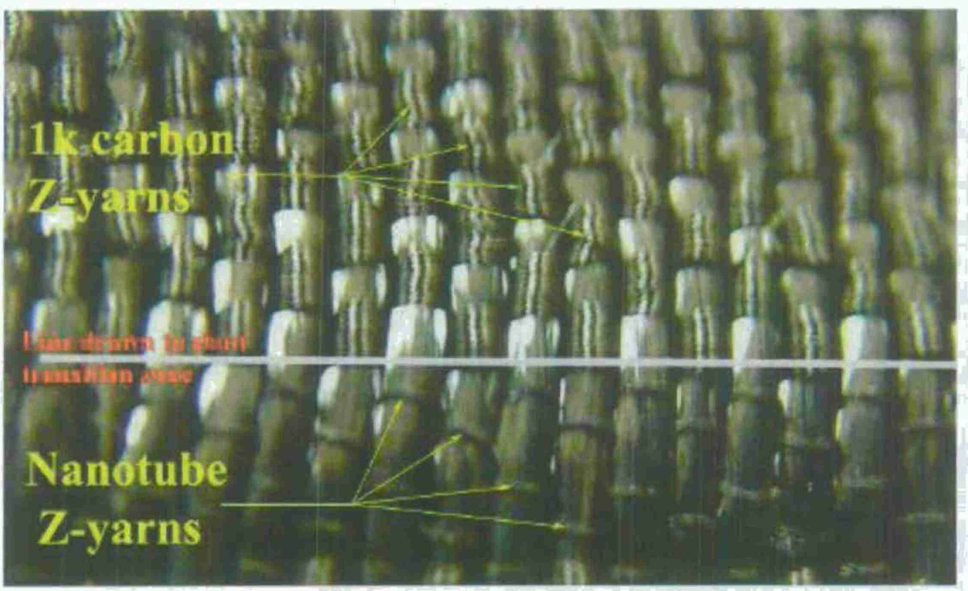

Figure 5.10. 3-D woven fabric with 25-ply nanotube yarns incorporated as the first five Z-yarns from the bottom.

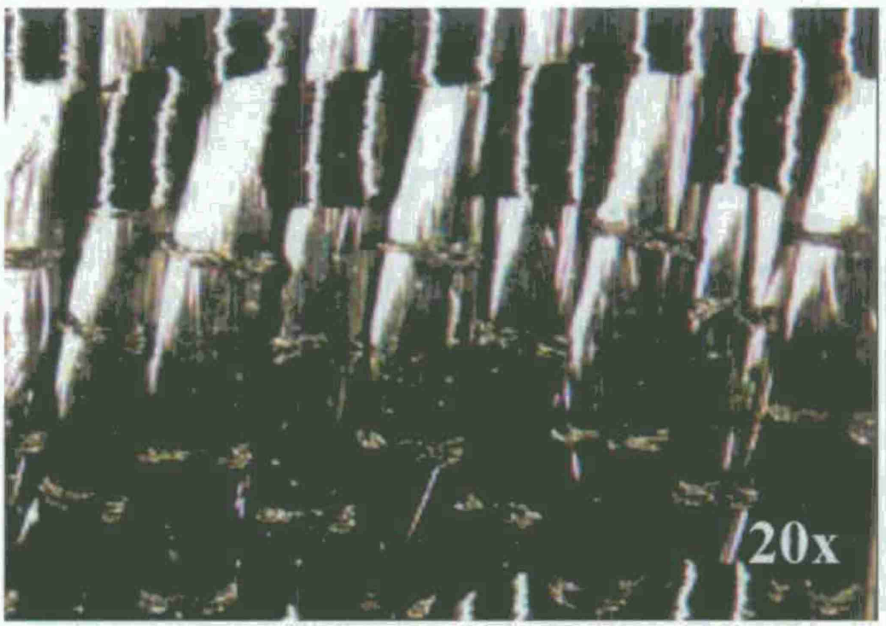

Figure 5.11. 25-ply nanotube Z-yarn crowns vs. regular 1K Z-yarn crowns on the 3-D weave surface (20x magnification).

Figure 5.12. 25-ply nanotube Z-yarn crowns vs. regular 1K Z-yarn crowns on the 3-D weave surface (65x magnification).

Results presented above have demonstrated that on this new specialty 3-D weaving machine 3TEX will be capable to process very fine carbon nanotube yarns, which are much smaller in size than the smallest commercially available 1K carbon yarns.

5.5. Automation of 3TEX's 3-D Weaving Machine

A specialized 3-D "Micro-weaving" machine described above was first operated in a manual regime with the use of actual plied nanotube yarns and 3-D braids made thereof. The primary purpose of those trials was gaining experience in weaving fabrics that incorporate carbon nanotube yarns. During Year 2 of this STTR Phase II the machine was fully automated, and its functionality has been demonstrated on the production of fabric with Z-directional 1K carbon yarns simulating carbon nanotube yarns to be obtained and utilized soon.

The main components of automated 3-D weaving machine are shown in Fig. 5.13. Of course, its purpose is to meet specific scale and processing requirements dictated by the use of very fine and relatively weak yarns constructed from carbon nanotubes. Careful considerations were made to accomplish this when the yarns have a breaking force of 20 grams or less. For good results, the research demands the optimal conversion of yarn to fabric without imparting considerable damage. The machine design has a size appropriate weaving zone, all motions are precisely controlled, and a flexible automatic control system is implemented.

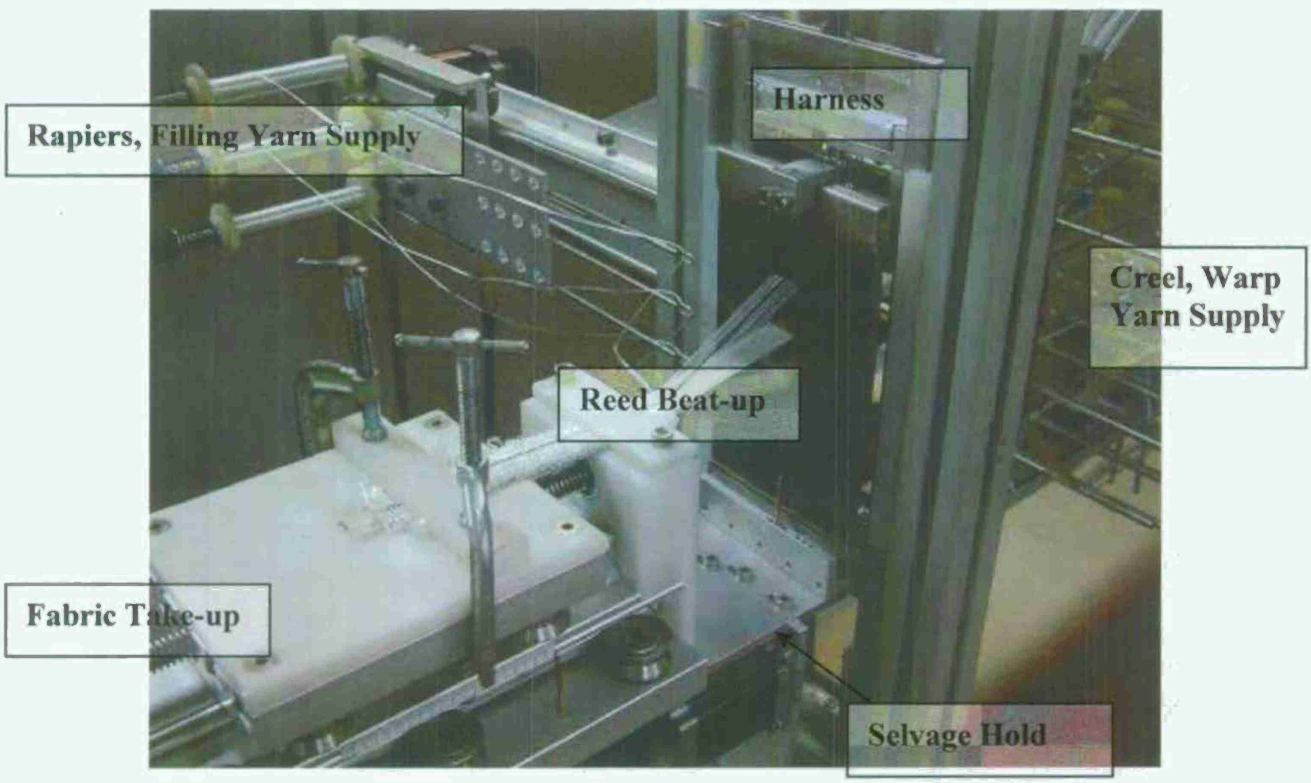

Figure 5.13. 3TEX's proprietary 3-D "Micro-weaving" machine.

The current small-scale 3-D weaving machines at 3TEX are predominantly pneumatic systems driven, which require extensive manual setup to accomplish fine yarn weaving. Those machines are 10 inch and 20 inch wide, respectively. They can effectively weave to small widths but with limited motion control. The newer 3-D weaving machines in 3TEX operation have multi-axis motor controls, but they were designed for even wider, 33 inch and 72 inch, fabric production.

The new specialized 3-D weaving machine shown in Fig. 5.13 takes the available technology to construct a scaled-down 3-D weaving machine for much smaller width (about 4 inches) fabric production, but enables using very fine technical yarns.

Fabric formation by weaving is a primary source to yarn damage. The motions of weaving have steel rubbing yarns, and yarn rubbing other yarns. The typical methods of reducing damage are well known, and those are also employed on all 3TEX machines. One of them is the use of large radius of curvature on all steel-to-yarn contacts. With the precise motion controls on the machine components, the yarn damage can be minimized. Slower speeds and accelerations give yarns the time needed to accommodate the motions and reduce friction. The result is lower stress on yarns and minimized damage.

The new 3TEX's weaving machine runs with the use of independently controlled motions. The motion profiles follow acceleration, velocity, and deceleration programmed into control system, see Fig. 5.14. The linear motions are driven by stepper motors. Rotation motor movement is translated to linear motion via belt drives or precision lead screws. This technology is commonly known as CNC and extensively used in machine shops for fabrication of complicated parts. The motions can be sequenced in step-by-step motions (or rather overlapped) to decrease processing time. The next motion is determined by a programmed position of another motion. These motion controls are essential for effective machine functionality.

Figure 5.14. 3-D weaving machine control system with 5-axis motion control.

The 3-D weaving machine has five linear motions sequenced to weave the yarns. These linear motions are in order of occurrence; rapier insertion, selvage hold, reed beat-up, fabric take-up, and harness change. Positions for each movement are set in the control system. Automatic operation moves each axis to the precise position in the required sequence. Positions are verified with use of proximity sensors. The weaving cycle is complete at the end of all the motor motions to provide one filling insertion (pick). The weaving continues until as many picks as necessary are inserted to produce a fabric.

The described motion controls help in other aspects of the weaving process. Yarn tension during the process is essential to fabric formation. The smoother motions allow for uniform tension throughout the machine movements by reducing tension spikes and abrasion in the yarns. These systems can also add tension during the proper times. Tension is added to stretch the filling yarns during the final beat-up stroke. The result of this is improvements in fabric quality and performance characteristics, as well as in minimized yarn damage.

5.6. First 3-D Weaving Trials in Automated Regime

The first fabric sample woven in automatic regime is shown in Fig. 5.15. This is an example of possible weaves that are enabled when the weaving machine is designed to process yarns into fabric with minimized damage. A fabric construction is determined by several variables; yarn type, number of warp layers, reed density (dents per inch, DPI), pick density (picks per inch, PPI), and harness configuration. The initial machine design and set-up was done for two warp yarn layers, three fill yarn layers inserted by rapiers, and two-harness weave pattern. Both DPI and PPI numbers are changeable in a broad range, but their maximum values are limited by the warp and fill yarn sizes.

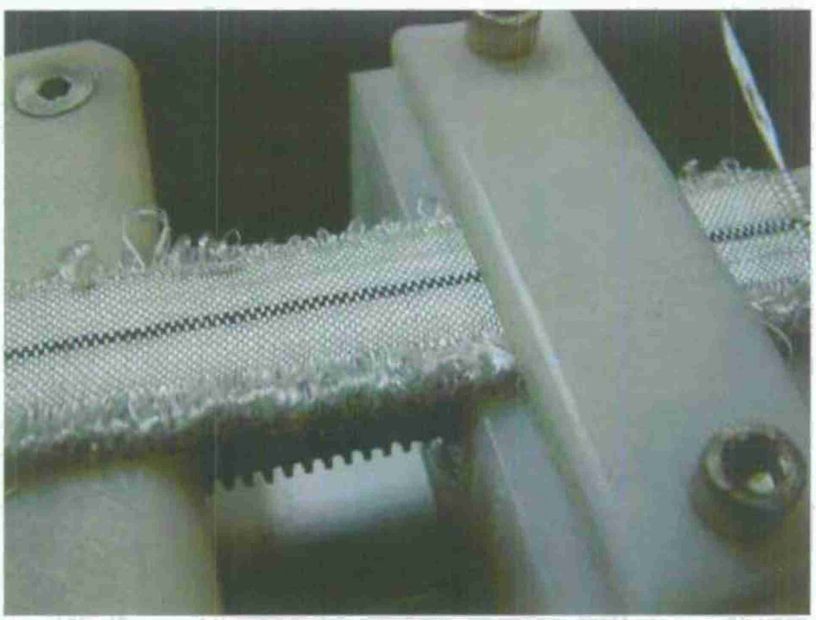

Figure 5.15. 3-D woven fabric produced on the new automated 3TEX's machine. Two black 1K carbon yarns were used in Z-direction to simulate carbon nanotube yarn weaving.

Regarding the fabric shown in Fig. 5.15, 3TEX was able to accomplish weaving with 5 in-plane yarn layers (2 warp and 3 fill) at 16mm width with 45 PPI and 40 DPI. Fine S-glass roving and a pair of 1K carbon yarns were used side-by-side in Z-direction. The rest of the fibers used was fine E-glass roving.

Again, this specialized 3-D weaving machine will be effective in producing relatively small width and thickness fabrics constructed of very fine and fragile technical yarns. Of course, weaving carbon nanotube yarns is the primary purpose of this machine utilization.

5.7. Automated 3-D Weaving with CNT Yarns

The newest plied CNT yarns produced by UTD proved to be strong enough to be used on 3TEX's automated 3D "Micro-weaving" machine. The extreme flexibility and durability of the yarns allowed them to be woven into a fabric with almost no observable damage. The five meters of 25-ply yarns were used as Z-yarns in a fabric made of S-2 glass fibers. Very bright white S-2 glass fibers were used to provide a sharp contrast to the CNT yarns and, therefore, to get best possible visualization of the hybrid fabric architecture. Two layers of 2500 yield E-glass warp yarns were used with a density of 40 dpi. Three layers of 2500 yield E-glass filling yarns were inserted with a density of 41 ppi. S-2 glass bundles were used for Z yarns due to the fact that the individual fiber diameter was smaller. The smaller diameter and higher strength of the S-2 glass bundles allowed them to be woven as Z-yarns with less damage.

Weaving trials with incorporation of the CNT yarn started by replacing a single S-2 glass Z yarn with a 25-ply CNT yarn. Because the CNT yarn had a limited length of approximately 20" (50 cm), it was impossible to use only the CNT yarn in a single dent. To keep tension on the CNT yarn during weaving a section of S-2 glass roving was removed and replaced with the CNT yarn. Super glue was used to connect the ends of the CNT yarn to the S-2 glass rovings. It was found that the action of the reed, which had a very high dent density, could catch on the glue points connecting the two type of yarns which in turn would break the CNT yarns during beat-up. To eliminate this problem, one end of the CNT yarn was glued directly to the S-2 glass Z yarn at the point of fabric formation as not be affected by the beat-up motion. After this modification was made, the 50 cm long section of CNT yarn was incorporated in the automated weaving process without stopping. Close inspection of the CNT yarns with a magnifying glass showed that there was no damage to any of the plies in the CNT yarn. In contrast, even relatively flexible S-2 glass Z yarns showed certain "hairiness" pointing at broken filaments, most likely caused by the sharp radius of the eyelets in the heddles.

Figs. 5.16-5.19 show the fabric samples incorporating the CNT Z yarns. Although they are much smaller than the S-2 glass rovings, the CNT Z-yarn crowns are easily distinguished due to their black contrasting color. Even though the original goal was only to incorporate the CNT yarns as Z-yarns, it might sometimes be useful to utilize the multifunctional properties of the yarns in either the warp or fill orientations, or both. To demonstrate this possibility, a 50 cm section of the 25-ply CNT yarn was used as the top filling layer. Although the insertions were successful, the tension control mechanism would need to be slightly modified to accommodate for continuous weaving.

Fig. 5.19 shows fabric sample woven with CNT yarns incorporated into it. The same process of superglueing the CNT yarn in line with the S-2 glass Z-yarn was used to replace the six S-glass Z-yarns in the middle of the fabric with CNT yarns. The final length of the produced fabric was 8 cm. Due to the thickness of the fabric, the length of the fabric that can be created is approximately one sixth of the length of the Z-yarns. Using 3WEAVE® Fabric Design software, the fabric parameters were calculated and are shown in Table 5.1. Most importantly, one can see the higher than usual total estimated fiber volume fraction, and much lower than usual Z-yarn fiber volume content. This proves the validity of the hypothesis of increasing in-plane properties of 3D woven fabrics with incorporated CNT Z-yarns [19].

It is important to emphasize again that all 3D weaving trials described in this section have been performed in a fully automated regime of machine operation. This means that continuous production of 3D woven CNT yarn fabric is feasible on 3TEX equipment with a relatively large speed and in industrial volumes.

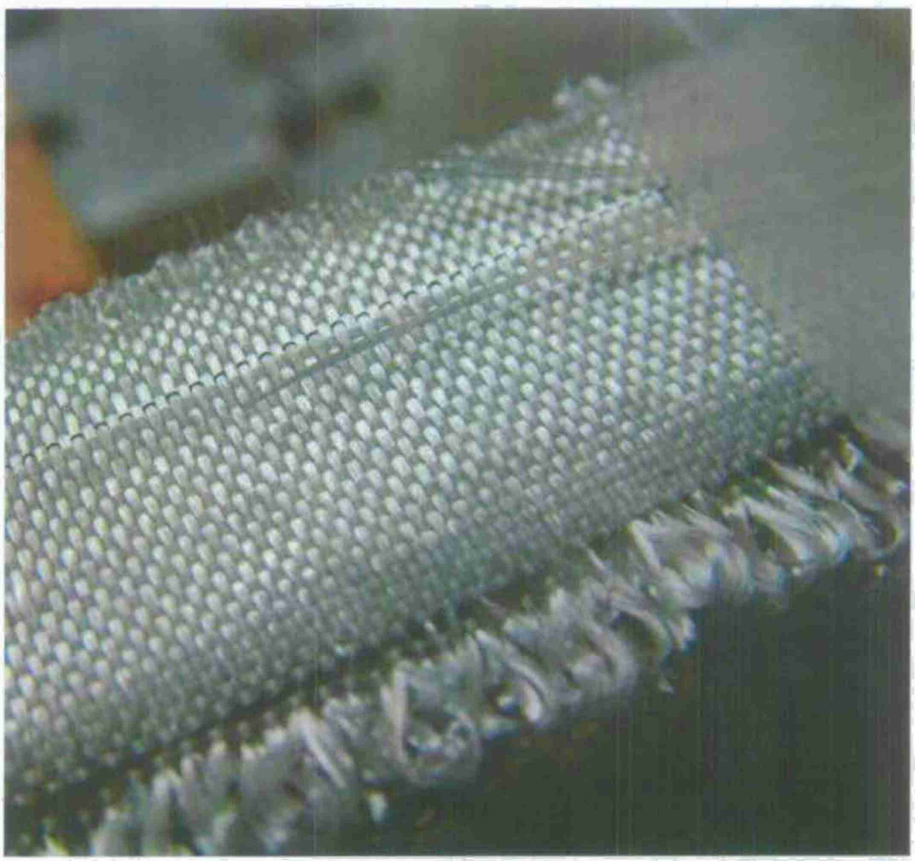

Figure 5.16. 3D woven fabric produced in the first weaving trial with incorporated 25-ply CNT yarn seen as black Z-yarn crowns near the top of the image.

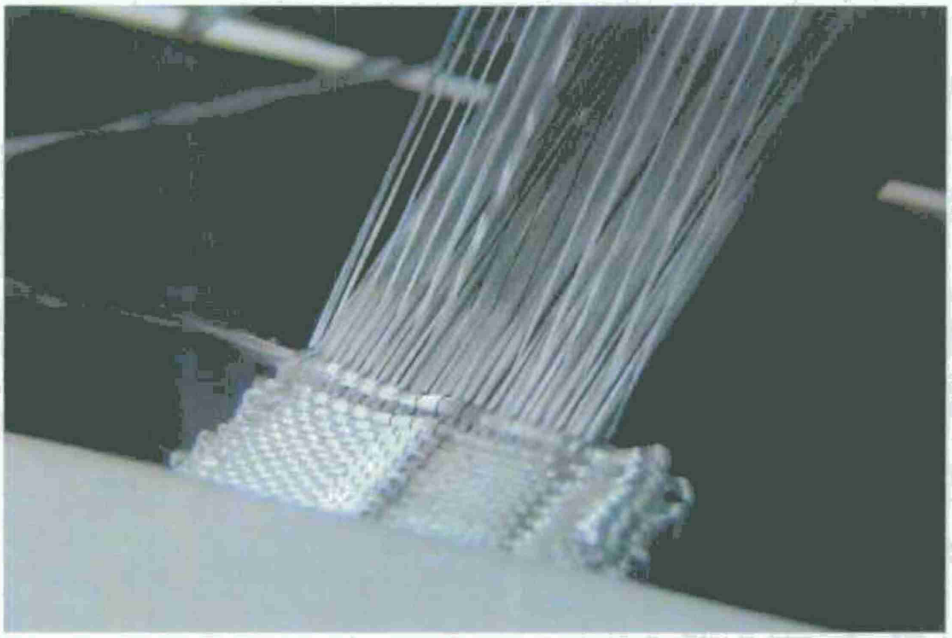

Figure 5.17. Fabric formation point when weaving with six 25-ply CNT yarns.

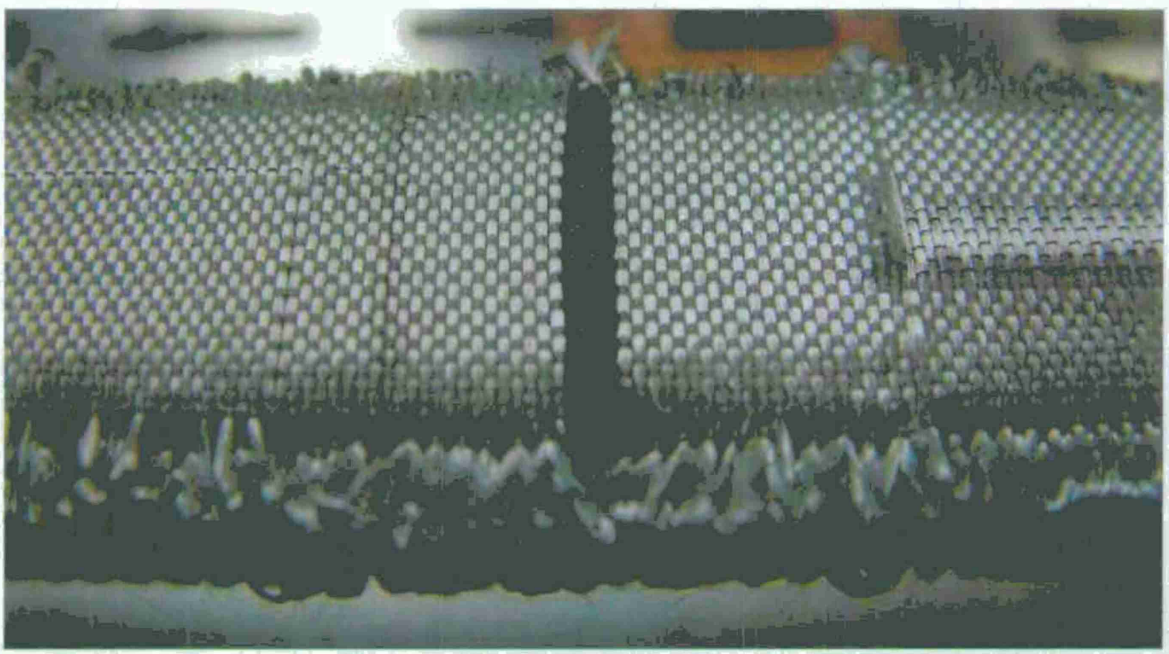

Figure 5.18. Produced sample of 3D woven fabric with 25-ply CNT yarns used as weft inserted yarns seen as the dark band in the central part of the image.

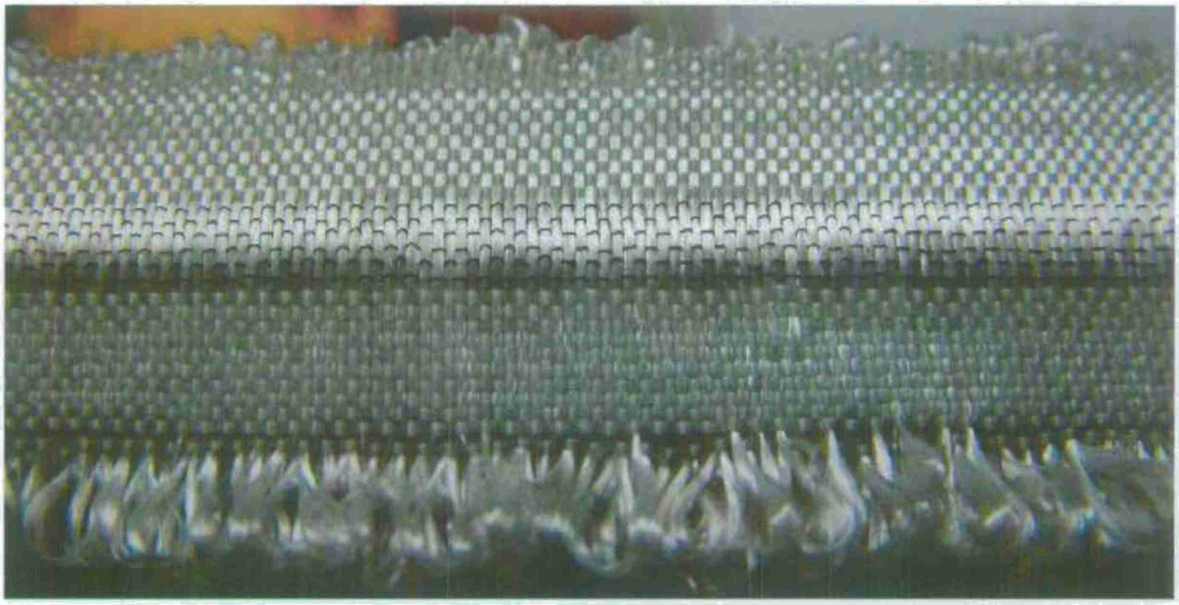

Figure 5.19. 8 cm long sample of 3D woven fabric with six 25-ply CNT Z yarns seen as a dark strip of Z-crowns in the central part of the fabric.

Table 5.1. Fabric construction parameters of 3D woven fabric with S-2 glass warp and fill yarns and 25-ply CNT Z yarns.

Fabric Parameter	Value
Specific Weight	94.8 oz/yd^2
Fabric Thickness	2.42 mm
Fiber Volume Fraction	53.5%
Volume of Resin Pocke	10.4%
Z- Fiber Volume Fractic	1.1%

SECTION 6

Geometrical, Structural and Mechanical Characterizations of the Dry CNT Yarns and 3-D raids

6.1. Baseline Tensile Testing of Carbon Fiber Filaments

Carbon nanotube yarns are only microns in diameter and thus have a low breaking force at failure. To test them in tension, an Instron 5544 tensile testing machine shown in Fig. 6.1 was used. The machine has a 5N load cell. This type of low force load cell is more accurate at extremely small loads and is commonly used for single filament fibers, small yarns, and thin films. Hexcel AS4 carbon filaments were tested to provide baseline data for future experiments. The obtained data could be compared to fiber manufacturer's test data for the same type of carbon fiber to make sure that the testing procedure was correct.

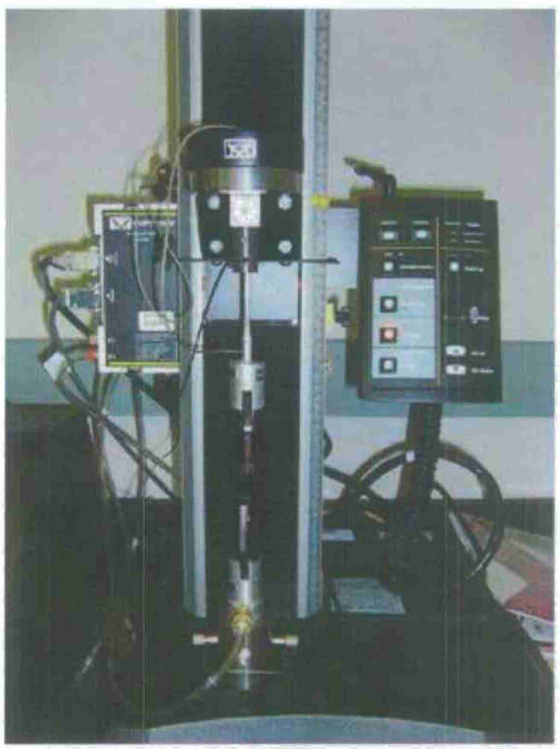

Figure 6.1. Instron 5544 Tensile testing machine.

A 50 mm length of 12K AS4 carbon fiber was cut off from a large yarn package. This piece was then soaked in a bath of water to remove the sizing. That allowed the individual filaments to separate much easier. After the fiber was dried, single filaments were carefully extracted from the large tow using fine tweezers. They were mounted and tested according to the ASTM C1557-03 standard. Tabs for securing the fibers were made by printing out a pattern on piece of

cardstock paper. The holes in the tabs were exactly 10 mm wide and were cut out using a razor blade. The tabs were secured to a piece of foam core board with tape for stability when mounting the carbon filaments. The carbon filaments were placed in the right position and taped at the ends to prevent them from moving while the epoxy was curing.

The epoxy system used for securing the fibers was an Epon 9504 and Epi-Cure 9554 mixture. Small drops of epoxy were applied to the tabs to permanently secure the filaments for testing. The epoxy was allowed to cure for 16 hours at room temperature and then was post cured at 90°C for one hour. The results of 15 tensile tests can be seen in Fig. 6.2. The average strength of 15 fiber samples was determined at 4034 MPa and average modulus was 205 GPa. These values are in good agreement with the manufacturer's data of 4278 MPa and 228 GPa, so it was deemed that equipment was operating properly and the method used for mounting and testing was correct.

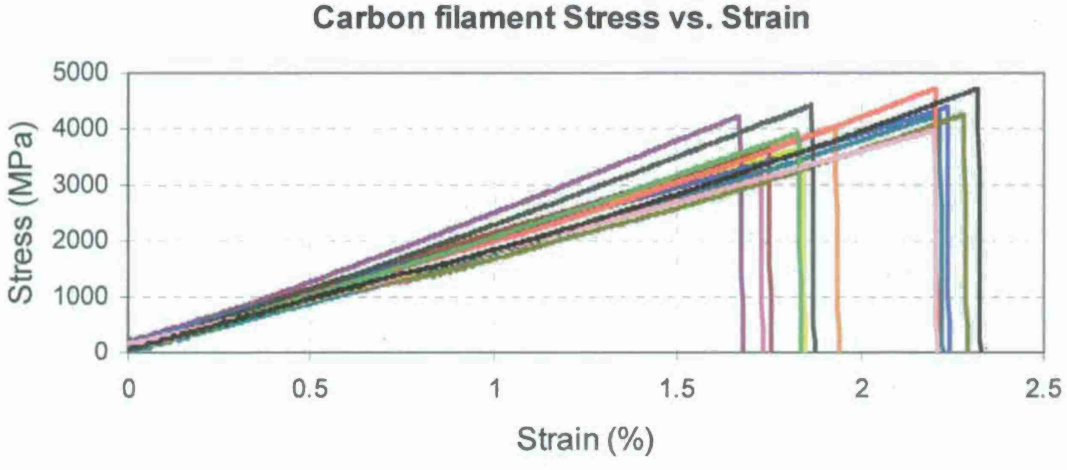

Figure 6.2. Stress vs. strain curves for AS4 carbon filaments.

6.2. Tensile Testing of 5-Ply Carbon Nanotube Yarn

Before any composite samples were made, the pure carbon nanotube 5-ply yarns, 25-ply yarns and 3-D braid were tested for tensile properties. It was thought that the dry yarns would behave much differently than the same yarns impregnated with epoxy. The yarns and the braid were tested on the same Instron machine which was used for the tests described in Section 6.1. The 5N load cell used to test the carbon filaments there was used to test the plied yarns, and a 100N load cell was used for the braided samples.

All samples had a gage length of ten millimeters and were secured to cardstock tabs using an Epon 9504 and Epi-Cure 9554 epoxy mixture. The yarns were tabbed in the same manner as the carbon fiber filaments. The first samples produced were viewed under optical microscope and resin could be seen coating the nanotube yarn about 1 mm away from the edge of the tab. It was thought that the epoxy had a low enough viscosity that it was being pulled down the surface of the yarn by small capillaries in the nanotube structure between the plies. When mixing the epoxy for the next set of samples, the mixture was allowed to become more viscous before application

on the tabs. When these samples were viewed under optical microscope, no epoxy was seen on the nanotube fiber. Fig. 6.3 shows a 5-ply nanotube yarn that has been tabbed with epoxy.

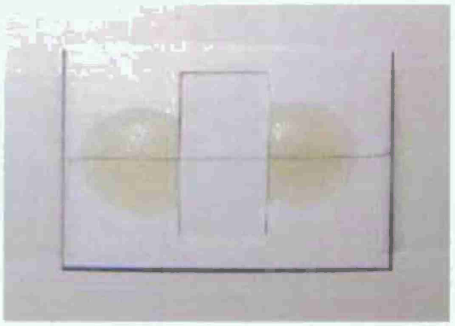

Figure 6.3. Tabbed 5-ply nanotube yarn sample.

All of the 5-ply yarn samples for the tensile tests reported below were taken from the same spool containing approximately 1 meter of yarn so that tensile properties between yarns from different spools (and, likely, having different diameters) would not be compared. The rest of the yarns were used in the braiding process. Because of the limited amount of yarn, some tests were conducted with only a few repetitions.

The first test conducted with the tabbed 5-ply samples was designed to test for viscoelastic behavior in the yarns. In normal polymeric fibers testing the same fiber at slow extension and fast extension rates produces different curves. In slow testing the polymer chains have time to disentangle and move past each other. With a high rate of extension the chains become trapped and do not have sufficient time to untangle. Polymeric material tested at a higher rate usually shows a higher modulus and lower strain to failure than if it is tested very slowly. Figs. 6.4 and 6.5 show that there was almost no difference between the 5-ply yarns tested at 10 mm/min and 0.1 mm/m rates. The observed minor difference among the curves can be rather attributed to the natural scatter of the yarn sample properties than to the difference in extension rate.

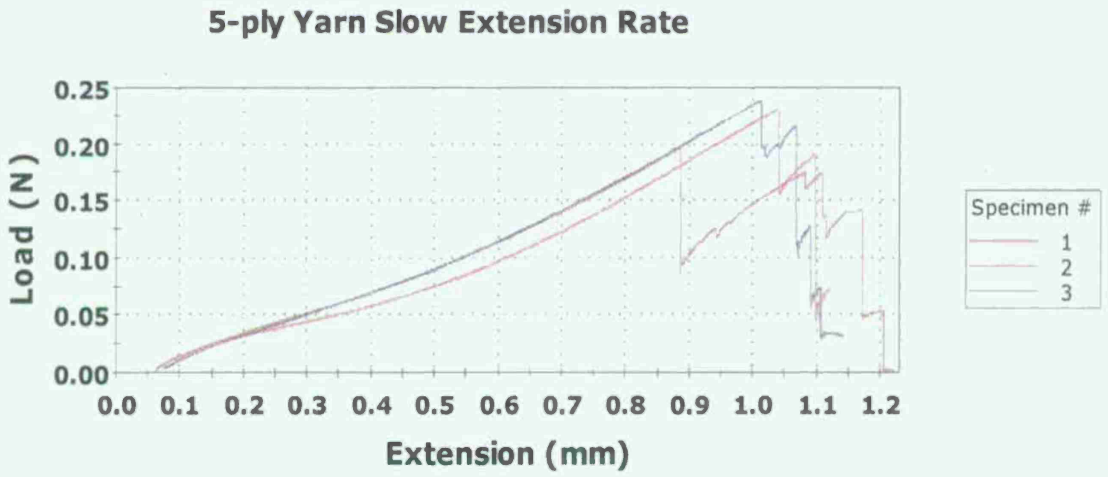

Figure 6.4. Load vs. extension curves for 5-plys nanotube yarn samples tested at 0.1 mm/m.

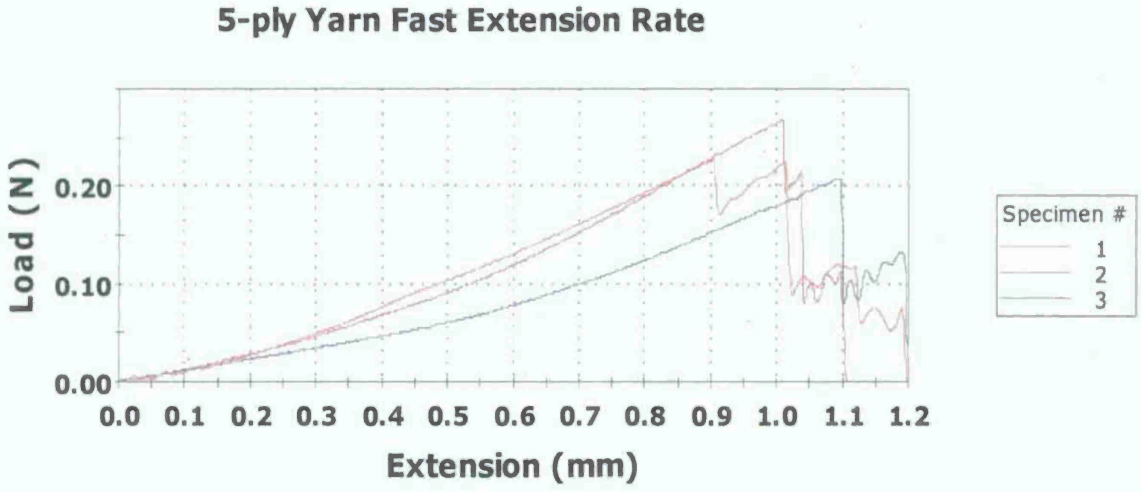

Figure 6.5. Load vs. extension curves for 5-ply nanotube yarn samples tested at 10 mm/m.

Five samples of the 5-ply yarn were then tested to measure the uniformity of breaking loads within the sample. The spool of yarn chosen was one that looked like having a visually average diameter. The load vs. extension curves for these five tests are presented in Figure 3.6. The yarns all failed within a small range of tensile load, between 0.22 and 0.25 N, and the failure strain varied from 8.4 to 9.5%.

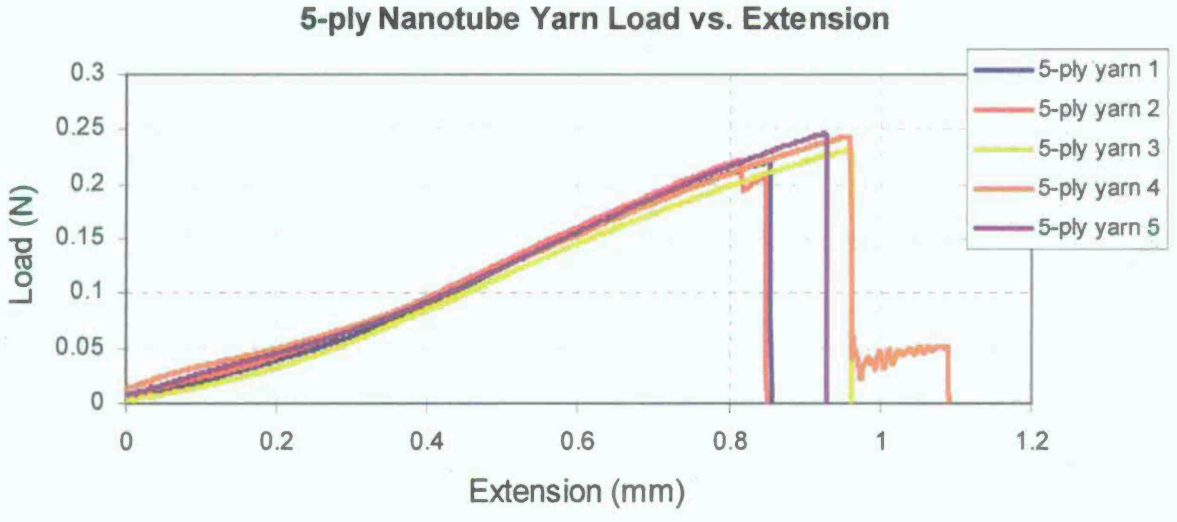

Figure 6.6. Load vs. extension curves for 5-ply nanotube yarns tested from the same spool.

The next test was conducted for 5-ply nanotube yarns with a gauge length significantly larger than the previous samples. Previous samples were tested at 10 mm while in this test two yarns of 50 mm gage length were tested. Fig. 6.7 shows results of these tests. Some difference between the group of five black curves (10 mm gage length) and two red curves (50 mm gage length) is

seen, however it is hard to say if this is due to the difference in gage length or simply due to a scatter in the yarn sample properties.

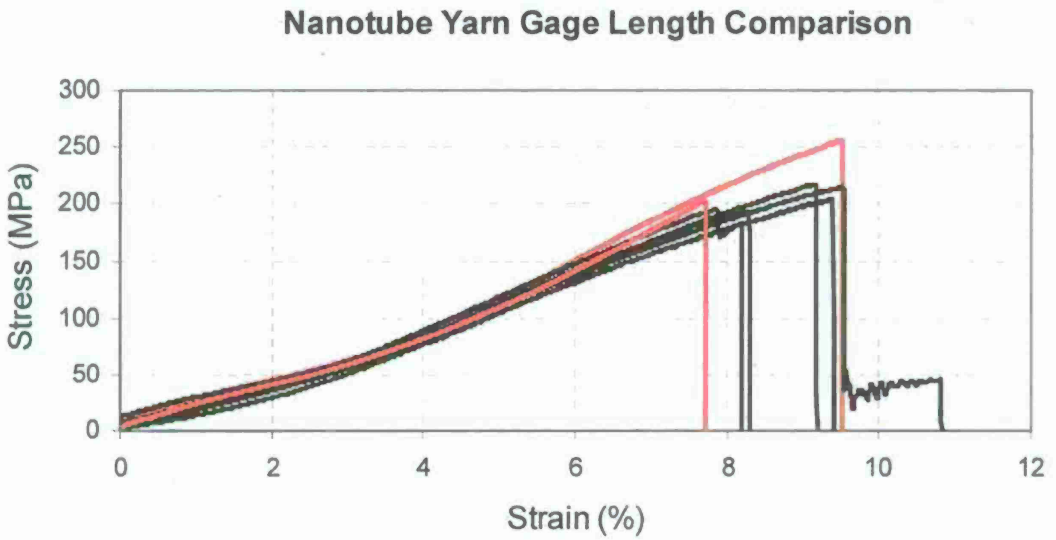

Figure 6.7. Tensile tests of 5-ply nanotube yarn samples with 10 mm gage length in black and 50 mm gage length in red.

It was noticed that the 5-ply nanotube yarns studied here have visibly different diameters when viewed on the spools with the naked eye. This is confirmed by the optical microscope picture shown in Fig. 6.8 - one can clearly see that there is significant variation in the yarns diameter when they are viewed at 63X magnification.

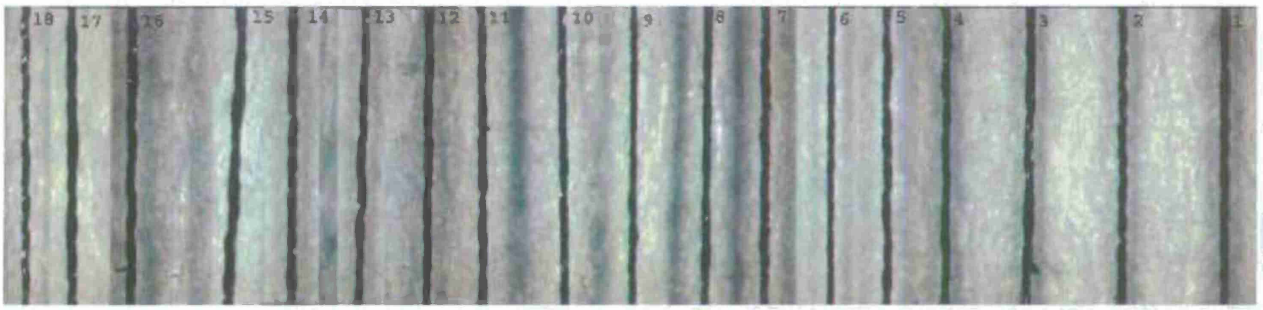

Figure 6.8. Yarns from 18 different spools used for braiding.

It is hard to tell whether the twist level is the only factor that significantly influences the 5-ply yarn diameter. Fig. 6.9 further shows a close-up of the first six yarns from Fig. 6.8 obtained with a SEM. It is recognized that even those yarns which have a similar level of twist vary significantly in diameter. This effect of the yarn geometry variation has significant meaning when comparing breaking loads of yarns taken from different spools.

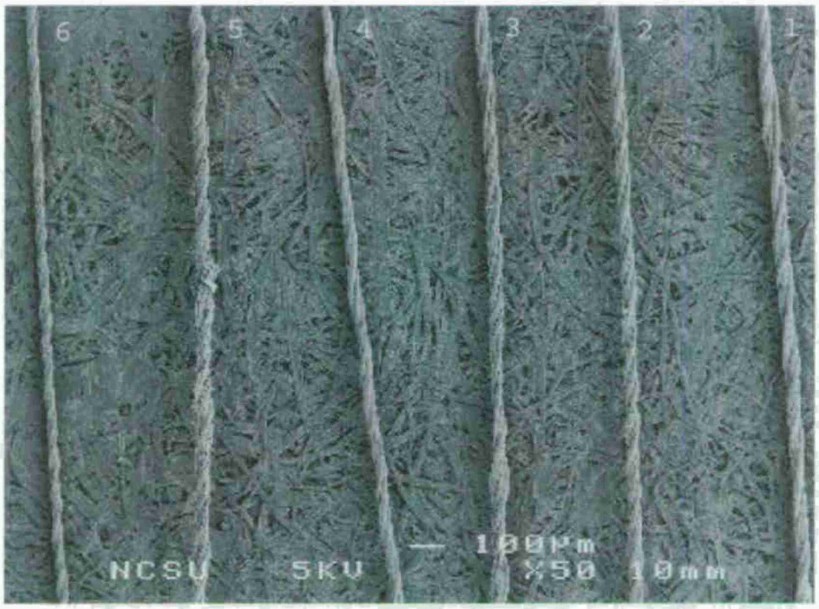

Figure 6.9. Comparison of 5-ply yarns from different spools.

6.3. SEM Study of Carbon Nanotube Yarns

The nanostructure of the 5-ply nanotube yarns was studied in a JEOL 6400F Field Emission Scanning Electron Microscope. This equipment allowed for extremely high magnifications where single nanotubes can easily be distinguished. Figs. 6.10-6.12 show a series of pictures taken at successively increasing magnifications. A preferred orientation of the nanotubes and nanotube bundles can be seen in Fig. 6.10. The nanotube orientation angle was measured using Scion Image software and was found to be 33°.

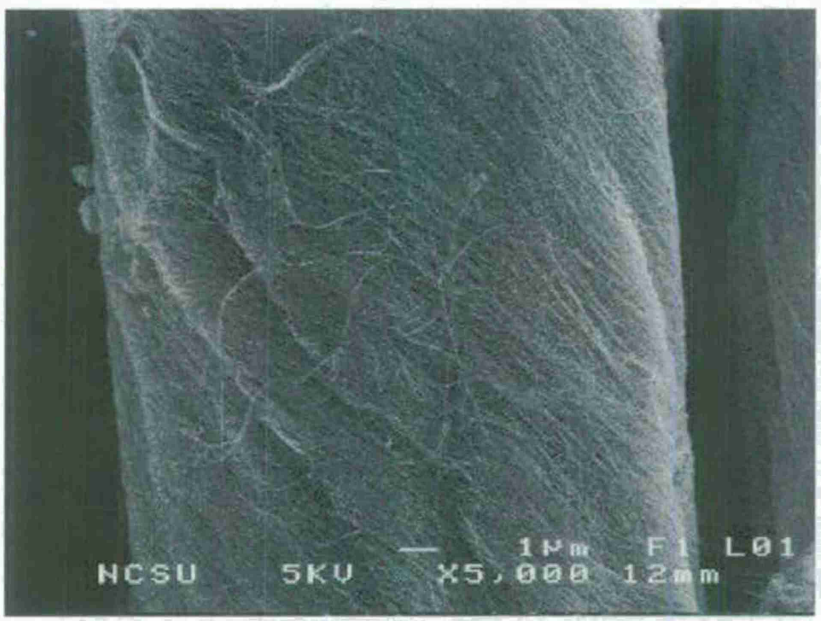

Figure 6.10. 5-ply nanotube yarn viewed at 5000x magnification.

Fig. 6.11 provides a closer view of the same yarn. Large bundles can still be seen with a preferred orientation but there are many individual nanotubes and small bundles thereof that are not in line with the aforementioned orientation angle. Fig. 6.12 further details the nanotube yarn morphology, and individual 10 nm diameter nanotubes can be distinguished. This close-up shows a much more disordered nanotube arrangement, and it becomes more difficult to determine the direction of preferred alignment.

Figure 6.11. 5-ply nanotube yarn viewed at 20,000x magnification.

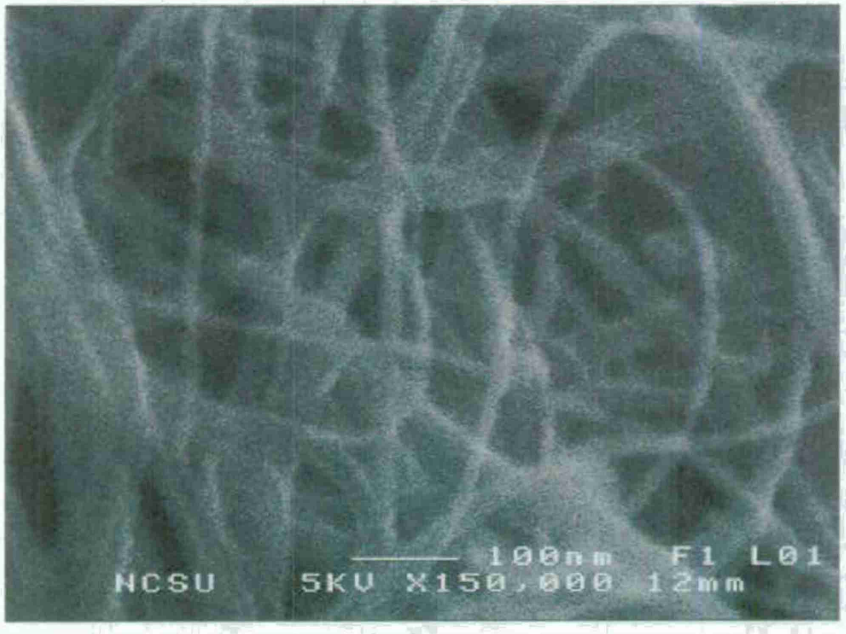

Figure 6.12. 5-ply nanotube yarn viewed at 150,000x magnification.

Clearly, in order to better utilize unique mechanical properties of carbon nanotubes, in the future work it is necessary to significantly improve alignment of the nanotubes and their bundles within the yarn and also reduce the angle between their preferred orientation and longitudinal axis of the yarn. Also importantly, improving orientation of the nanotubes would simultaneously increase their packing density.

6.4. Tensile Testing of 25-Ply Nanotube Yarn and 3-D Nanotube Braid

Two samples of the 25-ply nanotube yarns used in 3-D weaving and one sample of 3-D braid made of 5-ply nanotube yarns were also tested on the Instron machine described above. Load vs. extension curves for the three samples are shown in Fig. 6.13. For comparison, one curve that well represents the behavior of the previously tested 5-ply yarns is also included in the figure.

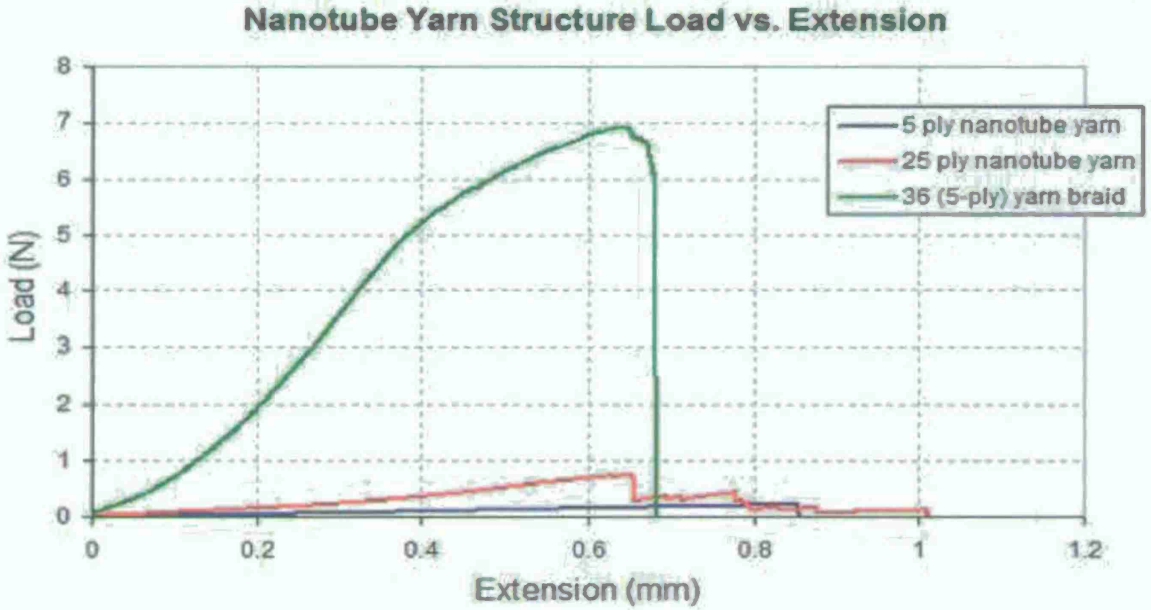

Figure 6.13. Load vs. extension curves for the nanotube yarns and 3-D braid.

Not to surprise, the braid containing 180 single yarns was able to withstand a much greater force than both the 25-ply and 5-ply yarns before failing. Therefore, it is more informative to determine what the difference is in the load per single yarn in each of these structures. Such load values were calculated and are presented in Table 6.1. It is seen that the single yarn in the braid holds 83% of the load that the single yarn holds in the 5-ply yarn (recall that the latter one was the raw material for braiding). This high value indicates that very little damage was imparted on the yarn during our 3-D braiding process (additional Optical Microscope and SEM observations of the surface of the braid confirmed that damage was practically non existent). It is further seen from Table 6.1 that the 25-ply yarn holds only 58% of the load that the single yarn holds in the 5-ply yarn. The single yarns in the 25-ply yarns could be seen fraying during the testing, causing the jagged downward slope on the load-extension curve. The fraying was caused by uneven load distribution across the single yarns. A large number of single yarns in 25-ply yarn allowed them to break gradually, without causing the whole 25-ply yarn to fail catastrophically. At the same time, this effect has substantially lowered the load bearing capability of the 25-ply yarn. Keeping

the discussed effects in mind, one could speculate that substantial reduction of the load bearing capability could have happened between the bundle of 5 parallel single yarns and the twisted 5-ply yarn. The conclusion is that it is desirable to minimize the twist rate and apply as even tension as possible to the single yarns when processing multi-ply nanotube yarns.

Table 6.1. Comparison of breaking load per single yarn in the plied nanotube yarns and in 3-D braid.

Plied Yarn/3-D Braid	Number of single yarns	Breaking load (N)	Breaking load per single (N)
5-ply yarn	5	0.233	0.0466 (100%)
25-ply yarn	25	0.674	0.0270 (58%)
3-D braid	180	6.95	0.0386 (83%)

6.5. Determination of the Yarn Cross-Sectional Area

To determine the stress and strength on each one of the tested yarns and braids, their cross-sectional areas have to be defined. For traditional textile plied yarns such as cotton or wool, the cross sections are not usually measured and used. The strength of such yarns is measured in tenacity, which is derived from the linear density and the breaking force. However, the stress values for fibers and yarns used in composites are usually measured by dividing the force over the fiber/yarn cross section, which is quite easy to determine for sufficiently rigid carbon, glass or ceramic fibers. For example, each kind of carbon fiber has well documented diameter value, which allows one to determine the cross section of 1K, 3K, 6K, 12K, etc. yarns with high certainty. Contrary to that, carbon nanotube yarns, especially twisted multi-ply ones, pose a challenge in cross-sectional area measurement. Once twisted, they loose their circular shape. This leads to three optional approaches to measuring their cross-sectional area, which are described next.

The first approach assumes measuring the cross section of one single yarn and then multiplying the result by the total number of singles in the multi-ply yarn, with account for some idealized packing model. This method is prone to error if the yarns are compressible, if they do not pack "perfectly" (in accordance with the model adopted), or if they vary in diameter. When using SEM measurements, what is assumed to be the "yarn diameter" may be just a randomly taken measurement of some dimension in the plane perpendicular to the yarn axis. For a single nanotube yarns such "diameter" measurement varied between 10 and 20 μm. Such a huge scatter of this geometric parameter obviously rules out this approach as the means of yarn cross-sectional area measurement.

The second, direct approach is based on SEM images obtained for the actual plied yarn or braid using Scion Image software. This allows for calculating an average diameter along the yarn length, as illustrated in Fig. 6.14. A representative sample from the group of 5-ply yarns that were used in braiding was chosen, and its "diameter" was measured at 36 points along the length. An average value of 46 μm was obtained with corresponding cross-sectional area of 1662 μm^2. The irregular (non-circular) cross section of a plied yarn may impart significant error on the cross-sectional area determination by this method, because it implies that all yarn cross sections are perfectly circular. In the case of elliptical cross section, for example, the observed "diameter"

variation along the yarn length could be simply due to rotation of the same ellipse in the plane perpendicular to the yarn axis, while the whole ellipse is not recognizable on SEM images.

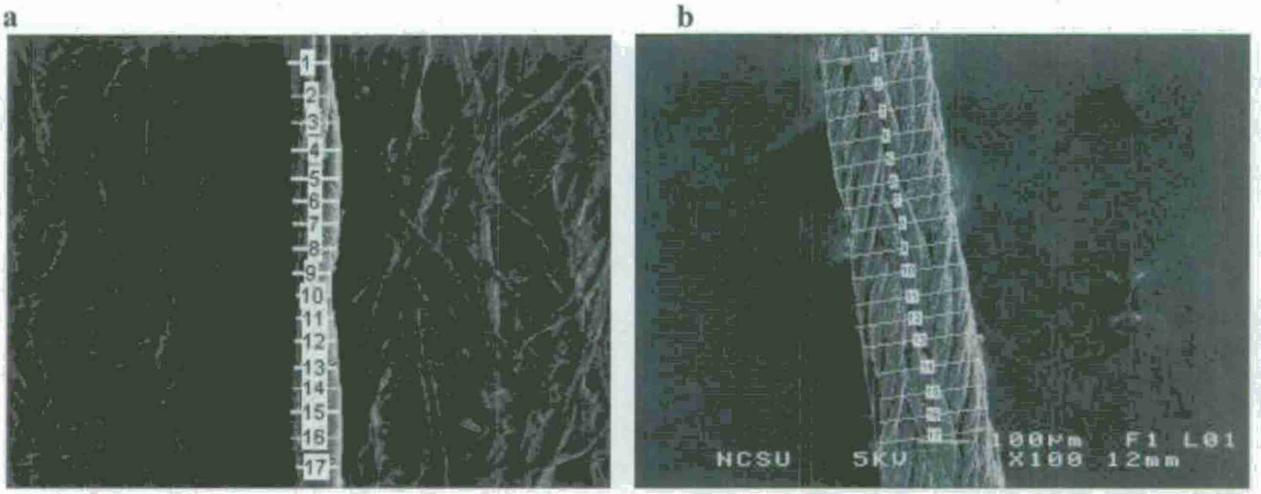

Figure 6.14. Application of the Scion Image method to the average diameter determination of the 5-ply nanotube yarn (a), where 17 of total 36 probes shown, and of the 3-D nanotube braid (b).

Measurements of the 3-D braid cross-sectional dimensions using this approach should be more accurate due to the use of thirty six 5-ply yarns results in kind of "smearing" their geometric non-uniformities along the yarn length. The braid's side length was determined as 211 µm from 17 measurements taken along its length.

The third method, which is much most complex, costly and time consuming, consists of taking measurements on the fracture surface of composite made from the yarn of interest. Areas of irregular shapes in the broken composite cross section can be directly measured using Scion Image software. With this type of software, a reference length is produced from the scale bar on the SEM picture and then an outline of the structure is traced on the picture using the freehand tool. Using the reference length, the software provides the total area within any closed contour line. Fig. 6.15 illustrates application of this method. The measurements were taken for five different 5-ply yarns inside the 25-ply yarn composite. The dark areas are nanotube-epoxy yarn regions, while the bright outlines are pure epoxy resin areas which were charging in the SEM because of the lack of conductive nanotubes in them. This method seems to be more accurate for determining the cross-sectional area of the plied yarns than the other two methods described above, because the actual shape and packing of single nanotube yarns can be easily viewed and quantified, rather than being assumed or fit to some geometrical model. As Fig. 6.15 illustrates, single yarn cross sections in each of the 5-ply yarns are far from circular; each of them changes its shape to pack more tightly in the twisted plied yarn than circular cylinders would do.

The above method has been adopted here for the plied yarn and braid stress-strain plotting and strength evaluation.

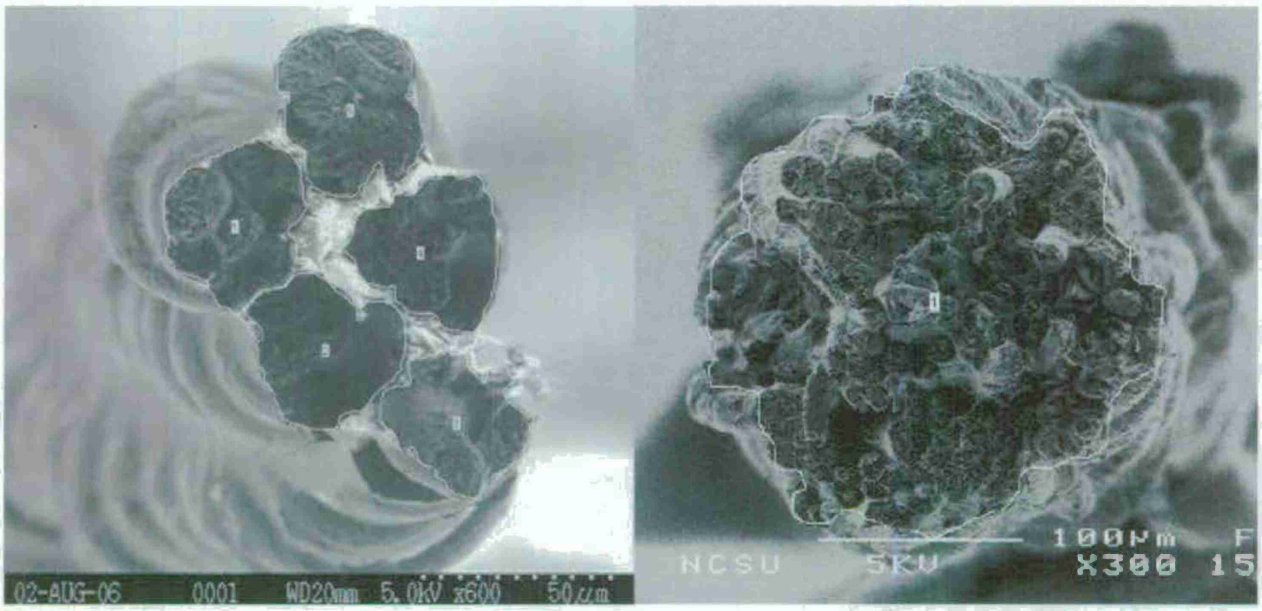

Figure 6.15. Cross-sectional area measurements of five 5-ply yarns within composite using Scion Image software.

6.6. A Comparison of Stress-Strain Curves for the Plied Yarns and 3-D Braid

Tensile stress vs. strain curves for the 5-ply yarn, 25-ply yarn, and 3-D braid are shown in Fig. 6.16. The following cross-sectional areas (determined with the third method of Section 6.5) were used here when calculating stresses from the recorded loads: 1137 μm^2 for 5-ply yarn, 5685 μm^2 for 25-ply yarn, and 39212 μm^2 for 3-D braid. It is seen from the figure that the highest strength (~200 MPa) is reached for the 5-ply yarn; the braid has ~155 MPa strength (78% of the 5-ply yarn strength), and the 25-ply yarn has ~125 MPa strength (62%). These values are in a good agreement with the failure load ratios from Table 6.1 (83% and 58%, respectively), which confirms the accuracy of cross-sectional area determination.

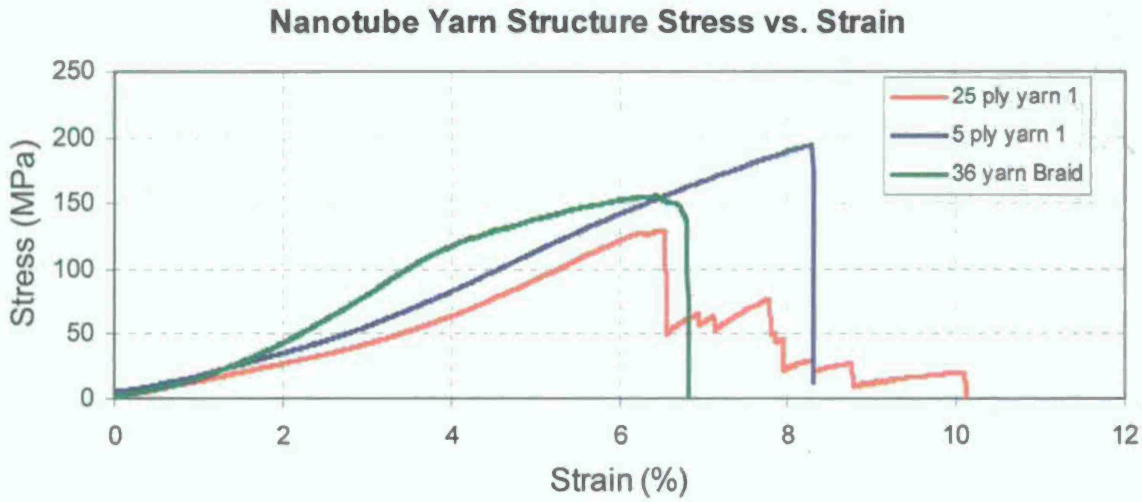

Figure 6.16. Stress vs. strain curves for 5-ply and 25-ply nanotube yarns, and 3-D braid.

Though the ultimate failure strain of the 25-ply yarn has the highest value (~10%), the load bearing capability of this material drops by more than a half at ~6.5% strain, which is even lower than the ultimate failure strain of the braid. The 5-ply yarn has the highest ultimate failure strain, above 8%, and breaks catastrophically.

Fig. 6.17 further illustrates the failure surfaces of the nanotube yarns in the braid. Each surface shows a necking effect caused by so-called "drafting", and a close-up shows bundles of nanotubes being pulled away at the very tip of the failure zone.

Figure 6.17. Failure surfaces of nanotube yarns in the 3-D braid.

The ultimate failure strain values, as well as related flexibility of the studied carbon nanotube yarns and 3-D braid are much higher than those of conventional carbon fibers and yarns used in high performance composites. Of course, this is due to the complex hierarchical structural organization of the novel textile materials fabricated and studied here. The nanotube yarns are held together primarily by van der Waals forces and mechanical friction. The yarns also contain free interstitial spaces that result mainly from the nanotube bundle misalignment in the "forest" and by various manufacturing artifacts in the drawing and twisting process from the forest. Different obstacles do not allow for perfect packing and alignment of the nanotubes in the spun yarns. Further loss of alignment and packing density is due to the secondary twist, which is applied when processing plied yarns.

Although mechanical characterization of the single nanotube yarns was not performed in this study, one can anticipate from experimental results presented in Fig. 6.16 that such yarns would probably have strength in the range of 350-400 MPa and would break catastrophically at about 10% strain.

SECTION 7

Fabrication and Mechanical Characterization of CNT Yarn and 3-D Braid Composites

7.1. Fabrication of Nanotube Yarn and 3-D Braid Composites

The resin system selected for processing first carbon nanotube yarn and 3-D braid composite samples was Epon 9504 epoxy with Epikure 9554 curing agent. This low viscosity resin system is often used for Vacuum Assisted Resin Transfer Molding (VARTM) applications. The manufacturer recommends mixing the resin at a 100:25 parts by weight ratio of epoxy to hardener and this combination produces a resin with initial viscosity of 300cp at room temperature. Heating the resin to 60°C lowers the viscosity to around 90cp. The pot life of the resin at 60°C is approximately 45 minutes. With the intent to get full resin penetration into the nanotube yarns and braids, a very low viscosity resin system was first selected. To achieve this, Heloxy 116 modifier was used in the fabricated samples to vary the viscosity of the resin system in a broad range. Heloxy 116 is a monoepoxide modifier, which can be added in large amounts without extreme changes in the hardened epoxy's properties. Unlike other solvents often used to lower the viscosity of epoxy resin systems, Heloxy 116 is bonded into the cross-linked network.

As the amount of modifier was increased and the viscosity of the resin was decreased, the mechanical properties of the matrix material were also somehow affected. To quantify this effect of the modifier on pure matrix properties, several samples were made with varying amount of the modifier. Samples of resin were mixed where modifier accounted for 0, 20, 30, and 40% of the epoxy's weight. As the amount of modifier increased, the amount of hardener had to be reduced accordingly. The mix ratios for the four samples fabricated and tested were 100:0:25, 80:20:22, 70:30:21 and 60:40:20 parts by weight of epoxy to modifier to hardener.

The resin was mixed thoroughly and then cast with a thickness of one millimeter on a level and polished aluminum plate. The resin was contained on the plate by "tacky tape", a thick rubbery sticky material used for sealing in VARTM processes. The plate was put in a vacuum oven for 15 minutes at 60°C to remove all the air bubbles. The viscosity was low enough to allow releasing the bubbles within first 5 minutes. The samples were then allowed to cure for 16 hours at room temperature and after that were post-cured at 90°C for one hour. The resin sheet was then removed from the plate and cut with a razor blade and a guide into 12 mm wide strips. Five strips of each kind were tested under tension on the same Instron machine described in Section 6.1.

7.2. Mechanical Test Data for Neat Epoxy Resins

Test results for fabricated four different epoxy matrix materials are presented in Table 7.1. It is clearly seen that the increase of modifier fraction results in a sharp reduction of modulus and strength, with as sharp increase of strain-to-failure. Of course, only the first recipe, without

modifier, would be considered for practical structural composites, however our intent here is to investigate how these four very different matrix materials would affect mechanical properties of the nanotube yarn and braid composites.

Table 7.1. Mechanical properties of Epon 9504 epoxy with different content of Heloxy 116 modifier.

Epoxy:Modifier:Hardner R	Modulus (GI	Tensile Strength (MI	Strain at Failure
100:00:25	2.43	64.71	3.6
80:20:22	0.48	33.8	22.5
70:30:21	0.19	11.61	62
60:40:20	0.03	6.58	89.3

7.3. Processing Composite Samples

The first composite samples were produced with the use of the smaller 5-ply and 25-ply yarns and with the lowest viscosity epoxy formulation, 60:40:20. The idea was to provide the most favorable conditions to the epoxy for penetrating inside the multi-ply and single yarns, and to wet and bond the nanotubes/nanotube bundles as well as possible. The nanotube yarns were placed in the epoxy bath and then heated and evacuated in a vacuum oven for 20 minutes at 60°C. Heating the resin further reduced the viscosity. The goal was to evacuate the microscopic air bubbles trapped between groups of nanotubes and allow the low viscosity resin to penetrate fully and diffuse into and around the most tightly packed areas of nanotubes. The samples were removed and placed on a paper towel to soak up any excess of resin and then were mounted on tabs under slight tension to prevent them from sagging. This lowest viscosity formula also ensured that no excess resin beaded on the surface of the yarn and thus a very uniform composite would be produced. After 16 hours, the mounted samples were post cured at 90°C.

To produce the 3-D braided nanotube composite samples, a 3" (7.5 cm) long piece of braid was placed into a bath of the mixed resin system. This was heated and evacuated in a vacuum oven for 20 minutes at 60°C. The infused braided samples were removed from the resin bath and attached to a spring loaded curing fixture shown in Fig. 7.1.

The springs provided approximately 25g of tension onto the curing sample. The curing fixture was placed in the oven at 60°C while the excess resin dripped off of the braid. After 10 minutes, any excess resin was blotted off of the braid and the fixture was set in a stable place for curing. The samples were allowed to cure for 16 hours at room temperature and then were post cured at 90°C in the oven. The first sample produced had a larger than expected cross-section and showed excess pockets of resin when the fracture surface was studied with a SEM. It was thought that the tension was too low during curing. The spring tension was increased to 100 grams for subsequent samples, and this eliminated the problem. Braided composite samples were fabricated with all four of the resin formulas listed in Table 7.1. Fig. 7.2 shows the size scale of the braided composite samples tested under tension.

Figure 7.1. Curing apparatus for braided composite samples.

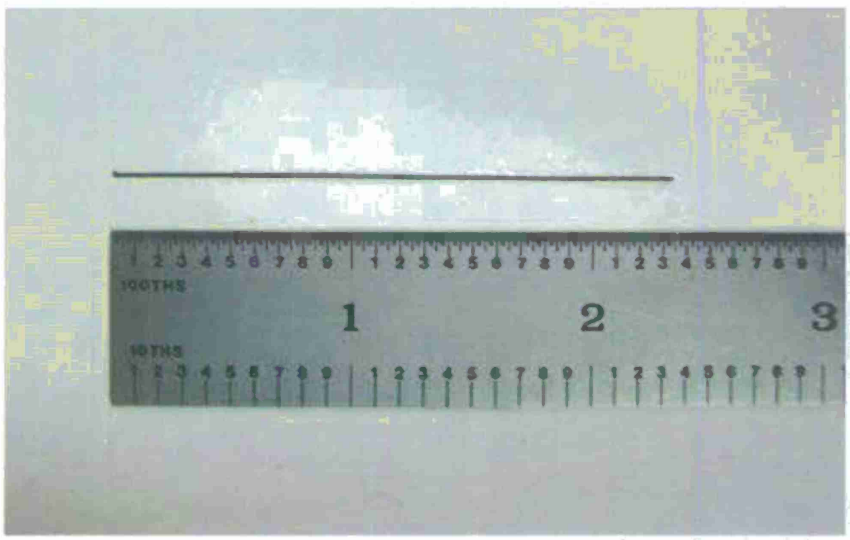

Figure 7.2. Scale of braided composite sample in inches.

Density of the 3-D braided nanotube composites was determined using the cross-sectional area measurements, the length measured with a micrometer, and the measured weight of each sample. The four composite samples ranged in density from 1.243 g/cm^3 to 1.247 g/cm^3 with an average of 1.244 g/cm^3. The density of the resin was calculated from a hardened and cured cylindrical sample and found to be 1.153 g/cm^3.

7.4. Tensile Testing of Nanotube Yarn and 3-D Braid Composites

The composite samples made with the 5-ply nanotube yarn, 25-ply nanotube yarn, and 3-D nanotube braid reinforcements, were all tested on the Instron tensile tester mentioned before. To ensure that the samples were properly aligned in the grips and to eliminate stress concentrations on the composites during testing, the samples were tabbed using epoxy as shown in Fig. 7.3. The gage length was 10mm for the 5-ply and 25-ply yarn composite samples, while it was 20 mm for the braided composite samples. All of the samples failed outside the gripping zone. To calculate stress values, cross-sectional area of each sample was experimentally determined. Each structure was viewed in SEM and Scion Image software was used to outline the fracture surfaces and directly measure the area. The following cross-sectional area values have been obtained and used for the stress calculation: 1137 μm^2 for 5-ply yarn composite, 6609 μm^2 for 25-ply yarn composite, and 39212 μm^2 for 3-D braid composite.

Figure 7.3. Tabbed braided composite sample.

The curves presented in Fig. 7.4 show that the highest strength value (~325 MPa) is achieved for the 5-ply yarn composite, similarly to what was observed in the dry yarn testing (see Section 6.2). The 3-D braid composites and the 25-ply yarn composite show close strength values between 240 and 314 MPa. The braid composite fabricated without modifier failed at 1.6% strain. It was initially thought that resin was not penetrating into the structure so that micro voids were causing premature failure of the epoxy matrix around the nanotubes. The viscosity of the resin was then lowered using the modifier, and we expected that better penetration of the epoxy will increase the strength and strain to failure of the composite. However, a rather little difference in strength and ultimate failure strain appears in Figure 4.4 between the four 3-D braid composite samples made with very different viscosity resin and characterized by very different mechanical properties of the matrix material (see Table 7.1).

Further, Figure 7.4 shows that there is a substantial drop of strain-to failure values for all six composite samples compared to the dry nanotube yarns and braid (see Section 6.2). The highest ultimate failure strain, just above 2%, is observed for the 25-ply nanotube yarn composite. The 5-ply yarn and the four 3-D braid composites show ultimate strain in the range of 1.6-1.8%.

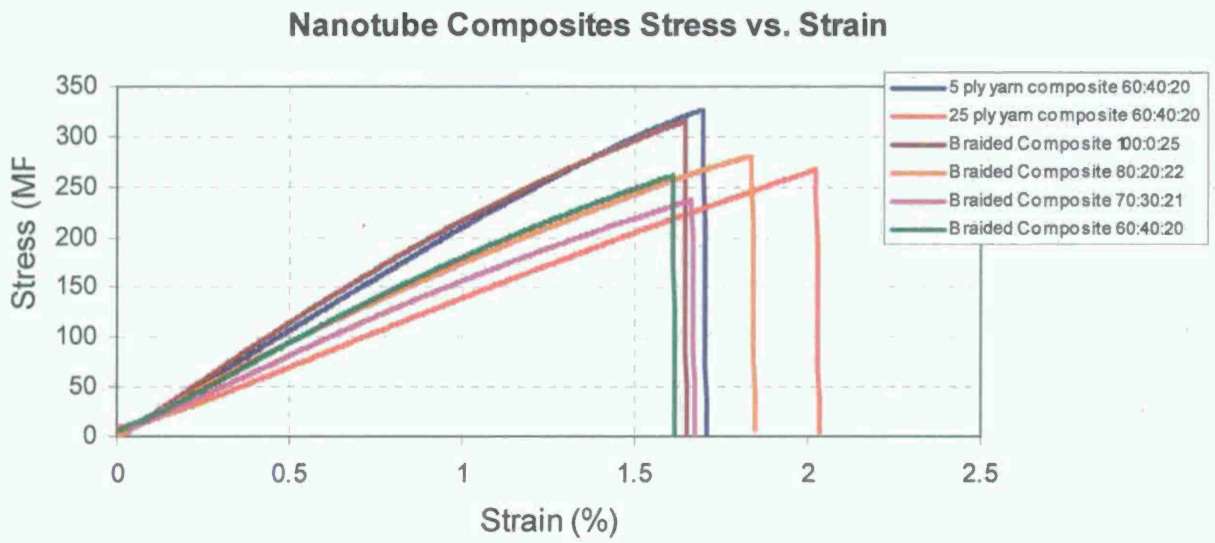

Figure 7.4. Stress vs. strain curves for different nanotube yarn composites.

7.5. Summary of the Tensile Testing Results and Initial Discussion

All obtained tensile test data for the dry reinforcements and their composites are summarized in Table 7.2. The results show that the modulus values of all tested composites are from 4 to 7 times higher than the modulus values for respective dry yarns and braids. The largest increase in modulus is observed for the 5-ply yarn composite. At the same time, the strength values have increased only by 35-100%. The largest increase in strength is again seen for the 25-ply yarn composite. It can be hypothesized that in this case the matrix material, bonding all single yarns together, provided more uniform load transfer across the 25-ply yarn cross section, and thus prevented gradual single-by-single yarn failure discussed in Section 6.

Table 7.2. Comparison of mechanical properties of dry 5-ply nanotube yarn, 25-ply nanotube yarn, 3-D nanotube braid, and their composites.

Material tested	Modulus (GPa)	Tensile strength (MPa)	Strain-to-failure (%)
5-ply dry yarn	3.04	190.44	8.95
5-ply yarn composite	21.07	319.78	1.7
25-ply dry yarn	2.35	127.47	4.62
25-ply yarn composite	14.18	261.42	2.02
3-D braid dry	3.98	173.63	6.52
3-D braid composite 100:0:25	23.91	314.77	1.63
3-D braid composite 80:20:22	19.74	274.16	1.8
3-D braid composite 70:30:21	16.07	232.01	1.72
3-D braid composite 60:40:20	18.87	255.43	1.61

The failure mode for these studied composite materials changed from a gradual slipping of nanotubes (or nanotube bundles) past one another, to a rather catastrophic nanotube breakage in the composites. This explains the dramatic decrease of strain-to-failure values in all composites compared to the dry yarns and braids. The similarly low ultimate failure strain values have been reported in other studies of carbon nanotube composites, in which nanotubes were added in high volume fractions to bulk epoxy, see for example.

One of the most interesting results following from the performed tests is that the Rule of Mixtures does not apply to the studied nanotube composites in conventional way, namely if the nanotube yarn/braid and epoxy matrix are viewed as the composite constituents. The common Rule of Mixtures predicts the modulus of a composite as a weighted average of the moduli of its individual constituents. For example, this rule well applies to predicting modulus of unidirectional carbon fiber composites in the fiber direction, considering that the constituents are a homogeneous carbon fiber and a homogeneous polymeric matrix. Contrary to that, in our case it is seen from the modulus values given in Tables 7.1 and 7.2 that the reinforcing constituent and the matrix have much lower moduli than their respective composite. The explanation of this highly synergistic effect is quite obvious: effective elastic modulus of this kind of composites is not determined by the modulus of nanotube yarn or nanotube braid, but by the modulus of individual carbon nanotubes or nanotube bundles.

The failure surfaces of the composites reinforced with the nanotube yarns/nanotube braids are much different than those observed for the respective dry yarns/braids. Fig. 7.5 shows the fracture surface of the 3-D nanotube braid infused with epoxy (recall that the braid was made of thirty six 5-ply nanotube yarns). These pictures reveal an increasing level in detail in the morphology of this 3-D braided composite fracture. Specifically, the twist of the nanotube yarns can be seen as the swirl on the surface of each fractured yarn. It is also seen that there is no significant pullout of the nanotubes and nanotube bundles. Also, it looks like the resin has penetrated well between the nanotube bundles, and no protruding nanotube exceeds 1 μm in length. The close-up images clearly show that the nanotubes are surrounded by epoxy resin. The dark spots seen in the picture are due to extremely high zoom level and the roughness of the fracture surface made it hard to focus on the whole surface.

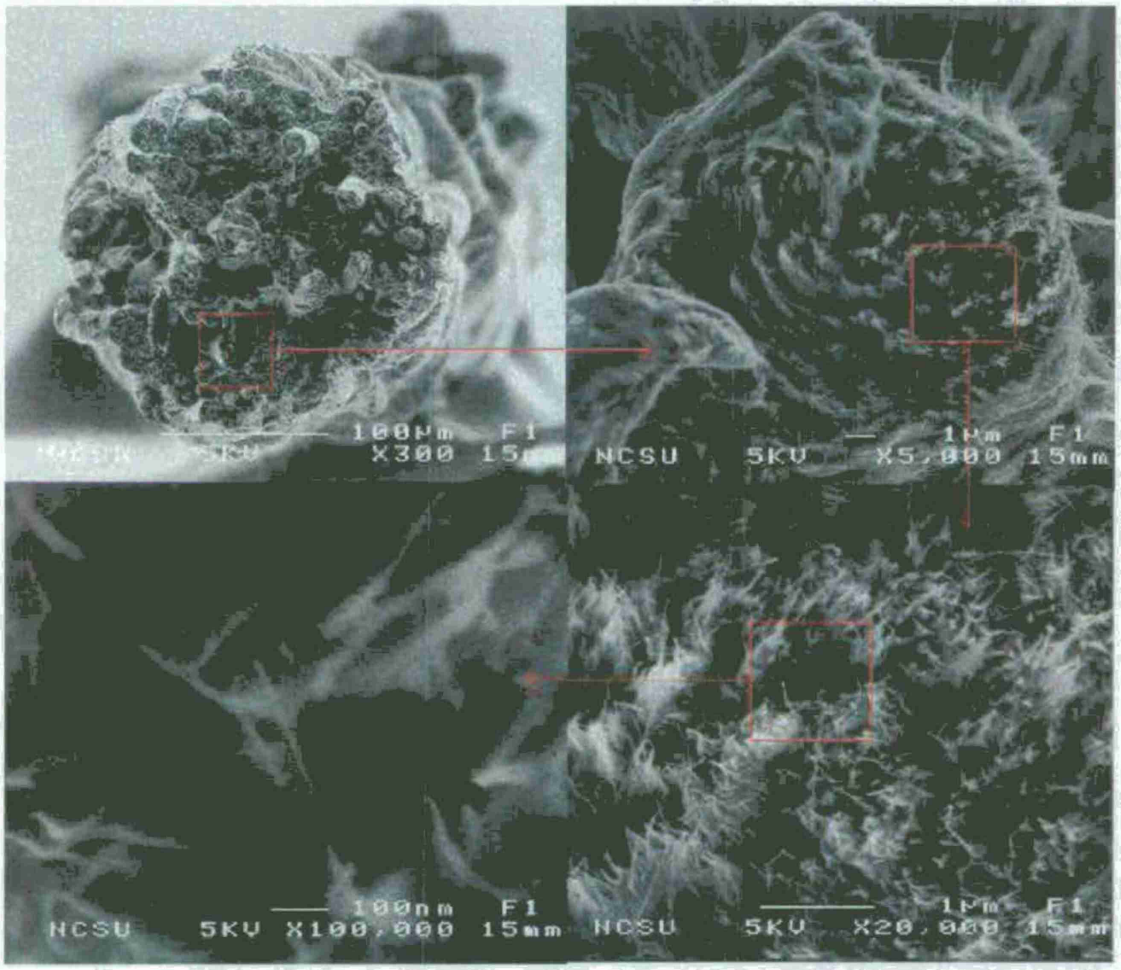

Figure 7.5. Cross section images of 3-D nanotube braid composite with increasing detail.

There is no question that conventional carbon fiber composites are many times stronger and stiffer than the nanotube composites produced so far in this project. Therefore, one may ask why, having so high theoretical stiffness and strength values of carbon nanotubes, we were not able yet to transfer those properties into our composite materials. There are several reasons for that.

First, the nanotubes that build up the nanotube yarns in the tested composite samples are about 300 µm long MWNTs, consisting of concentric walls. Stress applied to the outer wall may not be effectively transferred to the inner walls. This problem can be partly solved by using much longer nanotubes to make the yarns, and we are presently working on this. Note that individual SWNTs are stiffer and stronger because the whole nanotube can transfer load along its length. However, SWNTs bundle together, which causes the problem of insufficient stress transfer, similar to the problem mentioned above for MWNTs. This problem of insufficient stress transfer to inner nanotubes in a bundle will also become less pronounced as we go to longer nanotubes, either SWNTs or MWNTs.

Second, the nanotubes used here were not functionalized, so the interfacial bonding between the nanotubes (or bundles of nanotubes) and epoxy is far from being strong. Functionalization of

nanotubes forming yarns and braids would be another efficient approach to increase strength of nanotube composites.

Third, having nanotubes assembled in bundles can make it hard for the resin to penetrate inside the bundles which inhibits load transfer between the nanotubes. It is not clear at this point how to improve the situation from this perspective, because the approach of using less and less viscous resins which we tried to apply here did not make a significant effect on either stiffness or strength of the fabricated nanotube composites.

Fourth, the alignment of the nanotubes has a large effect on the stiffness and strength of the nanotube yarns, braids, and their composites. The single nanotube yarns used in this study show an apparent nanotube orientation angle 33° with respect to the longitudinal yarn axis, as measured with the use of Scion Image software. Decreasing this angle should also increase composite stiffness and strength. The nanotubes are further disoriented when five single yarns are plied together with twist, and disoriented even more when 5-ply yarns are again plied together with twist or braided. Minimizing twist in each of the processing steps should make significant property improvement.

Finally, the nanotubes are not packed as densely as possible. Their relatively low packing density directly correlates with the nanotube volume fraction in the composite and, consequently, with its mechanical properties.

7.6. Further Discussion of the Mechanical Test Data

Here we continue discussion of the obtained mechanical test data, started in Section 7.5. Figs. 7.6-7.11 use only numerical data from Tables 7.1 and 7.2. The longitudinal moduli E_c, strengths S_c and failure strains ε_c^u presented in these Figures for the three composites reinforced with 3-D nanotube braids, are normalized over respective epoxy matrix characteristics E_m, S_m and ε_m in Figs. 7.6, 7.8 and 7.10, and normalized over the dry braid characteristics E_r, S_r and ε_r in Figs. 7.7, 7.9 and 7.11. The bars shown in these figures make it easier to understand the major trends observed. Note that volume fraction of the nanotubes in the 3-D braid reinforcement has been estimated as ~40%, which is much higher than in any nanotube modified polymeric matrices reported in literature. This results in a very dramatic effect of the reinforcement when composites characteristics are compared with the respective characteristics of the neat matrices, as seen in the Figs. 7.6-7.8.

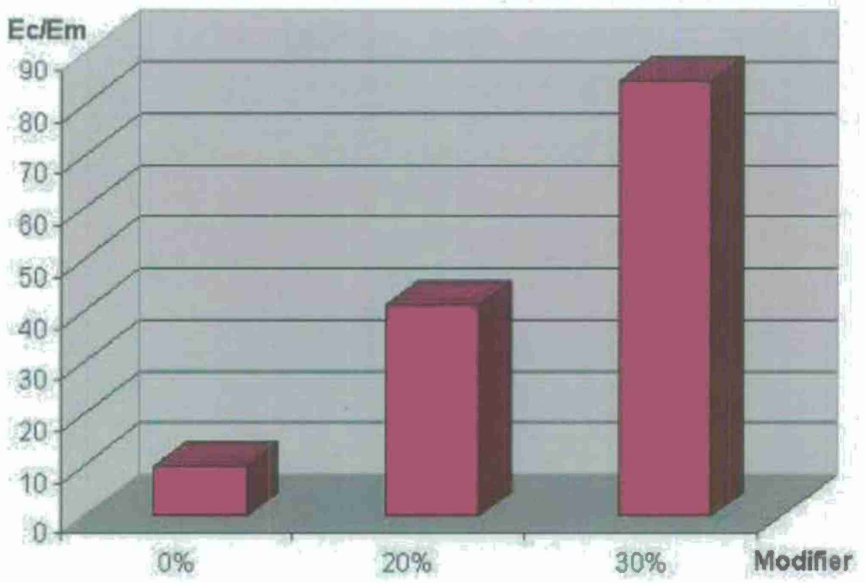

Figure 7.6. The ratio of longitudinal modulus E_c of three nanotube 3-D braid composites to respective modulus E_m of matrix at different amounts of modifier in epoxy.

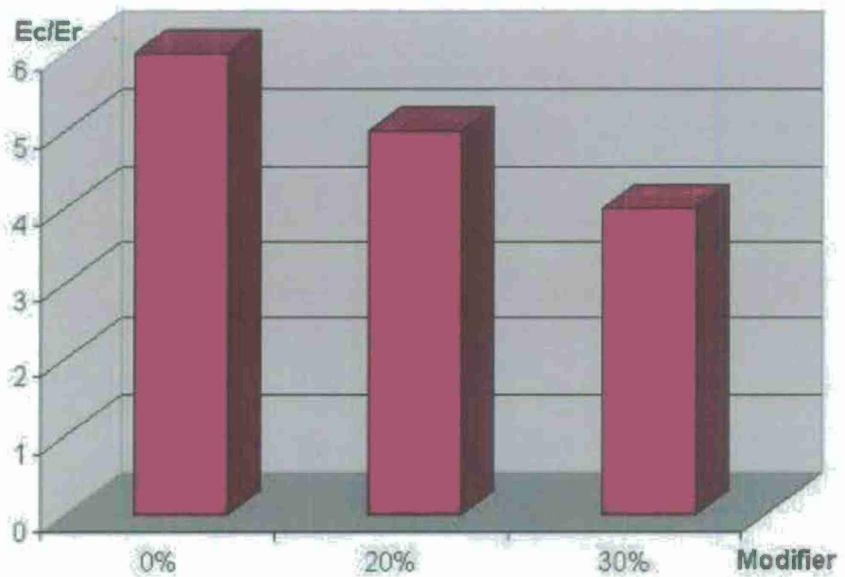

Figure 7.7. The ratio of longitudinal modulus E_c of three nanotube 3-D braid composites to the modulus E_r of dry 3-D nanotube braid at different amounts of modifier in epoxy.

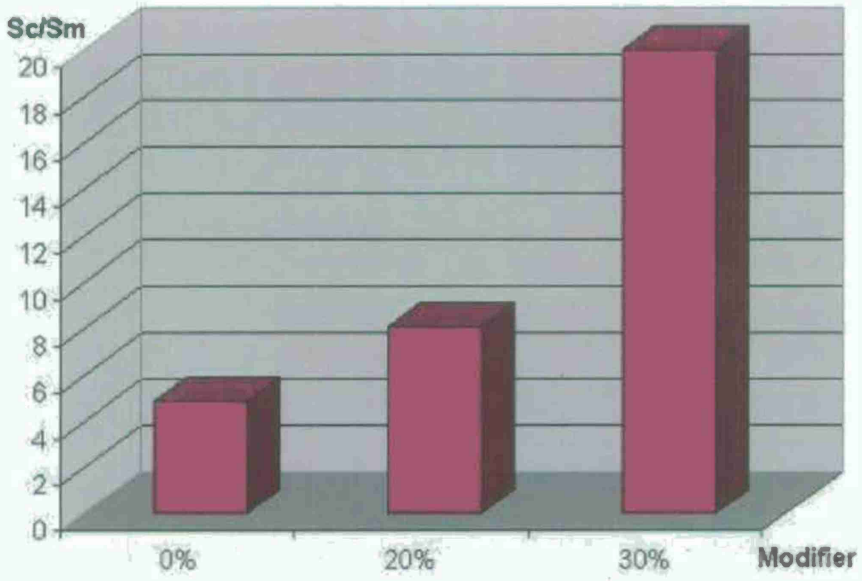

Figure 7.8. The ratio of longitudinal strength S_c of three nanotube 3-D braid composites to respective strength S_m of matrix at different amounts of modifier in epoxy.

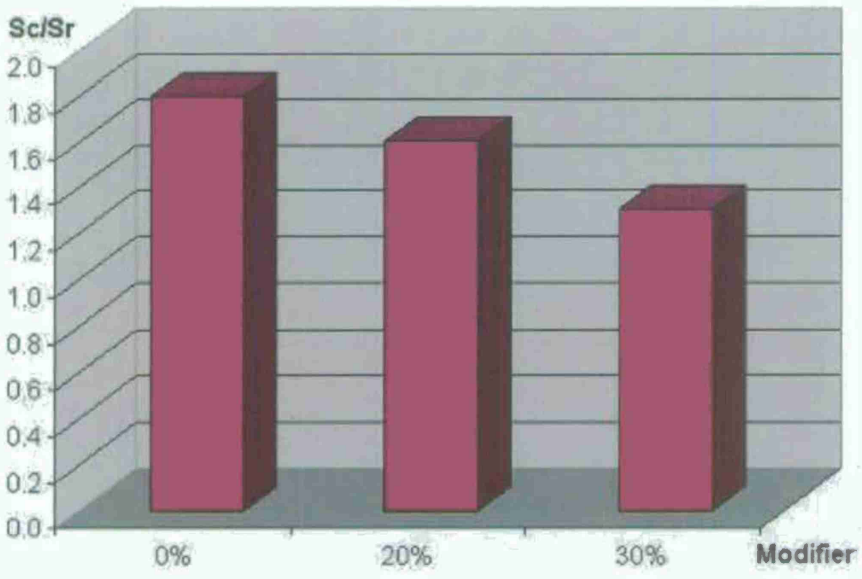

Figure 7.9. The ratio of longitudinal strength S_c of three nanotube 3-D braid composites to the strength S_r of dry 3-D nanotube braid at different amounts of modifier in epoxy.

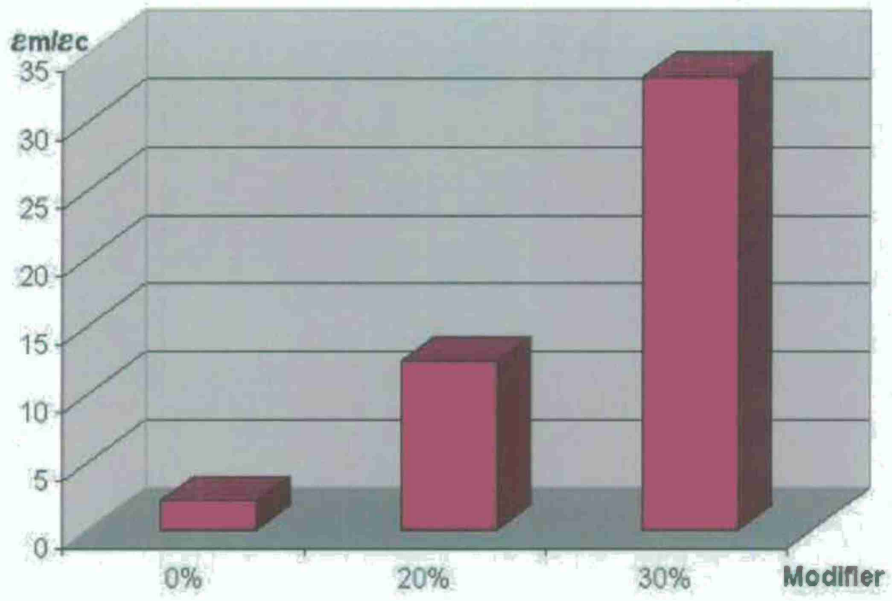

Figure 7.10. The ratio of longitudinal strain to failure of matrix ε_m to that of three nanotube 3-D braid composites ε_c at different amounts of modifier in epoxy.

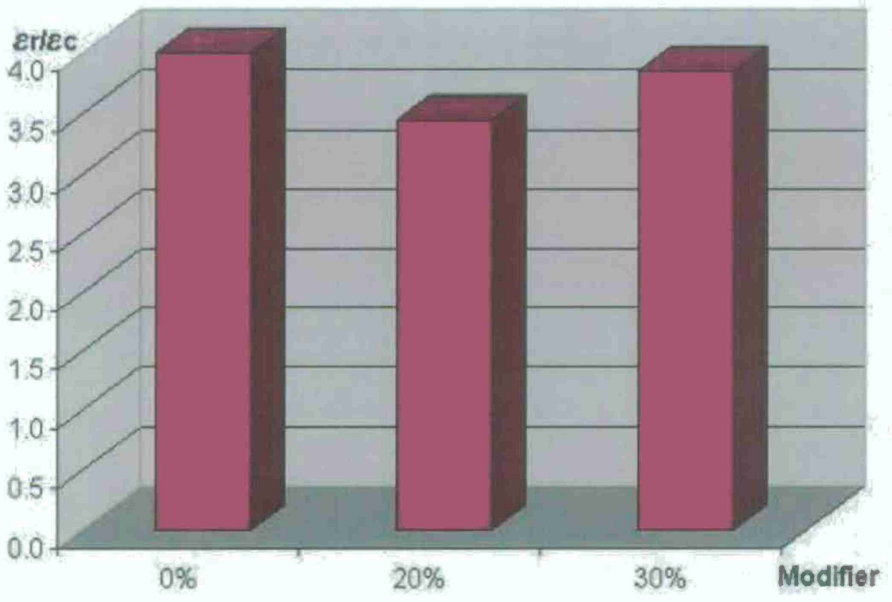

Figure 7.11. The ratio of longitudinal strain to failure of dry 3-D nanotube braid ε_r to that of three nanotube 3-D braid composites ε_c at different amounts of modifier in epoxy.

Fig. 7.6 shows that composites moduli are many times higher than the respective matrix moduli, and their ratio is growing with increasing amount of modifier. Specifically, with 30% modifier the ratio of moduli is close to 90. Fig. 7.8 indicates that the strength increase (which is also getting larger with increasing amount of modifier) in more modest, but it is still measured in times, not in percents or tens of percents. For example, in the case of 30% modifier the strength increase is 20 times. The ratio presented in Figure 4.3, $\varepsilon_m / \varepsilon_c$, is inverse and it reveals the same trend as direct ratios of moduli and strengths in Figs. 7.6 and 7.7: strain to failure values of matrices are many times higher that those of respective composites. Again, in the case of 30% modifier this ratio is about 35. These results clearly illustrate that, despite the fact that the obtained moduli and strengths of composites made with 3-D braid nanotube reinforcement are far below expectations, this reinforcement gave a huge increase in moduli and strengths of the respective matrix materials.

Contrary to the results in Figs. 7.6, 7.8 and 7.10, the ones shown in Figs. 7.7, 7.9 and 7.11, are much less dramatic. While several times increase of modulus is seen in Fig. 7.7, the strength increase in Fig. 7.9 is less than two times, and the strain to failure decrease of composites vs. matrix materials in Fig. 4.11 is between 3.8 and 4.0 times. In the other words, adding nanotube braid reinforcement to the matrices makes much more difference than adding matrices to the reinforcement. Also, the results in Figs. 7.6, 7.8 and 7.10 reveal consistent trend: the increase of matrix modulus and strength with simultaneous decrease of its strain to failure is somewhat linearly proportional to the volume fraction of modifier added to the regular epoxy resin.

Another very interesting effect, which needs special attention is, that as Fig. 7.11 shows, the ratio of strain to failure of the reinforcement to that of the composite is practically independent of the amount of modifier. In the next section this effect will be discussed from the Polymer Physics point of view, and some correlations with this effect will be revealed from the performed Dynamic Mechanical Analysis (DMA).

SECTION 8

Electrical Conductivity of CNT Yarns, Braids and Their Composites

8.1. Electrical Properties of Carbon Nanotube Composites

Carbon nanotubes are believed to be excellent conductors of electrons because of their unique graphitic tube structure. Extremely high current densities of $1x10^6$ A/cm^2, as reported in [28], and $2x10^7$ A/cm^2 [29] have been measured for carbon nanotubes. These are orders of magnitude above the maximum current density for copper wires used today. Resistivity measurements of carbon nanotubes have been measured as low as $5.1x10^{-6}$ ohm-cm using a four point probe method, see [30].

Nanotubes have been used as fillers in various matrix composites due to their extremely long aspect ratios enabling to create electrically conductive networks at very low volume fractions. For this reason, nanotubes have been added to epoxy matrices in many cases, see for example [31-33]. However, the conductivity of such networks is very low, right above the conductive percolation threshold. The range of electrical conductivity obtained in the above cited works was from 0.001 to 0.8 S/cm. Nanotube yarns studied for the first time in [21] have shown much better electrical conductivity; it was found to be 300 S/cm with the use of four point probe method. However, this is still orders of magnitude away from the theoretically predicted electrical conductivity of individual carbon nanotubes.

The limiting factor for the electrical properties of conductive carbon nanotubes and carbon nanotube networks is the contact resistance between crossing nanotubes, contact resistance between nanotube and matrix, conductivity of the matrix and, most importantly, the number of contact points between nanotubes in the network. In dispersed nanotube composites with insulating matrices, the high resistance is a result of few nanotube contacts that have a small conducting surface area. Contrary to a trivial case of two flat continuous contact surfaces, the least resistive path for electrons to flow within the nanotube network is through the small contact surfaces between adjacent tubes. The contact area has been theoretically estimated as ~1 nm^2 for SWNT [34].

The much denser and better organized carbon nanotube yarns exhibit substantially better electrical conductivity than dispersed nanotube networks due to the much larger number of contact points between nanotubes. In dispersed nanotube composites, short nanotubes may make intimate contact with tens of other tubes. In nanotube yarns, in turn, a single long nanotube could make thousands of contacts with other tubes. This is due to much higher packing density, better alignment and preferred orientation of nanotubes in the spun yarns. In dispersed nanotube composites, the nanotubes are deliberately separated from each other in order to maximize the physical properties of interest with the lowest volume fraction (so-called 'loading') of nanotubes. In carbon nanotube yarns, the nanotubes and nanotube bundles remain in the as spun form and therefore contain numerous contact points. For this reason, when carbon nanotube yarns were

infiltrated with a polyvinyl alcohol solution, as in [21], the electrical conductivity was decreased by only 30%. The majority of original contacts among nanotubes remained in place; therefore, the electrical conductivity was only moderately affected.

8.2. Experimental Study of Electrical Conductivity

Electrical resistivity, or the inverse characteristic called electrical conductivity, is a bulk material property. For a homogeneous isotropic solid material it is defined by the following equation:

$$\sigma = \frac{L}{R \cdot A} \tag{8.1}$$

where R is the measured resistance over length L, while A is the cross sectional area of the sample. This equation can be used, particularly, for solid isotropic metal wires. If using Strength of Materials analogy, σ in equation (8.1) can be viewed as equivalent of Young's modulus determined from Hooke's law under unidirectional loading of homogeneous isotropic solid. This analogy helps to explain to those skilful in Solid Mechanics what is the meaning of σ defined by equation (8.1) in the case of inhomogeneous material. Clearly, like in mechanics of inhomogeneous materials, in any case of inhomogeneous material exposed to electric current flow, σ may signify only "effective" electrical conductivity meaning the property "smeared" over entire material sample and, as such, it provides possibly only a coarse estimate. Besides, as in mechanics of anisotropic solids, more than one electrical conductivity characteristics, differing for different directions of electric current flow, should be involved.

With clear understanding of the aforementioned issues, and for simplicity of data processing, we used equation (8.1) to determine σ as effective electrical conductivities of the respective materials corresponding to the case of dominant current flow in the longitudinal direction of each tested material sample.

In a more sophisticated approach, if accounting that the sample is discontinuous along its width or length, internal contact resistances within the sample must be taken into account. The example of this kind is a tow of carbon fibers. Each single carbon fiber can be viewed as continuous material, therefore electrical conductivity measurements can be taken by placing probes on the surface of the material. Using the same procedure to find the resistivity of a carbon fiber tow would yield a much different result. Indeed, in this case the probe lies on the surface layer of fibers in the tow. The fibers within the core of the tow will contribute to electrical conduction, but their contribution will be a function of the number and closeness of the contacts made from fiber to fiber. Obviously, this creates additional resistance in the material and so the conductivity appears to be lower.

The same considerations readily apply to the cases of plied nanotube yarns and 3-D nanotube braids. Those single yarns in this type of structure which are exposed to the surfaces, may be in direct contact with the probes while the others, which are located inside the structure, are at some distances away from the probes. Even though the measured values of electrical resistance of the aforementioned structures cannot be used to evaluate their bulk conductivity, equation (8.1) can still be used to compare the relative conductivities based on the dimensions of the samples.

The described method was used to compare the relative conductivities of four types of samples: (i) continuous AS4 3K carbon fiber tow, (ii) 5-ply carbon nanotube yarn, (iii) 3-D braid made of solely carbon nanotube yarns, and (iv) the hybrid 3-D braid made of 9 bundles of S-2 glass fiber and 36 carbon nanotube yarns, as described above in Section 4.1. The samples were all tested on a Hewlett Packard 4145A Semiconductor Parameter Analyzer using two probes at room temperature. The electrical resistance was calculated from the slope of the voltage vs. current plot during a current sweep of -100 to 100 mA for the carbon fiber tows, the 3-D braided nanotube yarns and the hybrid 3-D braid. The current sweep for the smallest structure, the plied nanotube yarns, was from -1 to 1 mA.

Conductive silver epoxy was used to create contacts on each of the four structures. This was done because the testing probes were very small and would not come into contact with a very large surface area on the samples. On the hybrid 3-D braid, the probe would only touch a single (non-plied) nanotube yarn. The epoxy material had surrounded each sample completely at each contact point, so that multiple fibers or yarns would be contacted. On a glass microscope slide, the mixed silver epoxy was put down in thin lines. The sample was then placed on the slide and a second thin line of epoxy was deposited over the first, encapsulating the surface of the sample. The epoxy was extremely viscous, almost paste like, due to the presence of silver particles. With this extremely high viscosity, it was assumed that none of the silver epoxy penetrated into the structures but rather coated the surface. The epoxy was allowed to cure overnight. Fig. 8.1 shows two contacts on the hybrid 3-D braid sample. Each sample had four different contact points spaced apart at approximately same distance. The spacing between contacts was measured with a digital caliper. The multiple contact points allowed the resistance as a function of length to be determined.

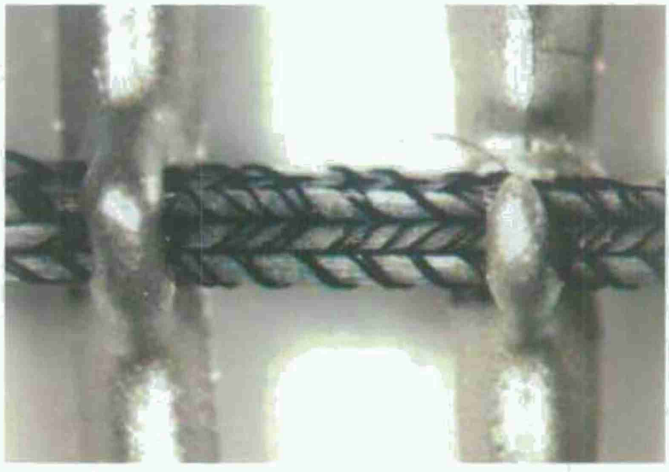

Figure 8.1. Test setup for a dry hybrid 3-D braided material with electrical contacts.

In application to composites, the electrical properties of the constituent materials or preforms are not as important as the electrical properties of the final composite part. The addition of an epoxy matrix can reduce the conductivity of the composite preform because the insulating matrix may coat the fibers, thus eliminating many electrical contact points between them. Hence, it was

important to measure the electrical conductivity of composites made from the previously tested preform samples.

Composites were made from the same preform samples used in the previous resistance testing for consistency. Using a syringe with a needle point opening, mixed epoxy resin was placed on the surface of each structure. As the structure absorbed the epoxy, more was added to the surface until the structure was saturated. At that point, extra epoxy began to pool around the structure. The samples were cured by heating in an oven for 3 hours at 90°C. Fig. 8.2 shows the hybrid 3-D braid after infusion and curing of the epoxy, taken with an optical microscope.

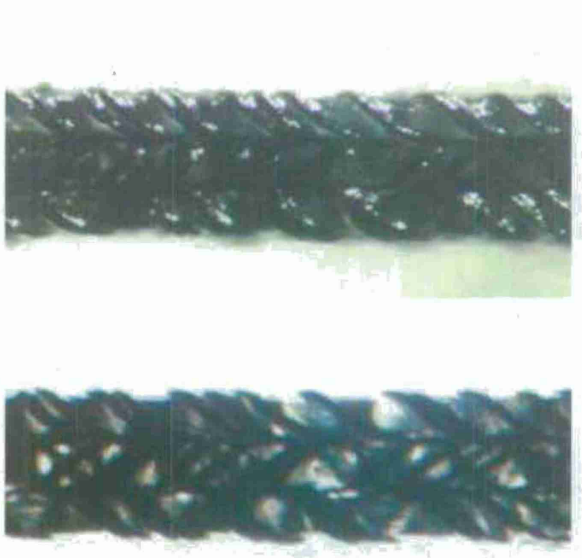

Figure 8.2. Hybrid 3-D braided composite illuminated from above (a) and below (b).

In Fig. 8.2a, the epoxy appears to be evenly distributed across the hybrid structure. Fig. 8.2b shows the same structure being illuminated from below. The glass fibers became translucent with the addition of epoxy, so that the dark nanotube yarns within the structure can be discerned. Notice the difference in appearance from Fig. 8.1.

The use of the extra fine syringe tip allowed the epoxy to be placed precisely, so that the silver epoxy contacts would be free of epoxy for testing. The method used here to test the composites was identical to the above described method used for testing dry yarns and braids. Therefore, the differences between results for the composites and their respective preforms can be attributed entirely to the presence of the epoxy matrix.

8.3. Experimental Results and Discussion

The measured resistances and the relative conductivities based on the geometry of each sample type are listed in Table 8.1. It is not surprising that the carbon fiber tow had the highest conductivity of all of the samples, considering that individual PAN based carbon fibers have a bulk conductivity of approximately 650 S/cm, see [35], while individual carbon nanotube yarns have a bulk conductivity of 300 S/cm [21]. However, the 5-ply nanotube yarn and the 3-D

nanotube braid were very close behind. Possibly, this is due to the size of each structure. The 3K carbon fiber tow has the largest cross section among the three comparable samples, therefore it would have the least amount of fiber surface contact regions.

Table 8.1. A comparison of electrical resistances and conductivities of dry yarns and 3-D braids, and composite made thereof.

Material Type	Cross-sectional area (mm^2)	Contact distance (cm)	Resistance (ohms)	Conductivity (S/cm)
AS4 3K carbon	0.119	0.527	4.52	97.977
5-ply nanotube yarn	0.00114	0.637	607	92.055
3-D nanotube braid	0.0472	0.489	13.38	77.430
Hybrid 3-D braid	0.178	0.402	12.63	17.881
AS4 3K carbon composite	0.119	0.527	6.96	63.629
5-ply nanotube yarn composite	0.00114	0.637	688	81.217
3-D nanotube braid composite	0.0472	0.489	16.7	62.037
Hybrid 3-D braid composite	0.178	0.402	14.68	15.384

The relative conductivity of the 3-D nanotube braid is lower than that of the 5-ply nanotube yarn due to not every yarn in the braid made contact with the silver epoxy. Only part of all yarns are simultaneously on the surfaces of the braid; the rest of the yarns are entirely inside. Those yarns which are in the interior of the braid could have contributed to electrical conduction, but the added contact resistance between the yarns lowered its overall value. Further, as is seen from Table 8.1, the electrical conductivity of the hybrid 3-D braid is lower than that of the 3-D braid made solely of nanotube yarns. This can be explained by the increase in the preform size due to the addition of the insulating S-2 glass fibers. The drop in conductivity well correlates with the change in the fiber volume content of the nanotube yarns within the preform. Specifically, in the hybrid 3-D braid, the nanotube yarns made up 26% by volume of the yarns in the structure, while the conductivity was 23% of that of the 3-D braided structure containing only nanotube yarns.

Infiltration of epoxy resin into the different studied textile structures lowered the electrical conductivity of each of them, which was expected. The electrical resistance and conductivity values for each composite structure are also shown in Table 8.1. Surprisingly, the nanotube yarn structures were the least affected by the addition of epoxy matrix. Specifically, the hybrid 3-D braid's electrical conductivity was only lowered by 14%, while it was lowered by 35% in the case of AS4 carbon fiber tow. Also quite surprisingly, the electrical conductivity of the 5-ply nanotube yarn composite shows higher than that of the AS4 carbon fiber tow composite. This is a significant find, considering that the carbon fibers are continuous across the contacts, while the carbon nanotube yarns are made up of discontinuous nanotubes. This result could be understood if the resin failed to penetrate into the carbon nanotube yarns. However, the same resin as used here was seen penetrating thoroughly into the nanotube yarn in one of the prior works [23].

The preservation of the conductivity in the nanotube yarn composite could be also due to the presence of nanotube bundling within the yarns. In addition, the extreme length of the nanotubes in the yarns ensures that nanotubes will meander from bundle to bundle creating a continuous network. The spacing between nanotubes in the nanotube bundles is small enough for preventing epoxy penetration into those areas. Thus, the resin infusion would not have as large effect on the

conductivity of the overall structure as in the case of AS4 unidirectional composite. The spacing between fibers in the carbon fiber tow allowed resin to penetrate and cover many of the fibers, thus reducing the amount of fiber contact area in the structure.

8.4. Conclusions

One major goal of this study was to show that carbon nanotube yarns can be used, along with traditional fibers, in the production of hybrid 3-D braided preform. To the best of the authors' knowledge, this is the first example of such 3-D braid ever made. Further, the braid was infused with epoxy resin and respective composite was consolidated.

The techniques used here to study electrical conductivity of various type dry textiles and composites made thereof, are not expected to provide very accurate conductivity values for the structures tested. One reason is that contact resistance between the probes and the silver epoxy, as well as contact resistance between the silver epoxy and the structures, was included in the resistance measurements. This means that the actual effective conductivities of these structures could be higher than the values presented in Table 8.1. However, identical mounting, testing and data processing techniques were applied to all samples tested, so the obtained information should be reliable at least for the mutual electrical conductivity comparisons among different materials. From this point of view, the results of this research are, certainly, useful. They provide insight into the effective electrical properties of carbon nanotube yarns and 3-D braids in composites.

The nanotube yarns and 3-D braids tested here acted as networks of electrically conductive paths embedded in epoxy matrix, and the resulting composite's electrical conductivity is many orders of magnitude greater than that of pure insulating S-2 glass. The electrical conductivity of the hybrid 3-D braided composite was found to be 15-1000 times greater than that of the composites made from dispersions of carbon nanotubes in epoxy, compare with data in [31-33].

Although the conductivity of the hybrid 3-D braided composites was found much greater than that of fiberglass, integrating the carbon nanotubes with carbon fiber tows would create negligible electrical conductivity enhancement. However, there is much room for improvement for the electrical properties of carbon nanotube yarns. As the length of the nanotubes increase and the methods to selectively grow only conducting nanotubes are discovered, the electrical conductivity of the yarns will increase accordingly.

With further development, carbon nanotube yarns could be the future of specialty high performance composites that demand multifunctional properties. As the yarns are further improved and become commercially available, continued research is needed to evaluate how these yarns perform both in a dry form and within composites. The planned future work will characterize the thermal properties and fracture toughness of the hybrid 3-D braided and 3-D woven composites that incorporate carbon nanotube yarns.

SECTION 9

Dynamic Mechanical Analysis of Epoxy Resins, CNT 3-D Braids and Their Reinforced Composites

9.1. Some Physical Hypothesis Brought to Explain the Mechanical Test Data

Mechanical test results were described in Section 7 of this report. Those correspond to four different epoxy resin systems with varying amount of modifier, dry nanotube yarns and 3-D braids made of those nanotube yarns, and composites fabricated from these matrix materials and reinforcements. Some of the results are extremely intriguing. Probably, most intriguing among them is the result that strain to failure at room temperature is nearly identical for all four tested composites that were made with four substantially different epoxy resin systems containing different amounts of modifier. Moreover, those strain to failure values of composites are about 4 times lower than the strain to failure of the dry reinforcement, about twice lower than strain to failure of unmodified neat epoxy, and many times lower than strain to failure of the modified epoxies. Indeed, it is not clear at all how to mechanistically explain the effects that (i) composite's strain to failure is much lower than that of both its constituents - matrix and reinforcement - tested separately, and (ii) composites made with very different, and very compliant, matrices show practically the same value of failure strain as the composite made with matrix having only 3.6% failure strain. Obviously, some kind of unusual "synergistic effect" takes place here.

In our continuing effort to find a satisfactory physical explanation to these effects, some new considerations and physical hypotheses are brought up here for discussion. First of all, one may suggest that the reason for the aforementioned very dramatic strain to failure reduction resulting from reinforcing epoxies with carbon nanotube yarns or braids might be that carbon nanotubes, when they interact with epoxy macromolecules, are able to somehow generate or facilitate generation of additional cross-linking (i.e., producing additional covalent bonds between macromolecules) in epoxy networks and thus reduce the cured epoxy network ability to deform, which ultimately results in lowering strain to failure. However, no argument has been found up to this point to validate this hypothesis. At the same time, there are some arguments contrary to this hypothesis. One of them is that no reason is seen, why CHEMICALLY INERT (non-functionalized) carbon nanotubes used in this research could cause so significant additional cross-linking of epoxy resins that the failure strain decreased many times. Even assuming some possible random impurities associated with the nanotubes (those might act as additional catalysts), it is hard to imagine that such impurities could cause so substantial increase in cross-linking density of the studied epoxies. Further on, no experimental data was found in the literature to support the point that by increasing cross-linking density in epoxies one was able to dramatically reduce their strain to failure values at room temperature, i.e., in the GLASSY STATE.

It is well known that cross-linking density strongly affects the Tg values and indirectly, through Tg, it also affects mechanical properties when transition from the RUBBERY state to the GLASSY state occurs. However, the obtained 3.6%, 22%, 62% and even 89% strain to failure values correspond to the GLASSY state (not to the RUBBERY state!) of the epoxies, and those strain to failure values have been obtained at the room temperature which, as we have all reason to assume, is significantly below the Tg values for those neat epoxy systems. Based on the above considerations, we ruled out, at least temporarily, the hypothesis that carbon nanotubes were able to induce significant additional chemical cross-linking it the matrices.

The alternative considerations assume that the presence of carbon nanotubes in such a large concentration (about 40% by volume in the studied composites) does not affect chemical cross-linking in the epoxies, but rather makes PHYSICAL changes. Specifically, it substantially reduces "free volume", constrains "local movability" and, through these factors, makes deformations of the composites exceeding 2% hardly possible. In the other words, instead of considering the effect of carbon nanotubes on Tg and so-called "α-transitions" (or "α-relaxation processes"), we should focus on the local movability effects associated with so-called "β-transitions" (or "β-relaxation processes"), which take place entirely in the GLASSY STATE of polymers. These relaxation processes are also often associated with the DUCTILE-BRITTLE transitions, which manifest themselves in a rather sharp reduction of "local mobility" of the polymer chains. In other words, when reducing temperature closer and closer to the β-transition peak, certain cooperative rotations of the groups of backbone links and side branches within polymer chains get "frozen". As the result, the polymer (still being in the glassy state) loses its "ductility" and shows more and more of a "brittle" behavior. Typically, β-transitions in epoxies occur in the temperature range between -30°C and -80°C with typical peaks at -50°C to -60°C. Accordingly, at room temperature the main local mobility mechanisms are practically unconstrained and relatively large "free volume" is available for the respective local chain movements. All this results in a more or less pronounced ductility and relatively high strain to failure values observed for the tested neat epoxies. Of course, these considerations are not new, they are "classics" of Polymer Physics, see for example [36].

Based on the above classical considerations, the following hypothetical explanation is proposed. When mixing and then consolidating ~40% by volume of very fine (about 10 nanometer diameter), very long (about 300 micrometer length) and very flexible carbon nanotubes with ~60% by volume liquid blend of epoxy and modifier, one obtains a very interesting three-phase media. Indeed, we have now two constituents (epoxy and modifier) that mutually engage in chemical reactions and form cohesive bonds, while the third constituent (carbon nanotubes) can only engage in physical interactions with them via van der Waals forces and other non-covalent interactions. The fact of really crucial importance here is, that the sizes of these interacting objects (i.e., the nanotube diameter, the epoxy macromolecule transverse size, and the modifier molecule size) are in the same nanometer scale. To support this point, the following citation from reference book [36] seems useful: "As in linear polymers, the relative influence of the molecular structure is on scale of nanometers…" and further: "In the glassy state, the physical behavior is essentially controlled by cohesion and local molecular mobility, both properties being mainly under the dependence of the molecular scale structure."

As we hypothesize now, the presence of a large amount (~40% by volume) of nanotubes mixed with epoxy macromolecules may (and, probably, should) result in their intermingling with epoxy chains, substantially reducing that free volume which was available in the neat epoxies and dramatically reduce LOCAL MOVABILITY of the macromolecules. In other words, nanotubes act as rigid (in comparison with much more flexible macromolecules) "inclusions", which obstruct otherwise relatively free rotations of the groups of backbone links and side branches that are responsible for ductility to the neat epoxies. In the result, at room temperature all epoxies in our composite systems become much less ductile, and even those characterized by 22%, 62% or 89% strain to failure in the absence of nanotubes, lose their local mobility and all of them behave almost identically, more like "brittle" polymers, with strain to failure below 2%. Of course, these effects strongly depend on the nanotube diameter and volume fraction in the composite. As anticipated, as smaller nanotube diameter is, as higher flexibility and larger volume fraction are, as more of a "brittle" behavior the epoxy matrix in the composite would show. Obviously, for all four studied nanotube composites with different epoxy matrices, the nanotube volume fraction was big enough and the nanotube diameter was small enough to suppress local mobility down to the same low level and thus making all four composites behaving like nearly identical material.

Now, one might ask the question: was this kind of effect, generated by the presence of carbon nanotubes, observed before? The certain answer cannot be given without exhaustive literature search, though to the best of our knowledge nothing like this has been ever reported in the literature. Next question may be: what is the reason for that? And our answer would be that in our studied composite systems there is unusually high nanotube volume fraction (~40%), which is incomparably higher than nanotube volume fraction ("loading") in all those polymeric materials which were modified by adding rather small amount (from fraction of percent to several percents) of nanotubes. Indeed, the uniqueness of our fabricated composite materials has resulted, firstly, in some "abnormal" mechanical test data and, secondly, has motivated us to search for the reasons of such abnormalities.

In addition to what was hypothesized above, the effect of significantly reduced "ductility" of epoxy matrices in our nanocomposites may also help to explain the lower-than-expected strength values observed in our tests. Indeed, as more of a "brittle" behavior is observed for polymer matrix, as more sensitive the composite is to any kind of micro-scale (in our case, nano-scale) defects, voids, inclusions, other irregularities. And any of them would reduce composite strength.

One may also ask the following question: why the effect discussed here (a dramatic drop of strain to failure in composites, far below the failure strains of both the reinforcement and matrix) has never been observed before on any existing composite system, like unidirectional composites, textile reinforced composites, etc.? The reasonable answer may be that polymer macromolecules do not penetrate inside regular carbon, glass, aramid and other fibers during composite fabrication and do not intermingle with sub-structural elements of those fibers. Fiber diameter is typically measured in micrometers, while the characteristic monomer scale is measured in nanometers. In conventional composites polymer matrix simply occupies (by forming micro-scale blocks of macromolecules) available spaces in-between fibers. If more or less strong interaction between fibers (or their coatings, sizings, etc.) and matrix takes place, that is always limited to a thin interfacial region, much thinner than the fiber diameter and the matrix block size. Contrary to such a situation, in the case of nanotube reinforced composites, the

diameter of nanotubes is measured in nanometers. This forces macromolecules during composite fabrication to find free spaces at a much smaller (nano-scale) level between closely packed carbon nanotubes. Obviously, local mobility of the macromolecules in such situation is much more constrained than in the case of micro-scale fibers in conventional composites.

New extensive and sophisticated experimental studies are required, that could directly or indirectly validate the proposed hypotheses. At this point, we can only bring up several practical questions and make certain suggestions for the future experimental studies:

1. One principal question is: how do carbon nanotubes and epoxy chains locate with respect of each other and how do they intermingle in the nanotube composite systems that were made and tested? We do not know the answer yet because SEM does not provide sufficient resolution to see individual macromolecules interacting with nanotubes inside composites. Probably, TEM imaging or other advanced imaging method could clarify the situation.
2. The Dynamic Mechanical Analysis (DMA) is the most common and relatively simple method to study beta-transitions in many polymer systems. We can now study three different material groups using DMA; (a) neat solidified epoxies containing different amount of modifier, (b) dry nanoyarn and/or nanobraid reinforcements, and (c) nanoyarn/nanobraid composites made with the same epoxy systems as used before. Studying β-transitions in aforementioned materials and mutually comparing them would bring some valuable information.
3. It is known from the literature that epoxies are characterized by highly active β-transitions, they typically show high-intensity β-relaxation peak, and as such they can be easily distinguished from some other polymer networks which have a low-intensity β-relaxation peak. The examples of latter type polymers are styrene cross-linked vinyl esters and polyimides. The suggestion is that the "strain to failure reduction effect" should be much less pronounced in similar nanotube composites if they are infused with a vinyl ester or polyimide resin. It seems practical making new composite samples using the same nanoyarn/braid reinforcements with a different resin system. Then their tensile tests can be performed and those new results compared with the previously obtained data for epoxy composites. This may be a good (though indirect) indication if the proposed hypotheses are right.

Next section presents first results of the DMA experiments which were conducted after accepted stated as additional research task.

9.2. A DMA Methodology

Dynamic Mechanical Analysis (DMA), also often called Dynamic Mechanical Thermal Analysis (DMTA) and Dynamic Thermo-mechanical Analysis (DTA) is now considered a common research tool in the analytical laboratory. DMA can be simply described as applying and oscillating force to a sample in a broad temperature range and analyzing the material response to that force and the temperature change. The other way to describe what is studied in DMA is the relaxation of the polymer chains. Another way to describe it is the changes in the free volume of the polymer that occur. Other interpretations are possible as well. One advantage of DMA is that

we can obtain modulus of the studied material each time a sine wave is applied, allowing us to sweep across a temperature or frequency range. Further background information on this method can be found in [37] and many other books.

Importantly, the modulus measured in DMA experiments is not the same as the Young's modulus obtained from a classic stress-strain curve. While Young's modulus is determined as the tangent to the curve, in DMA a complex modulus $E^* = E' + iE''$ is calculated from the material response to the applied sine wave. In the expression above, the real part, E', commonly called "storage modulus" signifies the elastic response, while the imaginery part, E'', commonly called "loss modulus", reflects inelastic (viscoelastic) behavior. The ratio $\tan\delta = E'/E''$ is commonly called "damping".

A lot of users exploit the greater sensitivity of the DMA to measure Tg values undetectable by the differential scanning calorimeter (DSC) or the differential thermal analyzer (DTA). However, more sophisticated users apply DMA to study relaxation processes in polymers. The thermal transitions in polymers can be described in terms of either free volume changes or relaxation times; both descriptions are essentially equivalent. Free volume is defined as the space a molecule has for internal movement. Changes in free volume can be monitored as a volumetric change in the polymer by the absorption or release of heat associated with that change, the loss of stiffness, increased flow, or by a change of relaxation time. As the free volume of the chain segment increases, its ability to move in various directions also increases. This increased mobility in either side chains or small groups of adjacent backbone atoms results in a greater compliance (lower modulus) of the polymer.

At low temperatures these local movements have been classified as $\gamma-$ and $\beta-$ transitions (or relaxation processes). There are several typical mechanisms of molecular motions corresponding to these transitions. Below $\gamma-$transition temperatures, only very limited local molecular motions are possible. As the material warms and expands, the free volume increases so that localized bond movements (bending and stretching) and side chain movements can occur. This is the $\gamma-$ transition. As the temperature and the free volume continue to increase, the whole side chains and localized groups of 4-8 backbone atoms get enough space to move, and material starts to develop some "toughness". This is called $\beta-$ transition. As we further move from very low temperatures, where the macromolecules are tightly compressed, we pass first through the solid state transition and get to the region of $\alpha-$transition (a.k.a. "glass transition", due to it occurs around Tg temperature). Here, the chains in the amorphous regions of polymer begin their coordinated segmental motions. One classical description of this region is that the solid amorphous material begins to melt. Finally, we reach the melt state, where large-scale chain slippage occurs and the material flows. Note that for a cured thermoset nothing happens above the Tg until the material begins to burn and degrade; this is due to the cross-links prevent the chains from slipping past each other.

The region of sub-Tg, or higher order transitions, which is of a special interest for us, has been heavily studies for different polymers, because these transitions have been associated with mechanical properties of polymers inn their solid (glassy) state. It has been shown, particularly, in cured thermosets, that increased freedom of movement in side chains increases the intensity of the transition. Specifically, it has been reported that $\beta-$transition can be considered the

"activation barrier" for solid-phase reactions, deformation, acoustic damping, etc. A working rule of thumb is that the $\beta-$ transition must be related to either localized movement in the main chain or to very large side chain movement to be able to sufficiently absorb vibration energy. Other observations reported for both mechanical and dielectrical properties indicate that both $\beta-$ and $\gamma-$transitions in bisphenol-A-based thermosets depend on the side chains and unreacted ends, and that both are affected by physical aging and postcure. It was also suggested that the intensity of the $\beta-$ transition can be taken as a measure of how effectively a polymer absorbs vibrations.

When analyzing a solid polymer, researchers typically look only at its transition as a function of temperature. However, the frequency at which the temperature scan is run, will also affect the temperature of the transition. The general trend is that transitions move to lower temperatures as frequency decreases. This dependency of transition temperature on frequency also has another implication which sometimes goes unnoticed. Namely, by changing the frequency, one can move a material through a transition. This is another reason why we need to know both the frequencies to which the material will be exposed in service and the frequency dependence of the material response.

9.3. DMA Studies

The most important results from our performed DMA testing of epoxy matrices and CNT yarn composites are shown in Figs. 9.1-9.6.

The results for DMA testing of a neat Epon epoxy are shown in Fig. 9.1. This testing was done to ensure the proper functionality of the machine and to provide a comparison basis for other tested materials. The storage modulus, loss modulus and tan delta curves followed the trends that are seen in many textbook examples of the DMA of epoxy resin. The large tan delta peak was taken as the glass transition temperature of the material and a β-transition peak is also clearly visible.

Adding the monoepoxide modifier to the epoxy should have the effect of bonding a monofunctional molecule into the network which will decrease the number of crosslinks in the system. Due to this lowered number of crosslinks, the resin should show an increase in the freedom of large scale molecular motion of its chains. This characteristic would be exhibited in a lowered Tg for the material as it takes less energy to allow the motions to occur. This trend is clearly seen in Fig. 9.2. As the amount of modifier is increased, the number of crosslinks is simultaneously decreased, and thus the tan delta and corresponding Tg peak is moved to lower temperatures. An increase in the magnitude of the β-transition peak is also seen for the highest modifier content indicating that the toughness of these resins at room temperature should be higher.

When these same resin formulations, with modifier content of 0, 20 and 40%, were used to infuse the 3D braided CNT preforms, their composites were expected to behave in a manner that is similar to the combination of the individual parts. In a system with a low dampening reinforcement, the ideal damping of the composite can be estimated by the rule of mixtures [44]:

$$\tan \delta_c = (1-\varphi_f)\tan \delta_m \qquad (9.1)$$

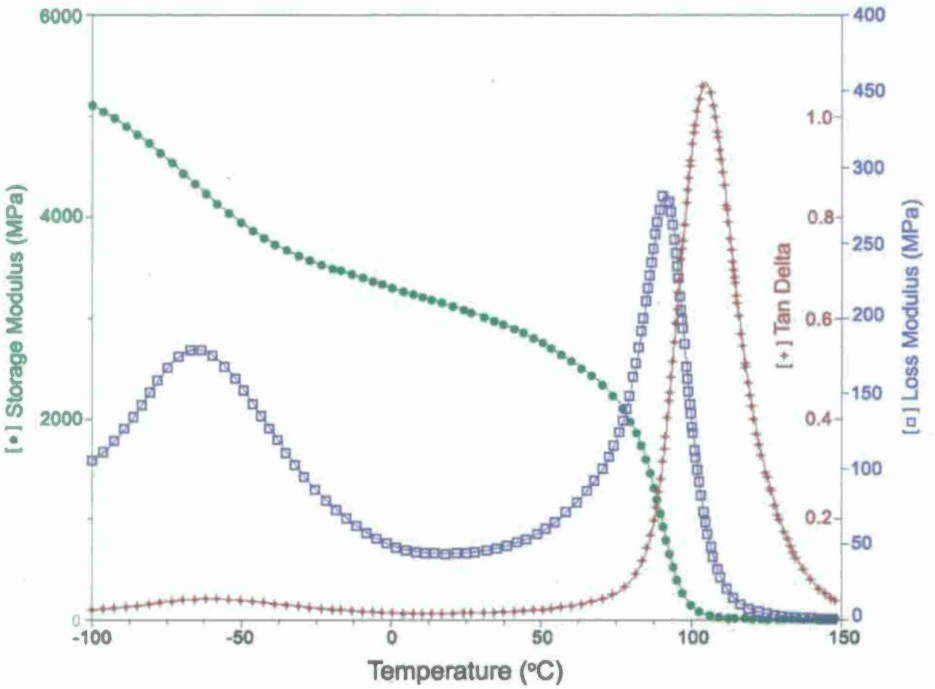

Figure 9.1. Characteristic DMA curves of Epon epoxy with no network modifier added.

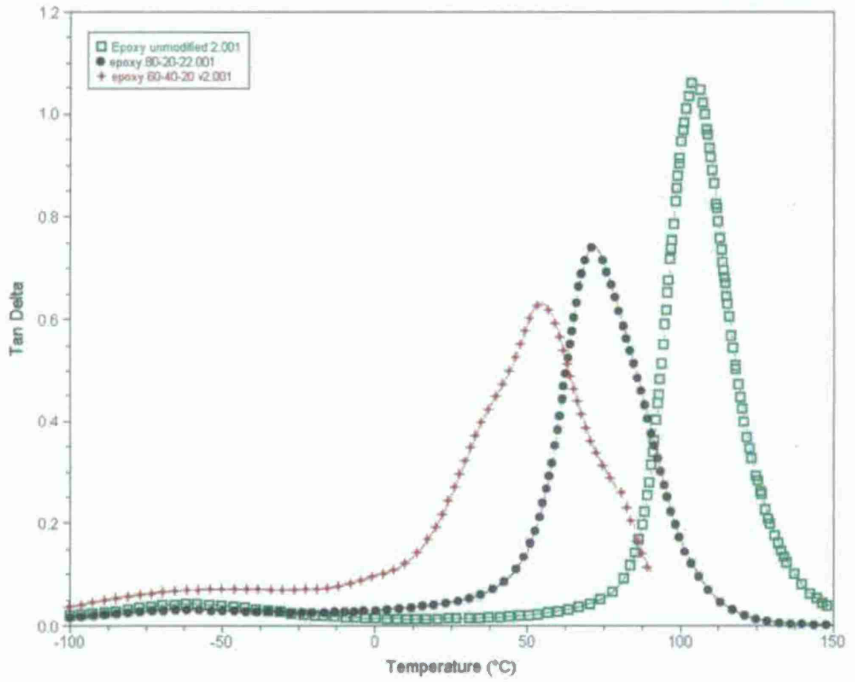

Figure 9.2. Tan delta curves for Epon epoxies with added network modifier; green corresponds to 0% modifier, black to 20% and red to 40% modifier.

Fig. 9.3 shows that this is not the case for the CNT yarn composites. Instead of taking on the characteristics of the matrices, the tan delta curves for each of the composites remain very close to each other, with a Tg value that remains in the same range as it was for the unmodified epoxy material. Not only are the Tg values of the composites uneffected, but the values of tan delta peaks are much lower than one would expect if a fiber volume fraction of 50% and the tan δ_m values from Fig. 9.2 are used in equation (9.1). The dampening is decreased significantly and can only point to an integration of the resin into the CNT yarn structure which changes the fundamental crosslinked epoxy networked structure. With such a large volume and close proximity of individual of CNTs to each other, there is a reduction in the number of chemical crosslinks in the epoxy network. However, for the same reason, the level of crosslinking remains determined not by chemical bonding but rather by a physical crosslinking of epoxy chains which are entangled in and bonded around the CNT network.

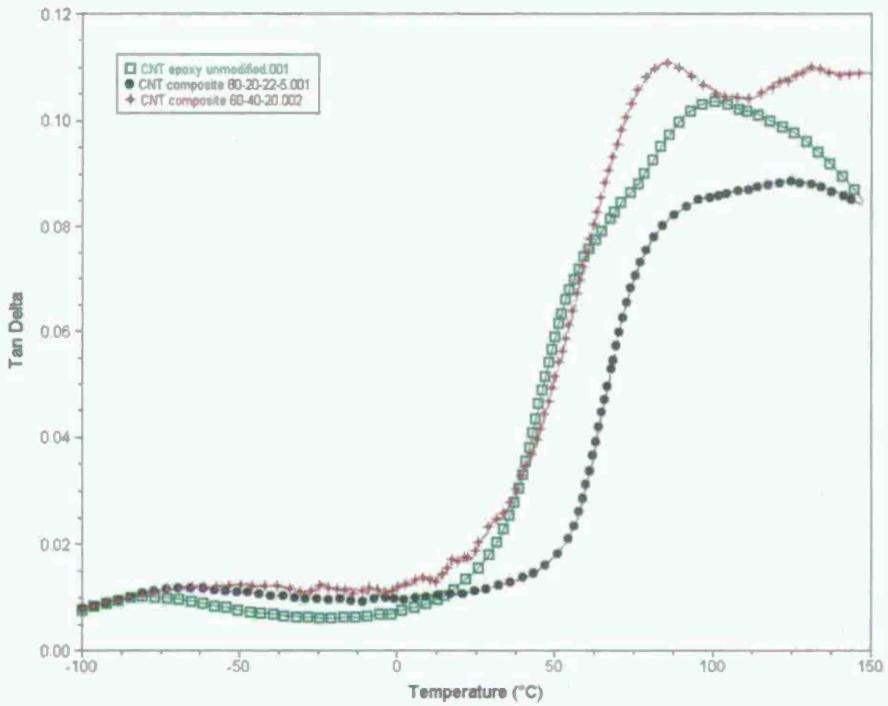

Figure 9.3. Tan delta curves for 3D braided CNT composites with the same epoxy formulations used in Figure 9.2.

Fig. 9.4 shows the results of storage modulus of the CNT yarn composites with unmodified epoxy and highly modified epoxy (40%) matrices. The elastic modulus of composites shown there is the same as the values in Fig. 7.4 and remains the same over the entire temperature range. The mechanical and thermomechanical properties remain the same and thus the network behavior of the epoxy is not influenced as much by the chemical crosslinking but rather the physical entrapment of the macromolecules by the CNTs. This could explain why no change in the strain to failure values between composites with vastly different epoxies was experienced and could help to explain the lower than expected values obtained.

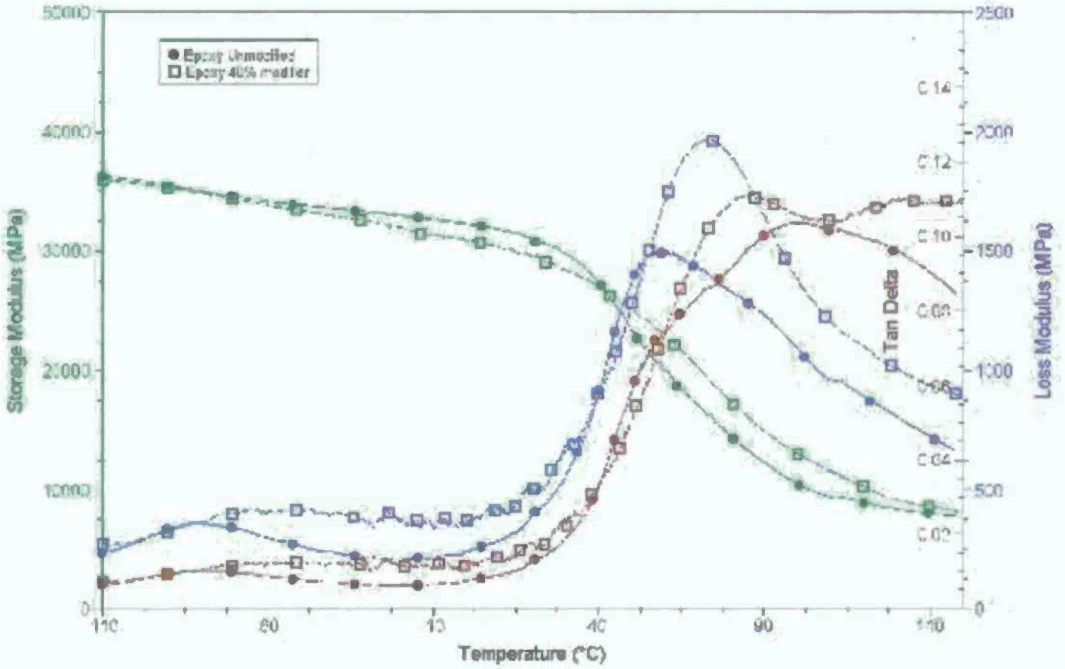

Figure 9.4. DMA curves showing the similarities between CNT yarn composites for vastly different epoxy formulations.

The lower order of transitions, such as β-transitions in polymer materials, also give some insight into the inherent brittleness of the material through the crack/defect initiation and propagation. In epoxy networks it has been shown that chain flexibility has a greater importance in the defect nucleation than the level of crosslinking [45]. Thus, increasing the stiffness or the local mobility of polymer chain in an epoxy network can increase the rate of defect initiation and propagation making the material behaving in a more brittle manner. It was hypothesized that the close proximity might not only affect the crosslinked structure but also hinder even smaller molecular motions which show up as lower order transitions. Fig. 9.5 shows the β-transitions of the epoxy samples and CNT yarn composite samples. The five curves with the highest tan delta values were collected from the tested modified epoxy samples. The lowest three curves were all collected from the CNT yarn composites. It is clear that both the tan delta curves are greatly reduced while also the amplitude of the peaks are reduced as well. Adding additional modifier to the epoxy samples increases the β-transitions intensity, while adding additional modifier to the CNT yarn composite samples has little effect.

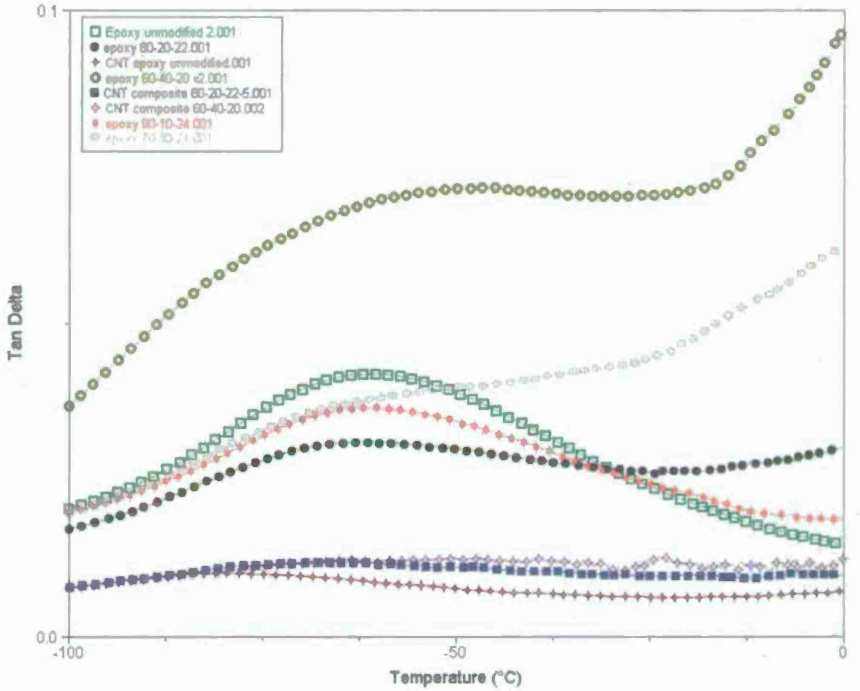

Figure 9.5. Tan delta curves for different modified Epon epoxies and the CNT yarn composites made with those epoxies.

9.4. Conclusions

Future high performance structural and multifunctional composites may utilize continuous carbon nanotube reinforcements. The interactions between carbon nanotubes and epoxy macromolecules in such composites open new areas of research and technology. Dynamic mechanical analysis used here for gaining an initial understanding of such interactions and explaining some unusual mechanical properties points to the fact that the nanotubes do, in fact, hinder small segmental motions of the epoxy molecules and are a paramount factor to take into consideration when determining the mechanical properties of composites made from CNT yarns.

REFERENCES

1. A. Thess, et al., Science, 1996, **273**, pp. 483-487.
2. A.G. Rinzler, et al., Applied Physics A, 1998, **67**, pp. 29-37.
3. C. Journet, et al., Nature, 1997, **388**, pp. 756-758.
4. P. Nikolaev, et al., Chemycal Physics Letters, 1999, **313**, pp. 91-97.
5. M. Endo, et al., J. Phys. Chem. Solids, 1993, **54** (12), pp. 1841-1848.
6. M. Ge and K. Sattler, Appl. Phys. Letters, 1994, **64** (6), pp. 710-711.
7. L.X. Zheng, et al., Nature Materials, 2004, **3**, pp. 673-676.
8. Q. Li, et al., Adv. Materials, 2006, Vol. 18, pp. 316-3163.
9. J. Fischer, in : Nanotubes and Nanofibers, Yury Gogotsi (Ed.), CRC Press, Boca Raton, FL, 2006, pp. 1-35.
10. R.H. Baughman, Nature Nanotechnology, November 2006, Vol. 1, pp. 94-96.
11. K. Hata, D.N. Futaba, K. Mizuno, T. Namai, M. Yumura, and S. Iijima, Science, 2004, **306** p. 362.
12. D. N. Futaba, K. Hata, T. Yamada, K. Mizuno, M. Yumura, and S. Iijima, Phys. Rev. Lett., 2005, **95**, 056104 (2005).
13. S. Chakrabart, T. Nagasaka, Y. Yoshikawa, L. Pan, and Y. Nakayama, Japanese Journal of Applied Physics, 2006, **45**, L720–L722 (2006).
14. P. Poulin, B. Vigolo, and P. Launois, Carbon, 2002, **40**, pp. 1741-1749.
15. P. Launois and P. Poulin, In: Encyclopedia of Nanoscience and Nanotechnology, 2004, Vol. 4, H.S. Nalwa (Ed.), pp. 763-774.
16. V.A. Davis, et al., Macromolecules, 2004, **37**, pp. 154-160.
17. Y.-L. Li, I.A. Kinloch, and A.H. Windle, Science, 2004, **304**, pp. 276-278.
18. R.H. Baughman, A.A. Zakhidov, and W.A. de Heer, Science, 2002, **297**, (5582), pp. 787-792.
19. A.E. Bogdanovich, Proc. 37th Int. SAMPE Fall Technical Conference, Seattle, WA, 2005.
20. K. Jiang, Q. Li, and S. Fan, 2002, Nature, **419**, p. 801.
21. M. Zhang, K.R. Atkinson, and R.H. Baughman, Science, 2004, **306**, pp. 1358-1361 (2004).
22. A. Bogdanovich, D. Mungalov, R.H. Baughman, S. Fang, and M. Zhang, Proc. 27th Int. SAMPE Europe Conference, Paris, France, 2006, pp. 455-460.
23. A. Bogdanovich, P. Bradford, D. Mungalov, S. Fang, M. Zhang, R.H. Baughman, and S. Hudson, SAMPE Journal, 2007, **43**, No. 1, January/February, pp. 6-19.
24. L. Zhu, D.W. Hess, and C.-P. Wong, J. Phys. Chem., 2006, **B 110**, pp. 5445-5449.
25. A.J. Hart and A.H. Slocum, J. Phys. Chem., 2006, **B 110**, pp. 8250-8257.
26. Q. Li, X. Zhang, R.F. DePaula, L. Zheng, Y. Zhao, L. Stan, T.G. Holesinger, P.N. Arendt, D.E. Peterson, and Y.T. Zhu, *unpublished.*
27. V.N. Shanov, Y. Yun, Y. Tu, and M.J. Schulz, 6th IEEE Conference on Nanotechnology, 2006.
28. A.J. Austin and C.V. Nguyen C.V., Journal of Applied Physics, 2006, **9**, No. 9, pp. 114304, 2006.

29. T. Shimizu, H. Abe, A. Ando, Y. Nakayama, and H. Tokumoto, Surf. Inerface Anal., 2005, **37**, pp. 204-207.
30. T.W. Ebbesen, H.J. Lezec, H. Hiura, J.W. Bennett, H.F. Ghaemi, and T. Thio, Nature, 1996, **382**, pp. 54-55.
31. A. Moisala, Q. Li, I.A. Kinloch, and A.H. Windle, Composites Science and Technology, 2006, **66**, pp. 1285-1288.
32. Y.J. Kim, T.S. Shin, H.D. Choi, J.H. Kwon, Y. Chung, and H.G. Yoon, Carbon, 2005, **43**, pp. 23-30.
33. A. Allaoui, S. Bai, H.M. Cheng, and J.B. Bai, Composites Science and Technology, 2002, **62**, pp. 1993-1998.
34. M.S. Fuhrer, J. Nygard, L. Shih, M. Forero, Y.G. Yoon, M.S.C. Mazzoni, H.J. Choi, J. Ihm, S.G. Louie, and A. Zettl, Science, 2000, **288**, pp. 494-497.
35. In: ASM Handbook, Volume 21 Composites. 4th edition, ASM International, 2006.
36. J.-P. Pascault, H. Sautereau, J. Verdu, and R.J.J. Williams, Thermosetting Polymers, Marcel Dekker, New York – Basel, 2002.
37. K.P. Menard, Dynamic Mechanical Analysis. A Practical Introduction, CRC Press, 1999.
38. Zhou, Y., Pervin, F., Lewis, L., Jeelani, S.., "Experimental study on the thermal and mechanical properties of multi-walled carbon nanotube-reinforced epoxy," Materials Science and Engineering A, 2007, Vol. 452-453, pp. 657-664.
39. Jin, Z., Pramoda, K.P., Xu, G., Hong Goh, S., "Dynamic mechanical behavior of melt-processed multi-walled carbon nanotube/poly(methyl methacrylate) composites," Chemical Physics Letters, 2001, Vol. 337, pp. 43-47.
40. Satapathy B.K., Weidisch, R., Potschke, P., Janke, A., "Tough-to-brittle transition in multiwalled carbon nanotube (MWNT)/polycarbonate nanocomposites," Composites Science and Technology, 2007, Vol. 67, pp. 867-879.
41. Goh, H.W., Goh, S.H., Xu, G.Q., Pramoda, K.P., Zhang, W.D., "Dynamic mechanical behavior of in situ functionalized multi-walled carbon nanotube/phenoxy resin composite," Chemical Physics Letters, 2003, Vol. 373 pp. 277-283.
42. Potschke, P., Bhattacharyya, A.R., Janke, A., Goering, H., "Melt mixing of polycarbonate/multi-wall carbon nanotube composites," Composite Interfaces, 2003, Vol. 10, No. 4-5, pp. 389-404.
43. Wang, Z., Liang, Z., Wang, B., Zhang, C., Kramer, L., "Processing and property investigation of single-walled carbon nanotube (SWNT) buckypaper/epoxy resin matrix nanocomposites," Composites: Part A, 2004, Vol. 35, pp. 1225-1232.
44. Nielson, L.E., Mechanical Properties of Polymers and Composites Vol. 2., Dekker, New York, 1974
45. Urbaczewski-espuche, E., Galy, J., Gerard, J.F., Pascault, J.P., Sautereau, H., "Influence of chain flexibility and crosslink density on mechanical properties of epoxy/amine networks," Polymer Engineering and Science, 1991, Vol. 31, No. 22, pp. 1572-1580.
46. T.W. Ebbesen, H.J. Lezec, H. Hiura, J.W. Bennett, H.F. Ghaemi, and T. Thio, Nature, 1996, **382**, pp. 54-55.
47. A. Moisala, Q. Li, I.A. Kinloch, and A.H. Windle, Composites Science and Technology, 2006, **66**, pp. 1285-1288.
48. Y.J. Kim, T.S. Shin, H.D. Choi, J.H. Kwon, Y. Chung, and H.G. Yoon, Carbon, 2005, **43**, pp. 23-30.

49. A. Allaoui, S. Bai, H.M. Cheng, and J.B. Bai, Composites Science and Technology, 2002, **62**, pp. 1993-1998.
50. M.S. Fuhrer, J. Nygard, L. Shih, M. Forero, Y.G. Yoon, M.S.C. Mazzoni, H.J. Choi, J. Ihm, S.G. Louie, and A. Zettl, Science, 2000, **288**, pp. 494-497.
51. In: ASM Handbook, Volume 21 Composites. 4th edition, ASM International, 2006.
52. J.-P. Pascault, H. Sautereau, J. Verdu, and R.J.J. Williams, Thermosetting Polymers, Marcel Dekker, New York – Basel, 2002.
53. K.P. Menard, Dynamic Mechanical Analysis. A Practical Introduction, CRC Press, 1999.

REPORT DOCUMENTATION PAGE

Form Approved
OMB No. 0704-0188

1. REPORT DATE *(DD-MM-YYYY)*	2. REPORT TYPE	3. DATES COVERED *(From - To)*
31-10-2008	Final Report	01-08-2005 - 31-10-2008

4. TITLE AND SUBTITLE
"3 Dimensional Nano-Scale Reinforcement Architecture for Advanced Composite Structures"

5a. CONTRACT NUMBER
FA9550-05-C-0088

5b. GRANT NUMBER

5c. PROGRAM ELEMENT NUMBER

6. AUTHOR(S)
Bogdanovich, Dr. Alexander - Principal Investigator

5d. PROJECT NUMBER

5e. TASK NUMBER

5f. WORK UNIT NUMBER

7. PERFORMING ORGANIZATION NAME(S) AND ADDRESS(ES)
3Tex
109 MacKenan Drive
Cary, NC 27511 USA

8. PERFORMING ORGANIZATION REPORT NUMBER
R051 Final

9. SPONSORING/MONITORING AGENCY NAME(S) AND ADDRESS(ES)
DCMA Southern Virginia
190 Bernard Road, Bldg. 117
Fort Monroe, VA 23651

10. SPONSOR/MONITOR'S ACRONYM(S)
DCMA/AFOSR

11. SPONSORING/MONITORING AGENCY REPORT NUMBER
AFRL-OSR-VA-TR-2012-0449

12. DISTRIBUTION AVAILABILITY STATEMENT
Dist. A - Approved for Public Release

13. SUPPLEMENTARY NOTES

14. ABSTRACT

Report developed under STTR contract for topic AF04-T020. Multi-walled carbon nanotube forests were used for draw-spin processing of continuous carbon nanotube yarns, which were then plied and utilized in a micro-3D braiding and 3D weaving on the specialty equipment developed for this project. The technology of growing spinnable multi-wall carbon nanotube forests has been comprehensively studied and moved towards industrial applications. Extensive experimental studies conducted for understanding the effects of different polymer infusion into carbon nanotube yarns on their mechanical properties. It was demonstrated, for the first time, that 3-D braids can be made solely of continuous carbon nanotube yarns, or as hybrids of those with conventional yarns, and then used as reinforcement for composites. The produced carbon nanotube yarn, hybrid 3-D braid and their composites were tested for tensile mechanical properties and electrical conductivity. Mechanical test results revealed some unusual effects, and their explanation required additional Dynamic Mechanical Analysis and insightful polymer physics considerations. Various potential applications of CNT yarns, their 3-D braids and 3-D weaves have been identified, specifically in the areas of sensors, actuators, artificial fuel-powered muscles, devices for energy storage and conversion. Initial steps were taken towards commercialization of this novel class of nanocomposites.

15. SUBJECT TERMS
Carbon Nanotubes, Nanocomposites, Carbon Nanotube Yarns, 3-D Braids, 3-D Weaves, Mechanical Properties, Electrical Properties, Multifunctional Composites

INSTRUCTIONS FOR COMPLETING SF 298

16. SECURITY CLASSIFICATION OF:			17. LIMITATION OF ABSTRACT	18. NUMBER OF PAGES	19a. NAME OF RESPONSIBLE PERSON
a. REPORT	b. ABSTRACT	c. THIS PAGE			Charles P. Gaylor, IV
U	U	U	SAR	119	19b. TELEPONE NUMBER (*Include area code*) 919 481 2500 x126

INSTRUCTIONS FOR COMPLETING SF 298

1. REPORT DATE. Full publication date, including day, month, if available. Must cite at lest the year and be Year 2000 compliant, e.g., 30-06-1998; xx-08-1998; xx-xx-1998.

2. REPORT TYPE. State the type of report, such as final, technical, interim, memorandum, master's thesis, progress, quarterly, research, special, group study, etc.

3. DATES COVERED. Indicate the time during which the work was performed and the report was written, e.g., Jun 1997 - Jun 1998; 1-10 Jun 1996; May - Nov 1998; Nov 1998.

4. TITLE. Enter title and subtitle with volume number and part number, if applicable. On classified documents, enter the title classification in parentheses.

5a. CONTRACT NUMBER. Enter all contract numbers as they appear in the report, e.g. F33615-86-C-5169.

5b. GRANT NUMBER. Enter all grant numbers as they appear in the report, e.g. 1F665702D1257.

5c. PROGRAM ELEMENT NUMBER. Enter all program element numbers as they appear in the report, e.g. AFOSR-82-1234.

5d. PROJECT NUMBER. Enter al project numbers as they appear in the report, e.g. 1F665702D1257; ILIR.

5e. TASK NUMBER. Enter all task numbers as they appear in the report, e.g. 05; RF0330201; T4112.

5f. WORK UNIT NUMBER. Enter all work unit numbers as they appear in the report, e.g. 001; AFAPL30480105.

6. AUTHOR(S). Enter name(s) of person(s) responsible for writing the report, performing the research, or credited with the content of the report. The form of entry is the last name, first name, middle initial, and additional qualifiers separated by commas, e.g. Smith, Richard, Jr.

7. PERFORMING ORGANIZATION NAME(S) AND ADDRESS(ES). Self-explanatory.

8. PERFORMING ORGANIZATION REPORT NUMBER. Enter all unique alphanumeric report numbers assigned by the performing organization, e.g. BRL-1234; AFWL-TR-85-4017-Vol-21-PT-2.

9. SPONSORING/MONITORS AGENCY NAME(S) AND ADDRESS(ES). Enter the name and address of the organization(s) financially responsible for and monitoring the work.

10. SPONSOR/MONITOR'S ACRONYM(S). Enter, if available, e.g. BRL, ARDEC, NADC.

11. SPONSOR/MONITOR'S REPORT NUMBER(S). Enter report number as assigned by the sponsoring/ monitoring agency, if available, e.g. BRL-TR-829; -215.

12. DISTRIBUTION/AVAILABILITY STATEMENT. Use agency-mandated availability statements to indicate the public availability or distribution limitations of the report. If additional limitations/restrictions or special markings are indicated, follow agency authorization procedures, e.g. RD/FRD, PROPIN, ITAR, etc. Include copyright information.

13. SUPPLEMENTARY NOTES. Enter information not included elsewhere such as: prepared in cooperation with; translation of; report supersedes; old edition number, etc.

14. ABSTRACT. A brief (approximately 200 words) factual summary of the most significant information.

15. SUBJECT TERMS. Key words or phrases identifying major concepts in the report.

16. SECURITY CLASSIFICATION. Enter security classification in accordance with security classification regulations, e.g. U, C, S, etc. If this form contains classified information, stamp classification level on the top and bottom of this page.

17. LIMITATION OF ABSTRACT. This block must be completed to assign a distribution limitation to the abstract. Enter UU (Unclassified Unlimited) or SAR (Same as Report). An entry in this block is necessary if the abstract is to be limited.